MODELING AND ANALYSIS OF LONGITUDINAL AND LATERAL DYNAMICS OF A TELE-OPERATED UNMANNED TRACKED VEHICLE

A THESIS

submitted by

SENTHILKUMAR D.

for the award of the degree

of

MASTER OF SCIENCE

(by Research)

DEPARTMENT OF ENGINEERING DESIGN
INDIAN INSTITUTE OF TECHNOLOGY MADRAS

MARCH 2017

THESIS CERTIFICATE

This is to certify that the thesis titled **MODELING AND ANALYSIS OF LONGITUDINAL AND LATERAL DYNAMICS OF A TELE-OPERATED UNMANNED TRACKED VEHICLE**, submitted by **Senthilkumar D.**, to the Indian Institute of Technology, Madras, for the award of the degree of **Master of Science (by Research)**, is a bona fide record of the research work done by him under our supervision. The contents of this thesis, in full or in parts, have not been submitted to any other Institute or University for the award of any degree or diploma.

Prof. T. Asokan

Research Guide
Professor
Dept. of Engineering Design
IIT-Madras, 600 036

Dr. C. S. Shankar Ram

Research Co-Guide
Associate Professor
Dept. of Engineering Design
IIT-Madras, 600 036

Place: Chennai

Date: 03rd March 2017

ACKNOWLEDGEMENTS

My research life has been a nice journey for me. It would not be fulfilled unless thanking all the people who helped me in doing this. First of all, I express my immense gratitude to my guide **Prof. T. Asokan** for given me this opportunity to work on a problem where I had a real-time experience and also for tendering me the constant support throughout my research journey. I am grateful to my co-guide **Dr. C. S. Shankar Ram** who gave me suggestions which really pushed me to explore many new areas. I thank to my panel members for their suggestions and particularly **Prof. R. Krishna Kumar** who actually provided me the base of my research with the course work of Vehicle Dynamics which helped me a lot to explore the problem very easily without much hindrances when I started the problem. Other course works such as Field and Service Robotics, Theory of Mechanism had given me the confidence so that I could easily deal with the problems I came across. And also other course works which gave me the idea of looking into the problem in different perspective.

I thank all my friends with whom I often put intellectual fights without which I would have never reached to this level. I particularly would like to thank my friend **Mr. R. Thiagarajan** for suggesting me how to implement a mathematical model in numerical tools and taught me some techniques as well. I thank my friends **Mr. C. Karthik, Mr. N. Ganeshram, Dr. Sourav Chandra, Mr. G. Nagamanikandan, Mr. Bhanu Chander, Ms. L. Prathyusha, Mr. Suraj Parameshwaran, Mr. Sai Sreekar Annamraju, Mr. Arjun, Mr. Irfan Habeeeb** and **Mr. K. Mithun** for their constructive criticism which really helps me to refine and improved the way I do research. I indebted to my dear friends **Mr. T. Edison Phoenix** and **Mr. Adithya Verma Sagi** who tendered their supports and suggestions. I thank my friends from automotive laboratory **Mr. Vignesh Rajaram** and **Mr. M. Jatheendra** for their suggestions.

It is incomplete without acknowledging the people of DRDO-CVRDE. I am very grateful to **Sct. Swarna Ramesh** who allowed me to work on the experimental vehicle in CVRDE for doing experiments and also suggested me in what way the results could be improved. I thank **Sct. N. Babu, Sct. Alexander** and **Sct. Lakshmi Prathiba** who were there with me in all the times when I was learning in CVRDE.

ABSTRACT

KEYWORDS: Tele-operation, Adams Tracked Vehicle (ATV) software, Tracked vehicle, Subsystems, Longitudinal, Lateral, and Yaw motion dynamics.

Tele-operation of an unmanned vehicle has received a lot of attention in the recent years due to its immense application in various fields where the risk to human is higher. These hazardous environments are mostly in off-road conditions where a pneumatic tyred vehicle would not tread effectively due to their undulations, obstacles, terrain condition variations, etc. In such scenarios, it is effective to use an unmanned tracked vehicle instead of a pneumatic tyred vehicle due to its better maneuverability and mobility in off-road conditions. It is important to model the dynamics of a tracked vehicle and its subsystems before developing a tele-operation or autonomous system.

In this research, efforts were taken to model the various subsystems, lower-level controller for the brake subsystem, and vehicle dynamics of a tracked vehicle. Three subsystems, namely, powertrain, brake, and steering were considered. In the powertrain subsystem, the components that were considered are engine, clutch, gearbox, and final drive, and mathematical models were derived for each. Since modeling the behavior of the engine is extremely complex, a two dimensional look-up table had been generated from the engine test data. The brake subsystem was modeled for the same configuration as in the experimental vehicle by making reasonable assumptions. The vehicle's steering was obtained by providing differential brake force to the sprockets since the skid-steering method was considered. For this purpose, the same brake components were used to obtain the steering action. Modeling and simulation of each subsystem's dynamics are also presented.

While modeling the tracked vehicle motion dynamics, only longitudinal (braking and acceleration), lateral, and yaw motions were considered. Effect of other motions such as pitch, bounce, and roll were not addressed. Modeling of terrain dynamics was followed from the literature and the scope was limited only to soft terrains that include snow, clay, sandy loam, etc. Longitudinal motion dynamics was modeled by considering variable resistances that the vehicle would possibly be acted upon and the results were presented. Accurate modeling of the lateral dynamics is quite complex since it deals with lateral skidding, track slippage, etc. An approximate model was obtained by considering the pressure distribution under the track as uniformly varying or uniformly distributed depending on the situation whether the vehicle is accelerated or maintaining constant speed. Finally, all the subsystems and vehicle dynamics were integrated and simulated for various cases. Lower-level subsystem controllers were also designed to obtain the desired output for the brake subsystems. These lower-level controllers play a significant role when the vehicle operates in autonomous or tele-operation mode.

The Adams Tracked Vehicle software was used to compare the proposed model results for various tests that were considered. The outputs of the subsystem models, which are the thrusts at the left and right sprockets, are the inputs to the proposed vehicle dynamics model and ATV model. The performance of the model was quantified using the Mean Absolute Percentage Error (MAPE). The corroboration with the experimental results was done only for the case of longitudinal dynamics due to experimental limitations. It was found that the model was able to predict the vehicle motion with reasonable accuracy both under transient and steady state conditions. This model could be used for developing automated systems for tele-operation.

TABLE OF CONTENTS

LIST OF TABLES

LIST OF FIGURES

ABBREVIATIONS

ATV	Adams Tracked Vehicle
BMP	Boevaya Mashina Pehoty
CVRDE	Combat Vehicle Research and Development Establishment
DBW	Drive-By-Wire
DOF	Degrees of Freedom
GPS	Global Positioning System
MAPE	Mean Absolute Percentage Error
PD	Proportional Derivative
RPM	Revolutions Per Minute
TPPMTV	Traction Performance Prediction Model for Tracked Vehicles

NOTATIONS

$\alpha(t)$	Yaw acceleration of the vehicle
β_f	Bulk modulus of the fluid
$\beta(t)$	Side slip angle of the vehicle
$\gamma_m(t)$	Mass factor
ς	Damping ratio
η	Transmission efficiency
$\theta(t)$	Orientation of the vehicle
$\theta_1(t), \theta_2(t)$ and $\theta_3(t)$	Angular displacements of link1, link2, and link3
θ_{lap}	Lapping angle of the band over the cylinder
θ_s	Sloping angle of the terrain
ξ_F	Final drive gear ratio
$\xi_T(t)$	Gear box reduction ratio
μ	Traction coefficient
μ_{band}	Friction coefficient between the band and the cylinder
μ_{dyn}	Dynamic viscosity of the lubricant
μ_{hyd}	Dynamic viscosity of the hydraulic fluid
μ_l	Longitudinal traction coefficient
$\mu_t(t)$	Lateral coefficient of traction
τ	Time constant
τ_1	Input torque, applied on the brake pedal
ρ	Air density
ϕ	Pressure angle
$\omega_E(t)$	Engine speed
$\omega_C(t)$	Clutch output shaft speed

$\omega_F(t)$	Final drive speed
$\omega_G(t)$	Gear output shaft speed
$\boldsymbol{\omega}_i$	Angular velocity of the i^{th} link in the body fixed frame
$\omega_o(t)$ and $\omega_{in}(t)$	Sprocket speed of the right and left sprocket of the vehicle
ω_n	Natural frequency
$\omega_z(t)$	Yaw speed
a_f	Frontal area
a_j	Joint perimeter area
a_t	Track area
b	Breadth of the track
B	Breadth of the vehicle
c	Cohesion
cl	Clearance between the link hole and the hinge surface
$c_x(t)$ and $c_y(t)$	Distance between the center of gravity of the vehicle and center of turn of the vehicle in x and y directions
C_d	Coefficient of drag
d_{mc}, d_{br} and d_{hos}	Diameter of the master cylinder, brake cylinder and hose
f	Magnification factor
$F_B(t)$	Brake force
$F_l(t)$ and $F_r(t)$	Force at the left and right sprocket
$F_{out}(t)$	Force that acts on the band
FR	Force ratio
$F_{rf}(t)$	Reactive force on the mechanism
$F_T(t)$	Ground thrust
$F_x(t)$	Lateral force that acts on the tracks
$F_y(t)$	Longitudinal force that acts on the tracks

I_C	Mass moment of inertia of the clutch about the rotational axis
$\mathbf{I}_{ci}$	Inertia matrix of the i^{th} link in the brake subsystem
I_F	Mass moment of inertia of the final drive about its rotational axis
I_T and I_w	Inertia of the track and the wheels
I_{zz}	Mass moment of inertia of the vehicle about the Z-axes
$i(t)$	Slip of the vehicle
$\mathbf{J}_{vi}(t)$	Translational velocity Jacobian
$\mathbf{J}_{\omega i}(t)$	Rotational velocity Jacobian
$\mathbf{j}_x(t)$	Jacobian for brake piston movement velocity
$j_o(t)$	Shear displacement
k_c, k_φ and n	Empirical constants for the terrain
K	Shear modulus
K_{band}	Stiffness of the band
K_{mc}	Stiffness of the master cylinder spring
K_{wc}	Stiffness of the brake cylinder spring
l_{mc}, l_{wc} and l_{hos}	Length of the master cylinder, brake cylinder, and hose
L	Lagrangian of brake subsystem
l	Length of the track
m	Mass of the vehicle
m_i	Mass of the i^{th} link in the brake subsystem components
$M_t(t)$	Moment of turning resistance
n_T	Number of tracks
n_w	Number of sprocket and track wheels
p_t	Pressure on the terrain
$\mathbf{p}_{ci}(t)$	Center of mass of the i^{th} link
r	Radius of the sprocket

r_1, r_2 and r_3	Lengths of link1, link2, and link3
$\mathbf{r_{03}}$	Ground link vector
$R(t)$	Turning radius
$R_a(t)$	Aerodynamic resistance
$R_{in}(t)$	Internal resistance
R_m	Motion resistance
R_G	Grade resistance
$s_o(t)$	Shift of the center of turn (C_T) from the center of gravity (C_G)
t_1	Time instant when the clutch is released from the completely pedaled position
t_2	Time instant when the clutch plate makes contact with the pressure plate
t_3	Time instant when the clutch starts transmitting power
t_4	Time instant when the clutch transfers power completely from engine to transmission
$T(t)$	Kinetic energy of the brake subsystem components
$T_2(t)$	Tension in the slack side
$T_C(t)$	Clutch torque
T_d	Time delay due to the communication lag
$T_E(t)$	Engine torque
$T_F(t)$	Final drive torque
$T_G(t)$	Gear torque
t_s	Settling time
$\dot{u}(t)$ and $\dot{v}(t)$	x and y components of the vehicle acceleration vector
$u(t)$ and $v(t)$	Vehicle speed in x and y direction
$\mathbf{v}_f\mathbf{(t)}$	Velocity vector of the vehicle
$V(t)$	Potential energy of the brake subsystem components

$\mathbf{v}_{pi}$	Translational velocity of the mass center
v_{fl}	Volume of the hydraulic fluid in the braking subsystem
W	Weight of the vehicle
$x_{act,i}$	Actual value of a variable
$x_{out}(t)$	Displacement of the brake cylinder piston
x_{pri}	Predicted value of a variable
$x_s(t)$	Displacement of the hydraulic piston in the master cylinder
z	Sinkage on the terrain

CHAPTER 1
INTRODUCTION

The demand for tele-operated unmanned vehicles has seen a rapid growth in the last few years owing to their applications in areas such as mining, defense, security, and surveillance, and many other hazardous environments where the risk to human is very high. In such scenarios, it is better to have an unmanned vehicle instead of employing a human to operate it and risking his/her life. Tele-operation is about human-computer co-operation in controlling the remote sensors and actuators. Tele-presence is a phenomenon in which a special sensing and display environment provides the driver a virtual feel of being in the operating environment (Sheridan, 1995). The field of tele-operation is an emerging field in which there are a lot of problems that are still to be addressed in terms of driver's capability such as loss of situational awareness, poor obstacle detection, etc. Even with expert operators, many other difficulties would arise in the form of poor communication between the vehicles, operator workload, etc. (Fong, Thorpe and Baur, 2001). Operator workload could be reduced by making the vehicle to make intelligent decisions by planning its vehicle path, obstacle avoidance, etc., which may be called as semi-automatic tele-operation. A tele-operation system is more prone to environmental changes since it has to transmit and receive data from a remote environment. Also, the remote vehicle should be capable of making its own decisions in scenarios when communication is lost between vehicles. In such cases, the vehicle should be able to take its own decisions by activating a fail-safe unit to avoid any dangerous situations.

A tele-operated unmanned vehicle will mostly be useful in environments such as mountains, deserts, forests, etc. In those off-road conditions, terrains are mostly filled

with undulations, obstacles in surfaces, and randomness in terrain properties (Li and Tang, 2015). In order to overcome challenges that arise in the environments, tracked vehicles will be more effective in terms of mobility when compared to a pneumatic tyred vehicle (Wong, 2001). Tele-operation systems have applications in various fields such as underwater, space exploration, toxic material handling in nuclear power plant, tele-presence, tele-medicine, remotely operated marine vehicles, firefighting, etc.

In the field of space exploration, there are so many examples of tele-robotics. Figure 1.1(a) shows the Russian Lunokhod-1, a remotely driven rover on the moon. This rover was driven in real-time (with a communication time delay of 2.5 *s*) by human operators on the earth. Robotic planetary exploration programs use spacecraft that are programmed by humans at the stations in the earth, essentially achieving a long-time-delay form of tele-robotic operation. Mars exploration rover is shown in Fig. 1.1(b). The spacecraft and the rover operated on stored programs, with the rover drivers on the earth programming each day's operation.

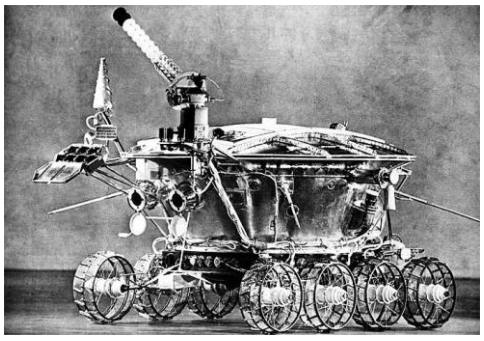

(a) Lunokhod 1
http://apod.nasa.gov/apod/ap100606.html

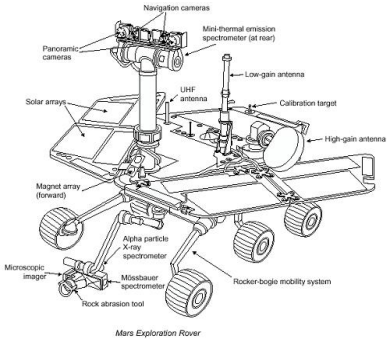

(b) Mars exploration rover
http://marsrovers.jpl.nasa.gov/newsroom/merlandings.pdf

Fig. 1.1: Space exploring tele-robots

Tele-surgery is being increasingly studied in the field of medical devices and minimal invasive surgical systems. In the conventional way of surgery, surgeon operates the patient that may last for hours, which induces tremor due to fatigue. Tele-operated surgical robots with master and slave manipulators have been used as shown in Fig. 1.2 to minimize the surgeon's effort and also filtering out the fatigue induced tremor during the surgery.

Fig. 1.2: Tele-surgical robots
https://doi.ieeecomputersociety.org

For monitoring deep ocean activities and surveillance, remotely operated vehicles are extensively used, which are tele-operated from a mother ship. Figure 1.3 shows a laboratory prototype of a remotely operated underwater robot. In nuclear power plants also, robotic manipulators are used for handling the nuclear waste and fuel rods. Usually in such scenarios, master and slave manipulators are used. Master manipulators will be operated by humans and the slave manipulators will do the operations on the toxic materials with scaled-up or scaled-down motion according to the design.

Fig. 1.3: Remotely operated underwater vehicle (Santhakumar, 2010)

1.1 TRACKED VEHICLES

A tracked vehicle is one that has a track wrapped around the road wheels as shown in Fig. 1.4. A track is a series of tread plates that are hinged to each other. The advantages of using tracked vehicles in off-road conditions are better mobility and improved maneuverability. Mobility is the ability of a vehicle to move easily over a range of terrains. Maneuverability is the ability of a vehicle to have planned or controlled motion in a particular terrain. Improved maneuverability of a tracked vehicle in rough terrain is due to its weight being distributed all along the track length (Lee, 2006). Better mobility is due to the improved contact area and the track being flexible enough to accommodate reasonably sized obstacles that the vehicle may encounter.

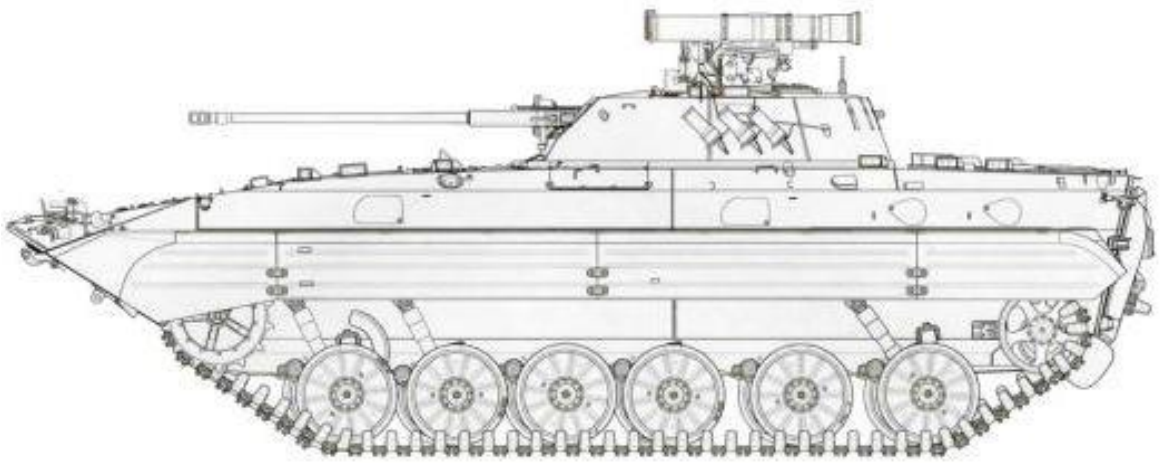

Fig. 1.4: Tracked vehicle

http://www.armyrecognition.com

Studying and replicating the behavior of a particular off-road terrain in a model is very complex since it possesses too many uncertainties, is dynamic in nature, and is highly influenced by weather conditions. Generally, off-road terrains can be classified as soft terrain and hard terrain. Classification of terrains are based on the terrain deformation caused by the vehicle. Soft terrain is where the terrain deformation is significant since the bonding between the molecules is weak. Hard terrain is where the terrain deformation is negligible since it has very strong bonding between the particles. Generally, these two terrains are characterized with different terrain properties. Soft terrain is characterized by certain properties such as cohesion, pressure angle, and shear deformation modulus (Wong and Chiang, 2005). Cohesion is a property of attraction between the same molecules and it is more predominant in the case of clay, mud, sandy loam, etc., where the moisture content is very high. Pressure angle indicates the friction between the sand particles and it is predominant in dry sand where the moisture content is very minimum. But in the case of hard terrains, properties by which the terrains defined are stiffness, damping, static transition, and friction transition.

Terramechanics is the study of interaction between the track and terrain. The dynamics of a tracked vehicle differs from that of a pneumatic tyred vehicle in many ways due to its inherent design variations and track-terrain interactions. In vehicles with pneumatic tyres, force generation is mainly decided by stiffness or compliance of the pneumatic tyre that is made of viscoelastic material. In tracked vehicles, force is generated by the soil shear strength in the track-terrain interface (Li and Tang, 2015). Generally, the strength of any soft terrain can be measured by the amount of deformation that the terrain would undergo for the applied shear stress, which is generally called as shear modulus. A number of test methods have been proposed by many researchers to determine the properties of soft terrains (Wong and Preston-Thomas, 1983). The interaction between the track and terrain is very complex and formulating an accurate model at each contact point under the track is very cumbersome due to its non-linearity (Lu and Hedrick, 2005). Further, the computational efforts involved in solving these models are high. A few approximate models have been developed and used to determine the behavior of the track-terrain interactions. Another important issue that needs to be addressed while modeling the track-terrain interaction is determining the nature of pressure distribution under the track, which is mainly decided by the terrain properties (Wong, 1984). Usually in soft terrains, the pressure distribution is uniformly varying in nature. When a vehicle is travelling at a constant speed, there will not be any load transfer. So the pressure distribution is uniformly distributed along the track length. But if a vehicle accelerates or decelerates, load transfer makes the pressure distribution trapezoidal or triangular variation in nature. That variation depends on the intensity of acceleration or deceleration of the vehicle (Kitano and Kuma, 1977). In some other scenarios where the vehicle is climbing over a slope, pressure distribution will become trapezoidal and triangular depending upon the

slope of the terrain. When a track segment under the road wheel penetrates inside a soft terrain, the adjacent track segments are also pulled and pressed against the terrain, which exerts some amount of pressure on all track segments adjacent to the road wheel. This behavior repeats at each road wheel that are placed at regular intervals; so it is reasonable that the pressure is uniformly distributed or varied along the track according to the center of gravity position. In hard terrain, the pressure distribution is generally assumed as sinusoidal along the length or approximated as a concentrated point load directly below the road track contact due to the negligible deformation of the terrain (Kitano and Kuma, 1977). But still the track will be useful in hard terrain because the obstacles on the terrain can be easily climbed over by the tracked vehicle.

Bull dozing effect is an additional mechanism of thrust generation when a blade is directly dug into the terrain and pressed in the direction opposite to that of motion, which helps the vehicle to propel when it maneuvers in soft terrains as shown in Fig. 1.5. Actually, blades are provided at each track segment, which are projecting downwards to push the sand mass present at the vicinity of the blades that helps to produce additional thrust.

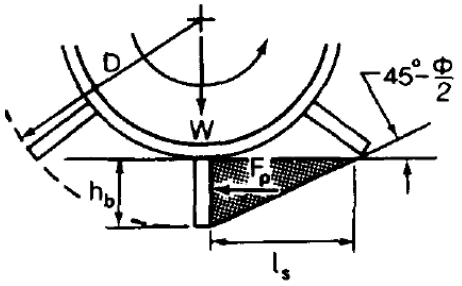

Fig. 1.5: Interaction between soil and blade (Wong, 2001)

In some situations, particularly in soft terrains, sinkage is so high that the bottom surface of the hull will get in touch with the terrain. In that scenario, the weight of vehicle is reduced at the tracks and the vehicle traction is reduced. This also adds additional drag to the vehicle that increases the resistance to the vehicle. Steering of a tracked vehicle is different from that of a pneumatic tyred vehicle. Generally, the steerable wheel of a pneumatic tyred vehicle will have two degrees of freedom (DOF) - one is about the wheel axis and the other one is about the axis perpendicular to ground plane. However, in the case of a tracked vehicle, the sprocket is allowed to have motion only about wheel axis. So the steering of the tracked vehicle should be done in differently, unlike the road vehicle. There are many ways to achieve the steering in tracked vehicle which are articulated steering, curved-track steering, and skid-steering. In articulated steering as shown in Fig. 1.6(a), two or more tracked vehicles are coupled to each other and steering actuators are provided between the vehicles that actually initiate the steering action. In curved track steering as shown in Fig. 1.6(b), steering is achieved through the lateral flexibility of the road wheels and tracks, where certain arrangements are provided at each track wheel to bend the track to a considerable amount to achieve the steering of the vehicle. But the disadvantage is that one cannot achieve a smaller turning radius due to the limitation of lateral flexibility of track wheel in the vehicle. The minimum turning radius will be very much higher compared to other steering methods. The most commonly used steering method is skid-steering. It does not need any additional attachments and is simple in construction. In skid-steering, as shown in Fig. 1.6(c), a differential force is applied to the tracks through sprockets that leads to the generation of a moment that in turn produces the steering action. The steering action happens due to the track slippage and lateral skidding of the tracks, which are inevitable in this case. Due to

this, it is quite tedious to model the exact nature of the skid-steering of the tracked vehicle (Wong and Chiang, 2005).

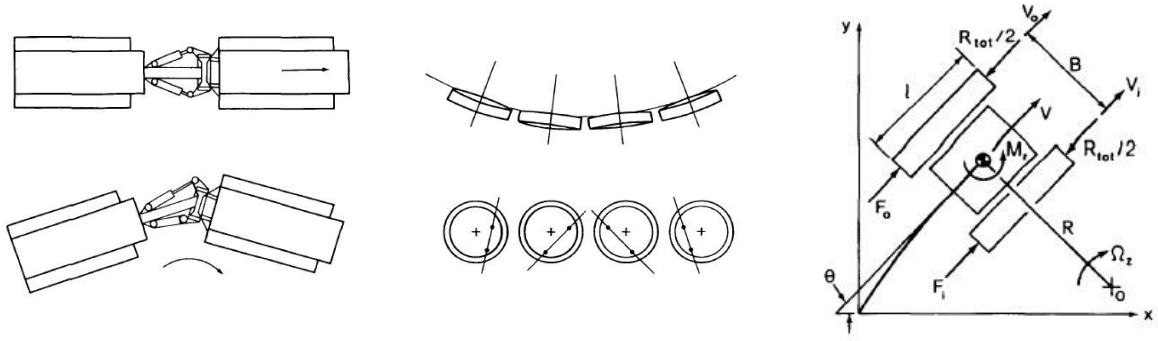

(a) Articulated steering (b) Curved-track steering (c) Skid-steering

Fig. 1.6: Steering methods (Wong and Chiang, 2005)

Modeling the subsystems of the vehicle is important because it may have significant impact on deciding the behavior of the vehicle in different input conditions. By giving importance to subsystem dynamics, the accuracy of the model could be improved (Shu, Ma and Liu, 2002). In particular, brake and steering subsystem dynamics of the tracked vehicle are completely different from that of a pneumatic tyred vehicle. For example, in a situation when a vehicle maneuvers a tight turn, the inner track will be acted upon by more resistances compared to the outer track. So, these forces on the sprockets will eventually affect the behavior of steering components. It is also important to model the subsystems for every tracked vehicle since the configuration of these subsystems varies from vehicle to vehicle. Brake of the tracked vehicle is mostly attained by an externally contracting brake, which will have more contact surface area to generate braking action. Accurate modeling of these subsystems will reduce the factors that cause uncertainties when the vehicle behavior is modeled.

1.2 TELE-OPERATION OF UNMANNED TRACKED VEHICLES

Tele-operation is a method by which a vehicle/system is controlled or operated from a remote location. The basic idea of tele-operation of a vehicle is shown in Fig. 1.7.

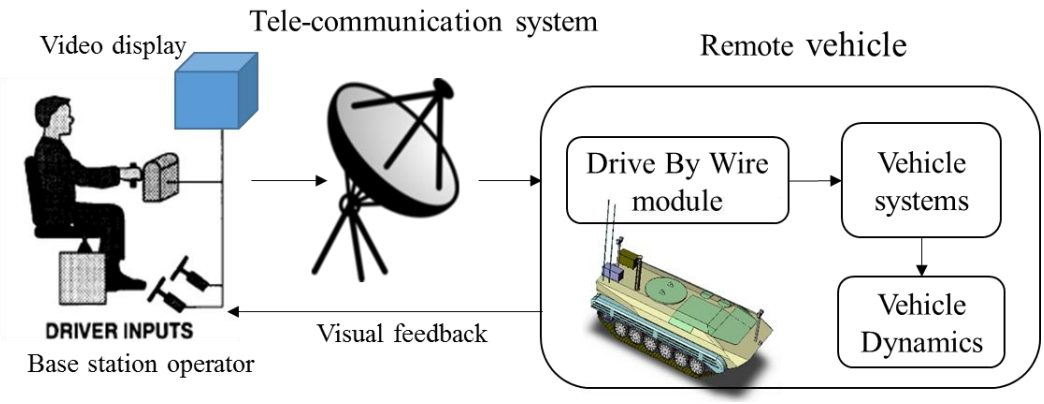

Fig. 1.7: Schematic of tele-operation of a remote vehicle

In the given scenario, there are two vehicles: a base station/vehicle and a remote vehicle. The base station/vehicle will be mostly in safer zones. The remote vehicle is the actual vehicle that will travel in unsafe or dangerous zones. The base vehicle will have input devices such as accelerator pedal, brake, steering, etc., feedback devices such as video display, signal screens, etc., and communication devices. The operator sits in the base vehicle and feeds the inputs according to the mission requirements and environmental changes such as change in terrain conditions, vehicle response, etc. The operator inputs are converted to electrical signals and transmitted to the remote vehicle. The remote vehicle receives, conditions, and processes the signals in the Drive-By-Wire (DBW) system. DBW system technology is most commonly used in the automotive industry where electro-mechanical systems are used for performing the vehicle's functions in order to partially replace the conventional mechanical linkages. The DBW system consists of signal processors, electrical motors, and controllers, and mechanical linkages

for actuating the throttle, brake, clutch, etc., of the remote vehicle. The remote vehicle will be operated based on the DBW outputs. There are many challenges in achieving the tele-operation of off-road vehicle as vehicle dynamics, terrain, DBW subsystems, and tele-communication systems bring in many uncertainties and practical difficulties such as delay in response, path tracking errors, etc.

Developing accurate models of vehicle, DBW system, etc., is very important in the study of tele-operation of vehicles. In order to model the tele-operation of vehicles, it is very important to consider the factors that influence its response. These factors include time delay, settling time, latency in the signal transmission, sensor noises, errors in the DBW system components, and extraneous factors. Considering these factors, it is necessary to develop a dynamic model of the tele-operation system to determine the behavior of a tele-operated vehicle. In this research, the DBW system was characterized as a linear first order system with time delay input.

1.3 LITERATURE SURVEY

Many researchers have tried to model the tele-operation of ground vehicles and simulate the vehicle behavior under various operating conditions (Fong, Thorpe and Baur, 2001), (Hainsworth, 2001). The design of a DBW system was presented in Sharon (1993), where the mechanical linkages were replaced and computerized control was used to improve the safety, reliability, and maneuverability of a vehicle. However, the dynamics of the vehicle was not given due importance as the focus was mainly on the tele-operation system. In the tele-operation of a tracked vehicle, the vehicle subsystem dynamics and

vehicle dynamics may play a major role as the dynamics of a pneumatic tyred vehicle and a tracked vehicle have significant differences.

Modelling of vehicle subsystems was considered by many researchers. In Kinagi *et al.* (2012), a methodology to design the brake system for light military vehicles was discussed. A transient model for the engine was developed and integrated with subsystems in the power train such as clutch, gear box, transfer case, and differential unit by Shu *et al.* (2002). An integrated powertrain model, coupled with either a multi-dynamics model or a point mass model of a vehicle, to find out the vehicle behavior in various operating conditions was reported in Assanis *et al.* (1999). Typical simulation and comfort optimization challenges in automatic gear shifting were discussed (Abel, Schreiber and Schindler, 2006), and the modeling solutions as well as applications were illustrated. A hydraulic brake system model was developed by Kuang *et al.* (1999) using bond graph method and a feedback control system with an adaptive gain scheduled PD controller was developed. A real-time simulation model for the transient analysis of a multi-cylinder engine that is linked with the powertrain components was presented (Janarthanan, Padmanabhan and Sujatha, 2009). A simplified transient analysis model was developed for various subsystems in the powertrain to predict the performance and fuel consumption of the tracked vehicle by Shu *et al.* (2002).

The longitudinal dynamics of tracked vehicle was characterized in Janarthanan *et al.* (2012) by considering various elements in the power train. Modelling of the terrain and the pressure-sinkage relationship was presented (Wong, 1984). A three dimensional multi-body simulation model was developed to simulate the dynamic behavior of the tracked vehicle and a platform called LMS-DADS simulation program was used to

analyze the derived model (Rubinstein and Hitron, 2004). A skid-steering model was developed by Maclaurin (2007) using track flexibility by considering compound slip function and shear stiffness of the pad. A modified general theory of skid-steering on firm ground was presented in Wong (2001), where the procedure was explained to calculate the lateral traction coefficient. Here, it was mentioned that the lateral coefficient is not a constant value and it is a function of turning radius and longitudinal speed. An extension of skid-steering theory from steady state to transient lateral dynamics was proposed by Wong and Chiang (2005), and the results were shown to have closer agreement with the experimental results than any other models. Maclaurin (2011) made use of Pacejka's magic formula (a popular tyre model that can be used to calculate various dynamic parameters such as forces and moments in longitudinal, lateral, and vertical directions) to calculate the force/slip characteristics of the tracked vehicle in skid-steer situation. The analysis of a skid-steer vehicle where the track force variations were assumed as a function of lateral slippage, turning radius, and longitudinal speed of a military vehicle, was presented in Kitano and Kuma (1977). Sensitivity of power and force requirements of a tracked vehicle when it maneuvers a turn is very important in determining the powertrain configuration and was investigated in Crosheck (2015), considering factors such as track geometry, vehicle configuration, and loading, and soil properties. Steerability of a tracked vehicle was investigated for steady state turning motion on a hard terrain flat level pavement (Kitano and Jyozaki, 1976). Here, the factors such as track slippage, vehicle configuration, etc., were considered when a vehicle maneuvers a turn. Bodin (1999) proposed the influence of different vehicle parameters on the mobility of a tracked vehicle, particularly for soft terrains such as deep snow and mud. A detailed explanation was given in Al-Milli *et al.* (2010) on how to calculate the

slip of vehicle as a function of thrust that is generated by the vehicle. Kar (1987) explained the importance of variable lateral coefficient of traction and it was indicated by the experiment corroboration that the lateral force generation is related to the turning radius and the longitudinal speed. A theoretical analysis of steerability of tracked vehicles during uniform turning on level pavement was described (Kitano and Jyozaki, 1976). A nonlinear real-time observer was implemented to estimate the track slip by tracing the difference between the desired vehicle path and the predicted vehicle path in Song *et al.* (2008). An analytical model has been developed to calculate the motion traction coefficient when the vehicle takes a turn. Previously this was used as a constant value but Ehlert *et al*. (1992) showed that the motion traction coefficient and the internal resistances are a function of radius. Also, it was shown that there is a considerable variation in this coefficient when the vehicle takes a harsh turn under high speed. Laughery *et al*. (2000) made use of Bekker's relations to find out the mobility of various tracked vehicles in different terrains. A slip circle model was developed by Schuring *et al.* (1996) to characterize the combined braking and cornering capabilities of tyres by showing how the longitudinal and lateral traction coefficients were split. A mathematical model had been developed to analyze the dynamic performance of the tracked vehicle when they are moving on the soft terrain and the coupled equations were solved (Li and Tang, 2015). Wismer and Luth (1973) described and derived a *Pull-Slip* equation, which helps to find out the longitudinal and lateral traction coefficients for tracked vehicles. A kinematic model was used in Solis and Longoria (2008) to estimate the shear displacement in the form of partial differential equation and it was used to calculate dynamic force of sprockets. A mathematical model for the spatial motion of a tracked vehicle was presented by Murakami *et al.* (1992), where the terrain was considered as an

inelastic material. Modelling the dynamics of a tracked vehicle using a commercial software was presented (Matej, 2010). A dynamic model for the tracked vehicle was developed by Xingguo *et al.* (2010) for both dry sand and road surfaces by using a multi-body dynamics software (RECURDYN). A kinematic approach was proposed by (Martinez, 2005) to predict the tracked vehicle motion in order to reduce the computational time instead of calculating it by the track speeds and the track slippages. Here the accuracy of the vehicle motion prediction was improved by considering the instantaneous center of rotation of treads. A multi-body dynamic model for a tracked mobile robot was developed in Ma and Akcabay (2016) for the purpose of predicting the mobility in two different scenarios such as steep terrains and urban terrains in the form of stair cases. Power loss in various subsystems of a tracked vehicle during high speed motion was analyzed (Wangl and Bini, 2014). Moghadam *et al.* (2013) developed a numerical method to calculate the turning radius of a tracked vehicle in steady state motion. A Traction Performance Prediction Model for Tracked Vehicles (TPPMTV) was developed in Park *et al.* (2008) by taking into account the characteristics of terrains, loading response, and primary design parameters of the tracked vehicle. Computer simulation program results were compared with the test results. The literature provided above shows that the extensive research has been made in the field of dynamics of the vehicle, and their subsystems, and terramechanics, and many models were proposed. The models are specific in nature with limited flexibility in their usage in different terrains. Detailed models for subsystem dynamics of steering and braking are not available, which can be integrated with the vehicle dynamics model.

1.4 MOTIVATION

In most of the above literature, focus was mainly on steady state motion dynamics of the vehicle. Transient dynamics was not dealt, particularly when the vehicle maneuvers a turn. Also, subsystem modeling was not given importance in the vehicle dynamics analysis. Subsystem dynamics may have a significant impact over the vehicle dynamics that in turn affects the behavior of the vehicle and also it will be essential in the point of vehicle autonomy and control. The corresponding models have not been developed to integrate the subsystems and vehicle dynamics model for tracked vehicles. There are a few commercial software available for simulating vehicle dynamics. However, the computation time to determine the behavior of the vehicle is very high and these software have limitations in changing the vehicle and terrain parameters. Further, higher order models may not be tractable for control applications. Hence, a lower order model with reasonable accuracy is preferable for characterizing the system behavior. An improved model for the lateral and longitudinal dynamics of tracked vehicles for tele-operation was found to be an essential requirement in the development of tele-operated off-road vehicles.

1.5 OBJECTIVES AND SCOPE OF THE RESEARCH WORK

The overall objective of this research work is to develop mathematical models for the subsystems such as powertrain, brake, steering, and tele-operation, and characterization of longitudinal and lateral dynamics of a tele-operated unmanned tracked vehicle.

The scope of the present work is limited to the following:

- Longitudinal, lateral, and yaw motions were only considered.
- Model for the soft terrain only was addressed.

1.6 OVERVIEW OF THE RESEARCH

A brief overview of the research work is shown in Fig. 1.8. The tele-operation was modelled as a first order system with time delay. The mathematical models for vehicle subsystems such as powertrain, brake, and steering were developed. The subsystem models were integrated with the vehicle and terrain dynamics model to determine the behavior of the vehicle under tele-operation mode. Extensive simulation studies were carried out and the results were compared with those from a standard commercial vehicle simulation software (Adams Tracked Vehicle (ATV)) for similar operating and input conditions. Finally, the simulation results were corroborated with limited real-time experiments.

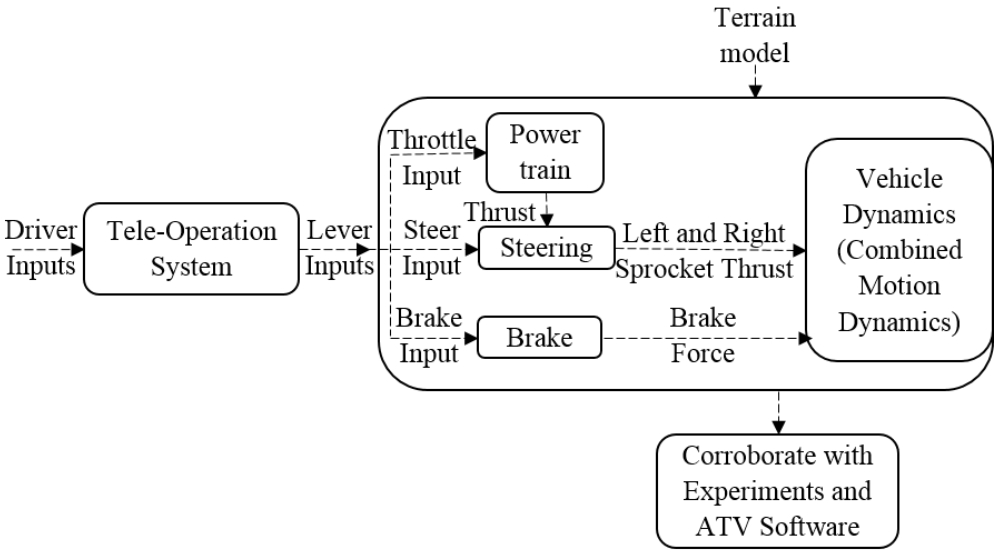

Fig. 1.8: Overview of the research

1.7 POTENTIAL CONTRIBUTION OF THE THESIS

The potential contributions of this thesis are listed below:

- An improved model for the tele-operation of tracked vehicle, taking into account the subsystem dynamics is presented.

- The developed model is computationally less intensive compared to the commercially available software for vehicle simulation.
- The tele-operation model will be useful for the design of controllers for autonomous tracked vehicles.

1.8 ORGANISATION OF THE THESIS

The thesis is organized in the following way. In chapter 2, mathematical modeling of various subsystem dynamics, terrain dynamics, and vehicle dynamics will be explained. The design of the lower-level controller for the brake subsystem will also be elaborated. The integration of all the subsystem dynamics and vehicle dynamics will be explained in a detailed manner. In chapter 3, simulation studies of the integrated model will be carried out to characterize the longitudinal and lateral dynamics. In chapter 4, a comparison of the ATV model results with the proposed model results for different scenarios will be explained in detail. In chapter 5, the corroboration of the proposed model with the limited experimental data would be presented. Conclusions and scope of future work will be explained in Chapter 6.

CHAPTER 2

MATHEMATICAL MODELLING OF TELE-OPERATED TRACKED VEHICLE AND SUBSYSTEMS

2.1 INTRODUCTION

In this chapter, mathematical modeling of the dynamics of various subsystems, vehicle, and terrain will be explained. Subsystem dynamics were given importance in this work since their effects may have significant impact on the behavior of the vehicle in transient conditions and in the point of vehicle autonomy and control. Modeling the transient dynamics of the tracked vehicle is also very important because the vehicle may experience frequent changes in the driving and terrain conditions that include sudden braking, acceleration, changes in orientation, and moving on from cross country terrain to mountainous terrain. Integration of subsystem models and the vehicle model will also be done to evaluate the combined motion behavior of the vehicle. The scope of the model was limited to consider the vehicle as a lumped mass and only longitudinal, lateral, and yaw motions were considered.

2.2 SUBSYSTEMS

The major sub systems of a tele-operated tracked vehicle are :

- Tele-operation module
- Powertrain
- Brake and
- Steering.

The powertrain module consists of the engine, clutch, gearbox, final drive, and the sprockets that drive the tracks. The modeling of each of these subsystems is explained in detail in the following sections.

2.3 TELE-OPERATION SUBSYSTEM

The dynamics of the tele-operation subsystem has been modelled as a first order system with a time delay. The model is given as

$$\tau\dot{y}(t) + y(t) = fc(t - T_d), \tag{2.1}$$

where $y(t)$ is the output of the system, $c(t)$ is the input to the system, f is the magnification factor, τ is the time constant, and T_d is the time delay due to the communication lag from driver input signal to the remote vehicle's input devices.

The corresponding transfer function is given as

$$G(s) = \frac{e^{-T_d s}}{\tau s + 1}. \tag{2.2}$$

The model parameters were estimated through experiments conducted using an experimental vehicle with tele-operation.

2.4 MODELING OF POWERTRAIN SUBSYSTEM

The powertrain transmits the drive energy from the engine to the sprocket through various components. The powertrain subsystem is an assembly of various components such as engine, clutch, gearbox, and final drive as shown in Fig. 2.1.

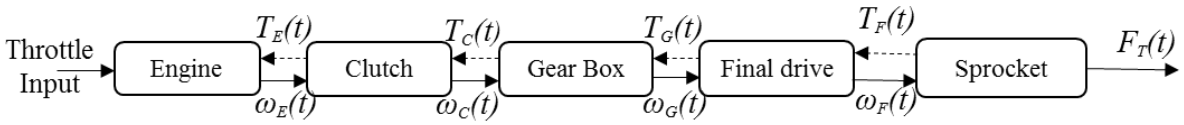

Fig. 2.1: Powertrain subsystem

The input to this system is the throttle input that indicates the amount of fuel that has been supplied and the output is the thrust available at the sprockets. The load torque transmitted from the sprocket to the engine is represented using dotted lines. Here, $T_E(t)$ is the engine torque, $T_C(t)$ is the clutch torque, $T_G(t)$ is the gear torque, $T_F(t)$ is the final drive torque, $F_T(t)$ is the ground thrust, $\omega_E(t)$ is the engine speed, $\omega_C(t)$ is the clutch output shaft speed, $\omega_G(t)$ is the gear output shaft speed, and $\omega_F(t)$ is the final drive speed. The following assumptions were made while developing the mathematical model of the powertrain:

- Changes in throttle position and corresponding changes in engine torque are instantaneous. Similarly, the time delay in clutch disengagement is negligible.
- Engine map was estimated based on steady state experiments for different fuel consumptions and engine speed.
- Gearshift happens when the clutch is being applied. So the gearshift time is not included.
- Thermal effects on efficiency, fuel consumption, etc., were assumed to be negligible.

2.4.1 Engine

Engine is the primary power source for the vehicle. It generates and supplies power to the other components of the vehicle according to the throttle input. Instead of using complex equations (Rajamani, 2006), an engine look-up table (Torque vs. speed for different throttle inputs) has been developed, which was adapted from an engine test data (provided by the engine manufacturer) as shown in Fig. 2.2.

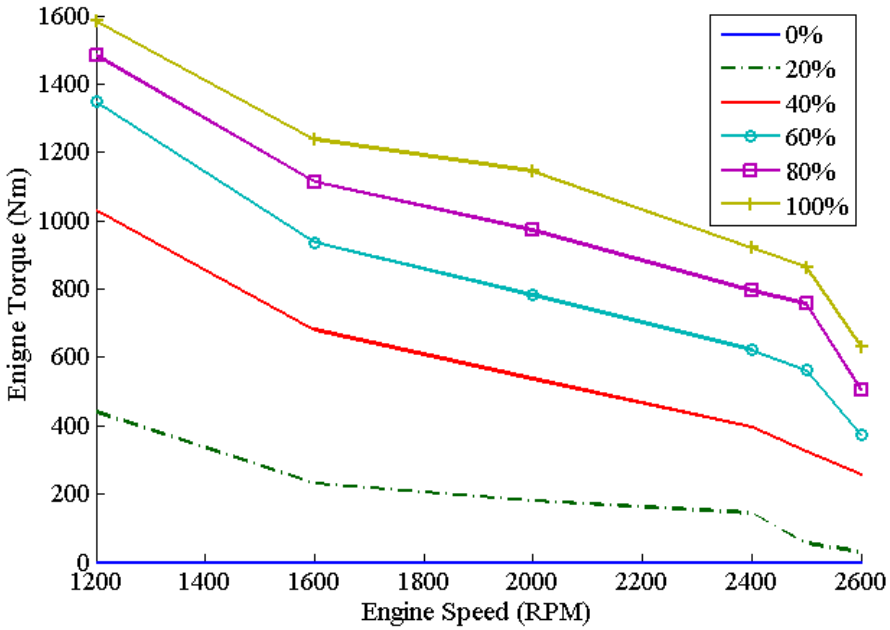

Fig. 2.2: Torque vs. speed table for different throttle inputs

(adapted from an engine test data)

The look-up table requires two inputs: engine speed and throttle input. With these two inputs, it locates a torque output value in the table. By using this table, it is possible to get the engine torque for any given throttle input and speed.

2.4.2 Clutch

Clutch is the mechanism that connects or disconnects the transmission from the engine while starting, gear shifting, and brake. Clutch has two plates, which are pressure plate and friction plate. Pressure plate is connected with the driving member and the friction plate is connected with the driven member. When the clutch pedal is pressed, the friction plate moves away from the pressure plate so that the energy is cut-off from the engine to the transmission.

The dynamics of the clutch was modelled by splitting the engaging time into three different time periods as shown in Fig. 2.3.

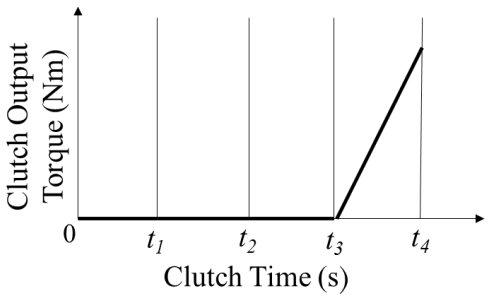

Fig. 2.3: Clutch time vs. torque at the clutch output

Here, t_1 is the time instant when the clutch is released from the completely pedaled position, t_2 is the time instant when the clutch plate makes contact with the pressure plate, t_3 is the time instant when the clutch starts transmitting power and t_4 is the time instant when the clutch transfers power completely from engine to transmission (Shu, Ma and Liu, 2002).

Period 1: $(t_1 \le t < t_2)$ It is the time period of the clutch plate to travel the distance from the completely open position to just engaged position with the pressure plate. There is no energy flow from the clutch input shaft to the transmission during this period. Hence, the torque available at the output shaft of the clutch is given as

$$T_C(t) = 0. \tag{2.3}$$

Period 2: $(t_2 \le t < t_3)$ It is the time period between the partial engagements of the clutch plate with the friction plate to the time when the output shaft starts transmitting the torque. During this period, the frictional pressure in the clutch plates is not enough to transmit energy to the output clutch plate. So the friction plate is just slipping away on the pressure plate so there would not be any energy flow. Hence,

$$T_C(t) = 0. \tag{2.4}$$

Period 3: $(t_3 \le t < t_4)$ In this period, the plate is engaged and the frictional pressure between the plates is just enough to compensate the resistant forces in the driveline. Hence, energy is transmitted from the input clutch shaft to the output clutch shaft. A linear relationship (Shu, Ma and Liu, 2002) is followed for the time period from t_3 to t_4 and the dynamic equation for the clutch can be expressed as

$$I_C \frac{d\omega_C(t)}{dt} = \left(\frac{t - t_3}{t_4 - t_3} \right), \qquad t_3 \le t < t_4 \quad (2.5)$$

where I_C is the mass moment of inertia of the clutch about the rotational axis.

2.4.3 Gearbox and Final Drive

Gearbox and final drive are used to increase the torque availability by reducing the speed. Gearshift takes place during the period when the clutch is in disengaged position. Automatic gear shifting is modelled here and the gearshift takes place when the longitudinal speed reaches a particular value. However, the model has been developed in such a way that a manual change also can be incorporated. The dynamic model for the gearbox is given as:

$$I_G(t)\frac{d\omega_G(t)}{dt} = T_C(t) - T_G(t), \quad (2.6)$$

where $I_G(t)$ is the mass moment of inertia of the gear about its rotational axis. The final drive is a constant gear reduction component that is placed before the sprocket.

The dynamic equation for the final drive is given as

$$I_F(t)\frac{d\omega_F(t)}{dt} = T_G(t) - T_F(t), \tag{2.7}$$

where I_F is the mass moment of inertia of the final drive about its rotational axis.

2.4.4 Sprocket Drive

The end shaft of the final drive is connected to the sprocket. So the same final drive torque is supplied to the sprocket. Sprocket is a positive drive that supplies the thrust to the tracks that wraps around the road wheels. The thrust at the sprocket is given as

$$F_T(t) = \frac{\eta T_F(t)}{r}, \tag{2.8}$$

where η is the transmission efficiency to take into account energy losses in the powertrain and r is the radius of the sprocket.

2.5 MODELLING OF BRAKE SUBSYSTEM

Brakes are essential safety components for any automobile. They are also important to provide a smooth stop in a minimum stopping distance. Generally, brake systems use hydraulic fluid or compressed air as the energy-transmitting medium. In the experimental vehicle considered in this study, a hydraulic brake system with an externally contracting brake was used.

The brake subsystem layout of the tracked vehicle is shown in Fig. 2.4. The vehicle uses a hydraulic brake system with an externally contracting band brake. It consists of the components such as brake pedal, master cylinder actuating mechanism, master cylinders, and band brakes. The band brake has bands wound around a cylinder that is connected to

the sprocket through the final drive. The master cylinder and the brake cylinder are connected by hydraulic lines.

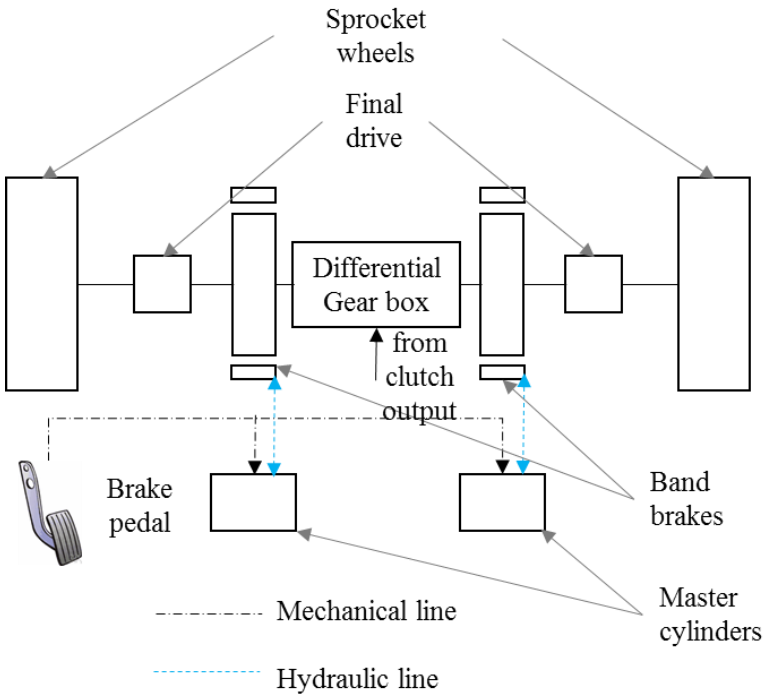

Fig. 2.4: Layout of the brake subsystem

While modelling the dynamics of the brake system, the following assumptions were made:

- Only viscous friction was considered in the mechanism. The dry friction at the mechanical hinges was not considered as it was assumed that the hinges are well lubricated.
- Frictional losses in the fluid flow and inertia of fluids were not considered in the fluid system modeling.
- Wall compliances were not considered.
- Frictional properties were assumed to be homogenous in the band and changes with respect to time and temperature were neglected.

2.5.1 Working of the Brake Subsystem

In order to develop a detailed model of the brake, it is necessary to understand the operation of the hydraulic band brake. A schematic of the working principle is shown in Fig. 2.5. The input torque, τ_1 is applied on the brake pedal that causes a displacement $x_s(t)$, of the hydraulic piston in the master cylinder. This, in turn, leads to the displacement $x_{out}(t)$, of the brake cylinder piston, which causes the band brake to apply the brake force $F_B(t)$.

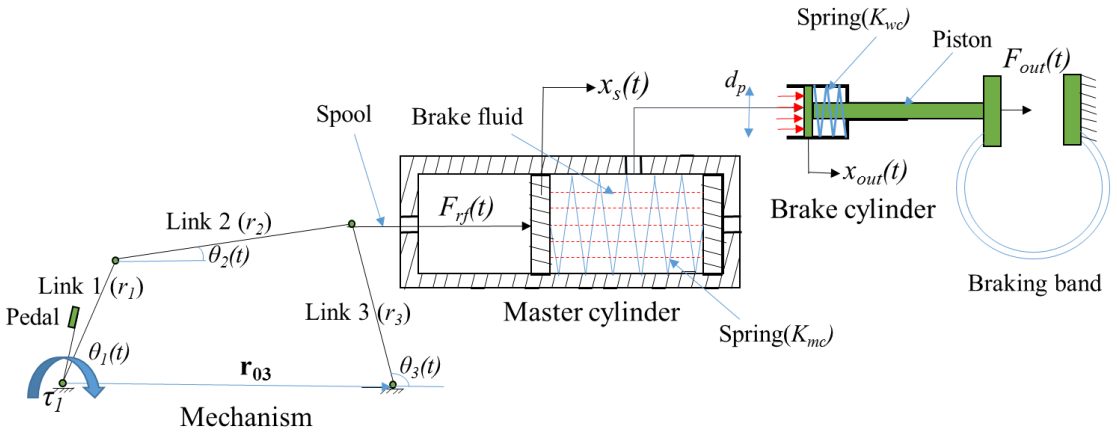

Fig. 2.5: Schematic representation of the brake system

Here, r_1, r_2, and r_3 are lengths of pedal, link1, link2, and link3, $\theta_1(t)$, $\theta_2(t)$, and $\theta_3(t)$ are the angular displacements of link1, link2, and link3, $\mathbf{r}_{o3}$ is the ground link vector, $F_{rf}(t)$ is the reactive force on the mechanism, K_{mc} is the stiffness of the master cylinder spring, K_{wc} is the stiffness of the brake cylinder spring and $F_{out}(t)$ is the force that acts on the band.

As the brake pedal is actuated, the spool is moved against the master cylinder hydraulic fluid pressure and the spring force. The volume of the fluid, which is being displaced in the master cylinder due to spool movement, will go to the brake cylinder that moves the brake cylinder piston. In steady state condition, the displacement of the brake cylinder piston can be calculated by using the area ratio of the cylinders of brake and master cylinder. The displacement of the brake piston causes the band to tighten or loosen and in-turn develops the brake force.

2.5.2 Model of the Brake Subsystem

In general, a hydraulic system can be modelled using three basic equivalent electrical elements i.e., Resistance (*R*), Inductance (*L*), and capacitance (*C*). Fluid resistance is due to the friction or the viscosity when the fluid flows, fluid inductance is due to the inertia of the flowing fluid, and fluid capacitance is due to the compliance that is offered by the fluid when it flows. Considering the small volume of fluid in the system and the limited flow of fluid during actuation, the effect of resistances and inductance on the dynamics is considered to be negligible. A detailed reasoning for this assumption is provided in Appendix (A.2). Dynamics of the mechanical linkages and the hydraulic systems in the brake subsystem to get the brake piston movement $x_{out}(t)$ is explained in Section 2.7.

The equation of motion for the brake piston is given as

$$p_{hyd}(t)a_{bc} - F_{out}(t) = m_{bc}\ddot{x}_{out}(t) + c_{bc}\dot{x}_{out}(t) + k_{bc}x_{out}(t), \qquad (2.9)$$

where $p_{hyd}(t)$ is the pressure due to the hydraulic fluid, m_{bc} is the mass of brake cylinder components, c_{bc} is the damping due to brake cylinder components, k_{bc} is the stiffness of

the brake cylinder spring, and $F_{out}(t)$ is the load force from the band. The band force output is given by

$$F_{out}(t) = K_{band} x_{out}(t) \exp(\mu_{band} \theta_{lap}), \tag{2.10}$$

where K_{band} is the stiffness of the band, μ_{band} is the friction coefficient between the band and the cylinder, and θ_{lap} is the lapping angle of the band over the cylinder. The brake force at the sprocket is given as

$$F_B(t) = \xi_F (F_{out}(t) - T_2(t)), \tag{2.11}$$

where $T_2(t)$ is the tension in the slack side and ξ_F is the final drive ratio.

2.6 MODELING OF THE STEERING SUBSYSTEM

The working principle of the steering subsystem is same as brake subsystem as it works with the same components of brake subsystem as shown in Fig. 2.6. The mechanism of steering in the tracked vehicle is skid-steering. In skid-steering, a differential force is applied between the sprockets, which makes the vehicle to carry out steering operation. As it is shown in the brake subsystem, the same components were used to get the steering action. The main difference here is that only one set of brake components is actuated at a time for steering action. Also, while braking, the power supply from the engine is cut off, but in steering it will be continuously supplied. Differential action takes place by supplying more force on one side and a lesser force on the other side according to the steering input given. This produces a moment that makes the vehicle to carry out steering action.

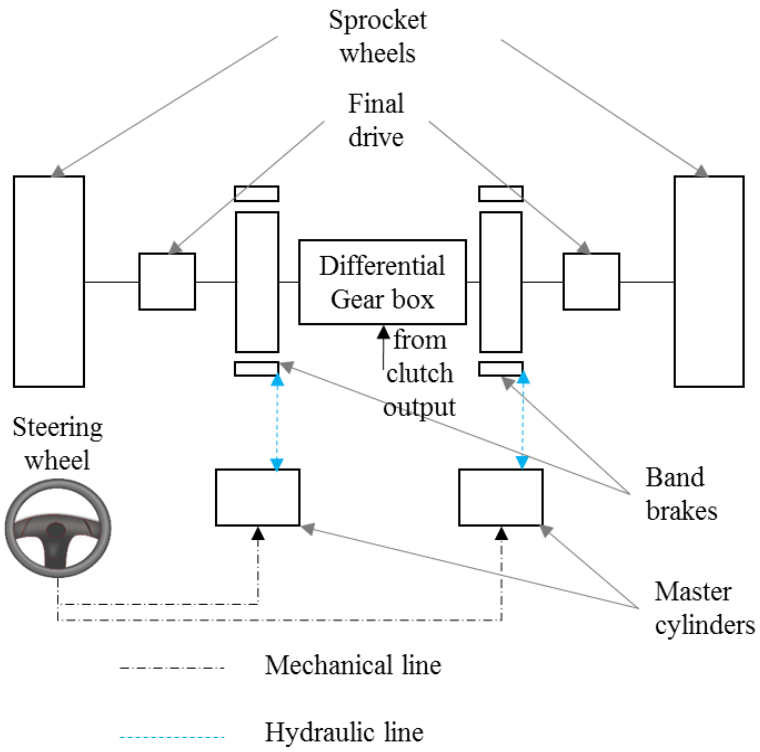

Fig. 2.6: Layout of the steering subsystem

2.6.1 Model of the Steering Subsystem

A differential gear box is used to obtain differential forces at the sprockets according to the steering input given. The force distribution model for a given steering input is

$$\begin{aligned} F_l(t) &= 0.5F_T(t) \pm F_B(t), \\ F_r(t) &= 0.5F_T(t) \mp F_B(t), \end{aligned} \tag{2.12}$$

where $F_l(t)$ and $F_r(t)$ are the forces at the left and right sprocket and $F_T(t)$ is the ground thrust which is available at the track-terrain interface. The force ratio, *FR*, between the sprockets is given by

$$FR = \frac{F_l(t)}{F_r(t)}. \tag{2.13}$$

2.7 BRAKE SUBSYSTEM WITH LOWER-LEVEL CONTROLLER

Subsystem models play an important role in the tele-operation/autonomous operation of the tracked vehicle. Subsystem dynamics are important in the remote control or autonomous control of the vehicle, especially in the design of lower-level controllers. Lower-level controllers are typically used to obtain desired responses in the subsystem output. These lower-level subsystem controllers would be useful in the overall control of the vehicle during its autonomous or tele-operation.

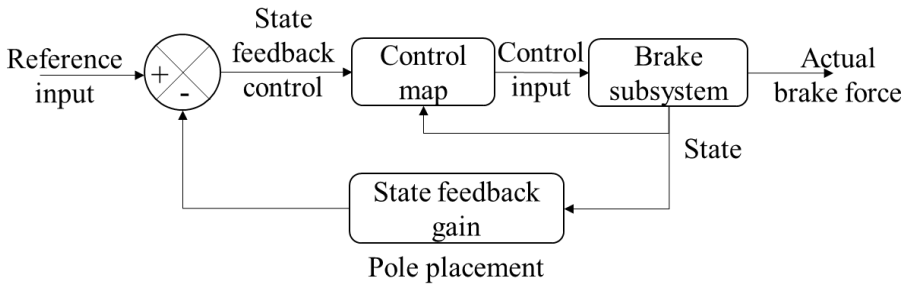

Fig. 2.7: Closed loop subsystem with controller

For example, the closed loop control of the brake subsystem to get a desired brake force is shown in Fig. 2.7. In order to demonstrate the use of the brake model developed in this thesis for brake control, a controller has been used here to control the response of the brake subsystem output.

The proposed brake subsystem model is non-linear. So, a feedback linearization technique was used to linearize the model. In this technique, a suitable control input is designed to transform the non-linear model into an equivalent linear model for the closed loop system (Khalil, 2014).

The Lagrangian formulation was used to derive the dynamic model of the brake system. The input to the system is pedal torque and the output is the brake piston movement. The

kinetic energy of the links, brake cylinder piston and hydraulic fluid were considered. The potential energy of each link and the strain energy of each spring were also considered.

The Lagrangian of the system is given as

$$L = T(t) - V(t), \tag{2.14}$$

where $T(t)$ is the kinetic energy of the system and $V(t)$ is the potential energy of the system.

The kinetic energy of the system is in two forms:

- Translational kinetic energy (Mechanical links, pistons and hydraulic fluid),
- Rotational kinetic energy (Mechanical links),

which can be derived as

$$T(t) = \sum_{i=1}^{n} \frac{1}{2} m_i \mathbf{v}_{pi}^{\mathrm{T}}(t) \mathbf{v}_{pi}(t) + \frac{1}{2} \boldsymbol{\omega}_i^{\mathrm{T}}(t) \mathbf{I}_{ci} \boldsymbol{\omega}_i(t), \tag{2.15}$$

where m_i denotes the mass of the i^{th} link, $\mathbf{I}_{ci}$ is the inertia matrix expressed in the body fixed frame located at the mass center of i^{th} link, $\mathbf{v}_{pi}$ is the translational velocity of the mass center, and $\boldsymbol{\omega}_i$ denotes the angular velocity of the i^{th} link in the body fixed frame.

In Eq. (2.15), translational and rotational velocities are expressed in the body fixed frame. Jacobians are introduced to transform it about the tip point (joint rotational angles). So Eq. (2.15) is rewritten as

$$T(t) = \frac{1}{2}\dot{\mathbf{q}}(t)\left(\sum_{i=1}^{n} m_i \mathbf{J}_{vi}{}^{\mathrm{T}}(t)\mathbf{J}_{vi}(t) + \mathbf{J}_{\omega i}{}^{\mathrm{T}}(t)\mathbf{I}_{ci}\mathbf{J}_{\omega i}(t)\right)\mathbf{q}(t), \tag{2.16}$$

where $\mathbf{q}(t)$ is the joint variables about the origin, which are $\theta_1(t), \theta_2(t), \theta_3(t)$, and $x_{out}(t)$. The simplified form of the kinetic energy of the system is given as

$$T(t) = \dot{\mathbf{q}}^T(t)\mathbf{M}(\mathbf{q}(t))\dot{\mathbf{q}}(t). \tag{2.17}$$

Comparing Eq. (2.15) and (2.16), the mass matrix of the system is obtained as

$$\mathbf{M}(\mathbf{q}(t)) = \sum_{i=1}^{n} m_i \mathbf{J}_{vi}{}^{\mathrm{T}}(t)\mathbf{J}_{vi}(t) + \mathbf{J}_{\omega i}{}^{\mathrm{T}}(t)\mathbf{I}_{ci}\mathbf{J}_{\omega i}(t). \tag{2.18}$$

Translational velocity $\mathbf{v}_{pi}(t)$ can be written as

$$\mathbf{v}_{pi}(t) = \frac{\partial \mathbf{p}_{ci}(t)}{\partial t} = \frac{\partial \mathbf{p}_{ci}(t)}{\partial \mathbf{q}(t)}\frac{\partial \mathbf{q}(t)}{\partial t}, \tag{2.19}$$

where $\mathbf{p}_{ci}(t)$ indicates the mass center of i^{th} link. The translational velocity Jacobian is given as

$$\mathbf{J}_{vi}(t) = \frac{\partial \mathbf{p}_{ci}(t)}{\partial \mathbf{q}(t)}. \tag{2.20}$$

The position vector of the center of mass of each element is given as

$$\mathbf{p}_{c1}(t) = \frac{r_1}{2}[\cos(\theta_1(t)) \quad \sin(\theta_1(t))]^T, \tag{2.21}$$

$$\mathbf{p}_{c2} = r_1[\cos(\theta_1(t)) \quad \sin(\theta_1(t))]^T + \frac{r_2}{2}[\cos(\theta_2(t)) \quad \sin(\theta_2(t))]^T, \tag{2.22}$$

$$\mathbf{p}_{c3} = r_0[1 \quad 0]^T + \frac{r_3}{2}[\cos(\theta_3(t)) \quad \sin(\theta_3(t))]^T, \tag{2.23}$$

$$\mathbf{p}_{c4} = r_0[1 \quad 0]^T + r_3[\cos(\theta_3(t)) \quad \sin(\theta_3(t))]^T + \frac{l_{eq}(t)}{2}[1 \quad 0]^T, \tag{2.24}$$

where r_1, r_2, r_3, and r_{o3} is the length of the link to its CG from the origin for link1, link2, link3, and ground link.

The hydraulic fluid is stored in the master cylinder, the hose pipe, and the brake cylinder which are of different diameters. When the brake action takes place, fluid from the master cylinder displaces to brake cylinder through the fluid hose. So the volume of the fluid occupied in the master cylinder is discharged to the brake cylinder keeping the volume of fluid in the hose constant, which is shown in Fig. 2.5. The equivalent length $l_{eq}(t)$ occupied by the hydraulic fluid in the cylinder is given as

$$l_{eq}(t) = \frac{a_{mc}}{a_{wc}} l_{mc}(t) + \frac{a_{hos}}{a_{wc}} l_{hos} + l_{wc}(t), \tag{2.25}$$

where a_{mc}, a_{wc} and a_{hos} denote the area of the master cylinder, brake cylinder, and the hose pipe respectively and $l_{mc}(t)$, $l_{wc}(t)$ and l_{hos} is the length of the master cylinder, brake cylinder, and the hose pipe respectively. Since the bulk motion of the fluid is translational, Eq. 2.25 is valid for calculating the equivalent length of the fluid.

The rotational velocity Jacobian is given as

$$\mathbf{J}_{\omega i} = \frac{\partial \boldsymbol{\theta}_{ci}(t)}{\partial \mathbf{q}(t)}, \tag{2.26}$$

where $\boldsymbol{\theta}_{ci}(t)$ is the rotational displacement of the links about the center of mass. By substituting the translational and rotational velocity Jacobian, Eq. (2.20) and (2.26) in Eq. (2.18), the kinetic energy of the system was calculated.

The potential energy of the system, which is due to the gravitational force and the strain energy of the spring, is given as

$$\begin{aligned} V(t) = &-\frac{1}{2}\left(m_1 g r_1 \sin\theta_1(t) + m_2 g r_2 \sin\theta_2(t) + m_3 g r_3 \sin\theta_3(t)\right).... \\ &+\frac{1}{2}\left(\frac{\beta_f}{l_{eq}(t)} a_{eq}(t) + K_{mc}\right)\left(r_3\theta_3(t)\right)^2 - \frac{1}{2}\left(\frac{\beta_f}{l_{eq}(t)} a_{eq}(t) - K_{wc}\right) x_{out}(t)^2, \end{aligned} \tag{2.27}$$

where β_f is the bulk modulus of the hydraulic fluid and $l_{eq}(t)$ is the equivalent length of the hose and cylinders that occupies with hydraulic fluid.

The non-conservative force vector $\mathbf{q}_{nc}(t)$ is given as

$$\mathbf{q_{nc}}(t) = \begin{bmatrix} \tau(t) \\ 0 \\ 0 \\ -K_{band}\, x_{out}(t)\, exp\ (\mu_{band}\, \theta_{lap}) \end{bmatrix}, \tag{2.28}$$

where K_{band} is the stiffness of the band, μ_{band} is the friction coefficient between the band and the cylinder, and θ_{lap} is the lapping angle of the band over the cylinder. The general equation of motion of the system is given as

$$\frac{d}{dt}\left(\frac{\partial L(t)}{\partial \dot{\mathbf{q}}(t)}\right) - \frac{\partial L(t)}{\partial \mathbf{q}(t)} = \mathbf{q}_{nc}(t). \tag{2.29}$$

Equations (2.16), (2.27) and (2.28) are substituted into Eq. (2.29) which yields

$$\mathbf{M}(\mathbf{q}(t))\ddot{\mathbf{q}}(t)+\mathbf{C}(\mathbf{q}(t),\dot{\mathbf{q}}(t))\dot{\mathbf{q}}(t)+\mathbf{g}(\mathbf{q}(t))=\mathbf{q}_{nc}(t), \tag{2.30}$$

where $\mathbf{M}(\mathbf{q}(t))$ is the mass matrix, $\mathbf{C}(\mathbf{q}(t),\dot{\mathbf{q}}(t))$ is the Coriolis and centripetal forces matrix and $\mathbf{g}(\mathbf{q}(t))$ is the potential term.

The Coriolis and centrifugal component of the system is given as

$$\mathbf{C}(\mathbf{q}(t),\dot{\mathbf{q}}(t))=\frac{1}{2}\sum_{k=1}^{n}\left(\frac{\partial \mathbf{M}_{i,j}(\mathbf{q}(t))}{\partial \mathbf{q}_k(t)}+\frac{\partial \mathbf{M}_{i,k}(\mathbf{q}(t))}{\partial \mathbf{q}_j(t)}-\frac{\partial \mathbf{M}_{j,k}(\mathbf{q}(t))}{\partial \mathbf{q}_i(t)}\right)\dot{\mathbf{q}}_k. \quad i,j,k=1,2,3,4 \tag{2.31}$$

The potential term of the system is given as

$$\mathbf{g}(\mathbf{q}(t))=\frac{\partial V(t)}{\partial \mathbf{q}(t)}. \tag{2.32}$$

Since the overall DOF of the brake subsystem is one, Eq. 2.30 was simplified by relating the input pedal torque and the brake piston displacement output using the Jacobian which is given as

$$\mathbf{j}_x(t)=\begin{bmatrix}\frac{\partial \theta_1(t)}{\partial x_{out}(t)} & \frac{\partial \theta_2(t)}{\partial x_{out}(t)} & \frac{\partial \theta_3(t)}{\partial x_{out}(t)} & 1\end{bmatrix}^T. \tag{2.33}$$

The final dynamic equation of the brake subsystem is shown as

$$\begin{aligned}&\mathbf{j}_x{}^{\mathbf{T}}(t)\mathbf{M}(\mathbf{q}(t))\mathbf{j}_x(t)\ddot{x}_{out}(t)+\left(\mathbf{j}_x{}^{\mathbf{T}}(t)\mathbf{M}(\mathbf{q}(t))\dot{\mathbf{j}}_x(t)+\mathbf{j}_x{}^{\mathbf{T}}(t)(\mathbf{C}(\mathbf{q})(t))\mathbf{j}_x(t)\right)\dot{x}_{out}(t)....\\&+\mathbf{j}_x{}^{\mathbf{T}}(t)\mathbf{g}(\mathbf{q})x_{out}(t)=\mathbf{j}_x{}^{\mathbf{T}}(t)\mathbf{q}_{nc}(t),\end{aligned} \tag{2.34}$$

where $u(t)=\mathbf{j}_x{}^{\mathbf{T}}(t)\mathbf{q}_{nc}(t)$. The state space form of the equation can be written as

$$\begin{bmatrix} \dot{x}_1 \\ \dot{x}_2 \end{bmatrix} = \begin{bmatrix} \dot{x}_{out} \\ -inv\left(\mathbf{j}_x{}^{\mathbf{T}}(t)\mathbf{M}(\mathbf{q}(t))\mathbf{j}_x(t)\right)\begin{pmatrix} \left(\mathbf{j}_x{}^{\mathbf{T}}(t)\mathbf{M}(\mathbf{q}(t))\dot{\mathbf{j}}_x(t) + \mathbf{j}_x{}^{\mathbf{T}}(t)(\mathbf{C}(\mathbf{q}(t)))\mathbf{j}_x(t)\right)\dot{x}_{out}(t)\ldots. \\ +\mathbf{j}_x{}^{\mathbf{T}}(t)\mathbf{g}(\mathbf{q}(t))x_{out}(t) - u(t) \end{pmatrix} \end{bmatrix}. \quad (2.35)$$

Equation (2.30) is nonlinear in nature and feedback linearization technique was used to transform the nonlinear system into an equivalent linear closed loop system by choosing a suitable input (Khalil, 2014). An input was designed in such a way to cancel the non-linearity present in the model. The non-linear control input is given as

$$u(t) = inv\left(\mathbf{j}_x{}^{\mathbf{T}}(t)\mathbf{M}(\mathbf{q}(t))\mathbf{j}_x(t)\right)\begin{pmatrix} \left(\mathbf{j}_x{}^{\mathbf{T}}(t)\mathbf{M}(\mathbf{q}(t))\dot{\mathbf{j}}_x(t) + \mathbf{j}_x{}^{\mathbf{T}}(t)(\mathbf{C}(\mathbf{q}(t)))\mathbf{j}_x(t)\right)\dot{x}_{out}(t)\ldots. \\ +\mathbf{j}_x{}^{\mathbf{T}}(t)\mathbf{g}(\mathbf{q}(t))x_{out}(t) + v(t) \end{pmatrix}, \quad (2.36)$$

where *v(t)* is the state feedback control. The non-linear brake system is converted into an equivalent controllable linear closed loop system by substituting the non-linear control input Eq. (2.36) in Eq. (2.35). The controllable linear closed loop system is written in the state space form

$$\dot{\mathbf{x}}(t) = \mathbf{A}\mathbf{x}(t) + \mathbf{b}v(t). \quad (2.37)$$

A controller was designed by using pole placement approach (Kuo, 2010). The state-feedback control (*v(t)*) is given as

$$v(t) = -\mathbf{k}^T\mathbf{x}(t) + r(t), \quad (2.38)$$

where **k** is the controller feedback gain and *r(t)* is the scalar reference input. By substituting Eq. (2.36) in Eq. (2.35), the closed loop system is represented by the state equation

$$\dot{\mathbf{x}}(t) = \left(\mathbf{A} - \mathbf{b}\mathbf{k}^T\right)\mathbf{x}(t) + \mathbf{b}r(t), \quad (2.39)$$

where **A** is (2x2), **b** is (2x1), the pair (**A**, **b**) is completely controllable (Khalil, 2014). The characteristic polynomial of the system was equated to the desired characteristic polynomial by using desired eigenvalues as shown

$$\left|s\mathbf{I} - \mathbf{A} + \mathbf{b}\mathbf{k}^T\right| = (s - \mu_1)(s - \mu_2). \tag{2.40}$$

where μ_1 and μ_2 are the desired eigenvalues. The choice of the closed loop eigenvalues of the brake subsystem were determined based on the performance criteria of settling time of 0.04 *s* for the critically damped (ζ =1) system. The location of the desired eigenvalues were determined to be -100 by using the above performance parameters and the controller feedback gains were found appropriately.

2.8 MODELLING OF TRACKED VEHICLE DYNAMICS

In this section, modeling of the tracked vehicle dynamics is discussed. Force inputs to the left and right sprockets, various resistances, and terrain parameters such as lateral and longitudinal traction coefficients are the inputs to the vehicle dynamics model. Vehicle behavior is determined by considering the terrain dynamics, subsystem dynamics, and environmental parameters.

While modelling the vehicle, the following assumptions were made:

- Vehicle was assumed as a rigid body.
- Only the longitudinal, lateral, and yaw motion dynamics of the vehicle were considered.
- Position of center of gravity was assumed to be at geometric center of the vehicle.
- It was assumed that the terrain is perfectly flat and the pressure distribution under the track along the length is uniform.
- It was assumed that the maximum tractive force at the track-terrain interface is directly proportional to the weight of the vehicle.
- Effect of coupled dynamics of the vehicle is negligible.

2.8.1 Coordinate System Representation

The planar motion of the ground vehicle can be represented using two coordinate frames as shown in Fig. 2.8. Frame XY with origin O1 is the global frame with respect to which the vehicle position and orientation is represented. The moving frame xy with origin O2 is attached to the body center of the vehicle and moves with the vehicle. The longitudinal, lateral, and yaw speed of the vehicle will be represented with respect to the global frame.

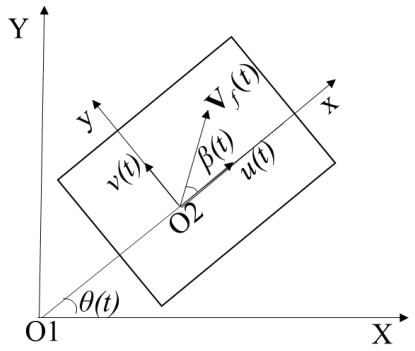

Fig. 2.8: Coordinate system representation of the tracked vehicle

Here, $\mathbf{v}_f(t)$ is the velocity vector of the vehicle and $u(t)$ and $v(t)$ are the components of vehicle velocity vector in x and y directions respectively with respect to the body frame. The orientation of the vehicle with respect to the global frame is represented by the angle $\theta(t)$ and $\beta(t)$ is the side slip angle of the vehicle.

2.8.2 Model of the Tracked Vehicle

The free body diagram of a tracked vehicle is shown in Fig. 2.9 below. Here, *b* is the breadth of the track and *B* is the breadth of the vehicle. When the vehicle is taking a turn with respect to O with a turning radius $R(t)$, $s_o(t)$ is the shift of the center of turn (C_T)

from the center of gravity (C_G) of the vehicle. The longitudinal and lateral forces acting on the tracks are represented by $F_x(t)$ and $F_y(t)$ respectively.

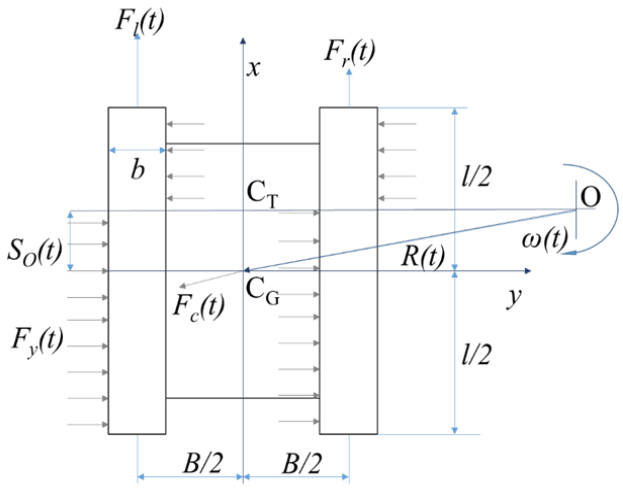

Fig. 2.9: Free body diagram of the vehicle when maneuvering a turn

Lateral force generated at the interface is balanced by the centrifugal force while maneuvering a turn as shown in Fig. 2.9.

The equation of motion along longitudinal direction (x- direction) can be expressed as

$$m\gamma_m(t)(\dot{u}(t)-\omega_z(t)v(t)) = F_T(t)-R_a(t)-R_{in}(t)-R_m-R_G, \qquad (2.41)$$

where m is the mass of the vehicle, $\dot{u}(t)$ and $\dot{v}(t)$ are the x and y components of the vehicle acceleration vector, $\omega_z(t)$ is the yaw speed, $R_a(t)$ is the aerodynamic resistance, $R_{in}(t)$ is the internal resistance, R_m is the motion resistance, and R_G is the grade resistance. $\gamma_m(t)$ is a factor that takes into account the power consumed by various rotating components inside the vehicle and is given as (Wong, 2001)

$$\gamma_m(t) = 1+\frac{n_T I_T + n_w I_w + \xi_F^2(t) I_F + \xi_T^2(t)\xi_F^2(t) I_F}{mr^2}, \qquad (2.42)$$

where n_T is the number of tracks, n_w is the number of sprocket and track wheels, I_T and I_w represent the inertia of the track and the wheels respectively, ξ_F is the final drive gear ratio, $\xi_T(t)$ is the gear box reduction ratio, *m* is the mass of the vehicle and *r* is the sprocket radius of the vehicle.

To maintain the stability of the vehicle, vehicle should not drift in the lateral direction. Drifting happens when the centrifugal force is so high that the lateral force generated at the track-terrain interface could not balance it. It can be controlled by limiting the steering input and the vehicle speed. The equation of motion along lateral direction (y-direction) can be expressed as

$$m(\dot{v}(t)+\omega_z(t)u(t)) = \frac{2\mu_t(t)Ws_o(t)}{l}, \tag{2.43}$$

The equation of motion about the axes pointing perpendicular to the ground can be expressed as

$$I_{zz}\alpha(t) = (F_l(t)-F_r(t))\frac{B}{2} + m\frac{u^2(t)}{R(t)}s_o(t) - M_t(t), \tag{2.44}$$

where $\alpha(t)$ is the yaw acceleration of the vehicle, $M_t(t)$ is the moment of turning resistance, $\mu_t(t)$ is the lateral coefficient of traction, *W* is the weight of the vehicle, I_{zz} is the mass moment of inertia about the axes pointing perpendicular to the ground and *l* is the length of the track.

The moment of turning resistance was derived by considering uniform ground pressure. The pressure distribution under each track is given by (Wong and Chiang 2005):

$$p(x) = \frac{\mu_t W}{2l}. \tag{2.45}$$

To calculate the lateral force, Eq. (2.45) needs to be integrated over the length of the track as

$$F_y = \int_{-\left(\frac{l}{2}+s_o(t)\right)}^{\left(\frac{l}{2}-s_o(t)\right)} p(x)dx. \tag{2.46}$$

Therefore, the lateral force of the tracked vehicle is given by

$$F_y = \frac{2\mu_t(t)Ws_o(t)}{l}. \tag{2.47}$$

To calculate the turning moment, Eq. (2.46) needs to be integrated over the length of the track as:

$$M_t(t) = \int_{-\left(\frac{l}{2}+s_o(t)\right)}^{\left(\frac{l}{2}-s_o(t)\right)} p(x)xdx, \tag{2.48}$$

and the moment of turning resistance of the tracked vehicle is given by

$$M_t(t) = \frac{\mu_t(t)W}{2l}\left(\frac{l^2}{2} + 2s_o{}^2(t)\right). \tag{2.49}$$

Aerodynamic resistance is the drag force that acts against the motion of the vehicle and is given as

$$R_a = \frac{1}{2} C_d \rho a_f u^2(t), \tag{2.50}$$

where C_d is the coefficient of drag, ρ is air density and a_f is the frontal area. No generic analytical model is available to represent the internal resistances as it mainly depends on the friction between the components and the vehicle configuration. It is normally represented by an empirical relationship developed by (Bekker, 1957), applicable for modern light tracked vehicle which weighs less than 25 *Ton* (Wong, 2001). The relationship is given as

$$R_{in}(t) = \frac{W(133 + 2.5u(t))}{9810}, \tag{2.51}$$

The motion resistance is the resistance due to the sinkage that is produced on the ground. If a vehicle is treading on any soft ground, it produces some amount of sinkage on the ground that will consume considerable amount of power. It can be represented using an empirical relationship which was proposed in (Wong, 2001) as

$$R_m = \left(\frac{b}{(n+1)(k_c/b + k_\varphi)^{n+1}} \right) \left(\frac{W}{bl} \right)^{\frac{n+1}{n}}, \tag{2.52}$$

where k_c, k_φ and n are empirical constants for the terrain. These constants can be obtained using the pressure sinkage relationship proposed in (Wong, 2001). The pressure sinkage relationship is given by

$$p_t = \left(\frac{k_c}{b} + k_\varphi \right) z^n, \tag{2.53}$$

where p_t is the pressure on the terrain and *z* is the sinkage on the terrain by the vehicle. The grade resistance is given as

$$R_G = W \sin\theta_s, \tag{2.54}$$

where θ_s is the sloping angle of the terrain.

The shift of turn is given by

$$s_o(t) = \frac{lu^2(t)}{2R(t)\mu_t g}. \tag{2.55}$$

The dynamics of the tracked vehicle can be modelled using the Equation (2.52) to (2.55).

2.9 MODELING OF TERRAIN DYNAMICS

Terrain dynamics play a very important role while modeling the dynamics of the tracked vehicle and decides the capabilities of the terrain in force and moment generation through the parameters such as slip, traction coefficients, slip angle, etc.

2.9.1 Lateral Traction Coefficient

While modeling the vehicle, there are important terrain parameters that need to be estimated such as slip of the tracks and traction coefficients. In general, traction coefficient is available in the terrain irrespective of the direction. So when a tracked vehicle maneuvers a turn, traction coefficient is shared between the lateral and longitudinal directions as a frictional ellipse model (Schuring *et al.*, 1996). Here, the ground is assumed as isotropic as it possesses similar properties in all directions. So it became frictional circle model (Schuring *et al.*, 1996) and it can be expressed as

$$\mu = \sqrt{\mu_l^2 + \mu_t^2}, \tag{2.56}$$

where μ_l is the longitudinal traction coefficient, μ_t is the lateral traction coefficient, and μ is the traction coefficient. When a vehicle moves in straight line direction, all traction is utilized only in the longitudinal direction and no lateral force is generated. But if a vehicle maneuvers a turn, lateral and longitudinal forces come in to picture. In that scenario, traction is shared among the longitudinal and lateral directions. The lateral traction coefficient is not a constant value since it is a function of vehicle speed and turning radius (Kar, 1987). The value of lateral traction coefficient increases when the vehicle make a tight turn with high speed. Value of the traction coefficients in both the directions is determined by the frictional circle model. If the steering input is increased above the ground capable limit, the reactive force generated from the ground could not counter the centrifugal force that is generated by the vehicle, which leaves the vehicle in unstable condition. The procedure to calculate the lateral traction coefficient is explained in Appendix (A.1). By following the procedure shown in Appendix (A.1), a lateral traction coefficient look-up table has been generated for a range of longitudinal speed and speed ratio between the sprockets and it is shown in Fig. 2.10.

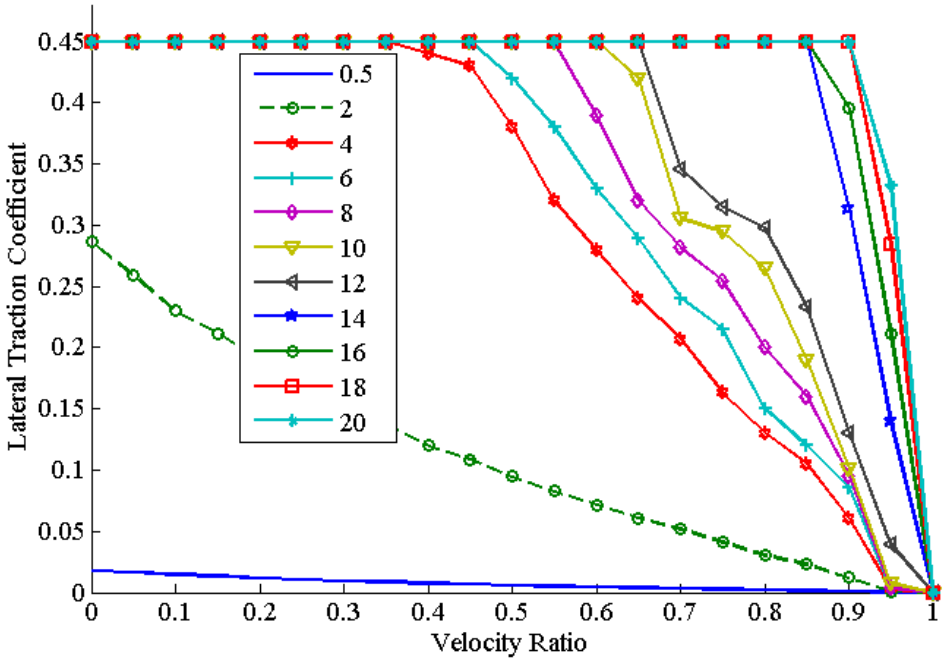

Fig. 2.10: Lateral traction coefficient of the tracked vehicle for different speed

2.9.2 Slip of the Vehicle

Slip of the vehicle is defined as the difference between the sprocket speed and longitudinal speed of the vehicle. For soft terrains, the properties that determine the slip of the terrain are cohesion, shear modulus, and pressure angle. The slip of the tracked vehicle on soft terrain (Wong and Chiang, 2005) is given by

$$F_T(t) = \left(a_t c + W \tan\phi\right)\left(1 - \frac{K}{i(t)l}\left(1 - \exp\left(\frac{-i(t)l}{K}\right)\right)\right), \qquad (2.57)$$

where K is the shear modulus, ϕ is the pressure angle, a_t is the track area, c is the cohesion, and l is the length of the track. Force at the track-terrain interface $F_T(t)$ is calculated from Eq. 2.8. By substituting it into Eq. 2.57, the slip $i(t)$ of the tracked vehicle on the given terrain is calculated. Here, another look up table has been generated for a range of thrust force that is generated at the interface, as plotted in Fig. 2.11.

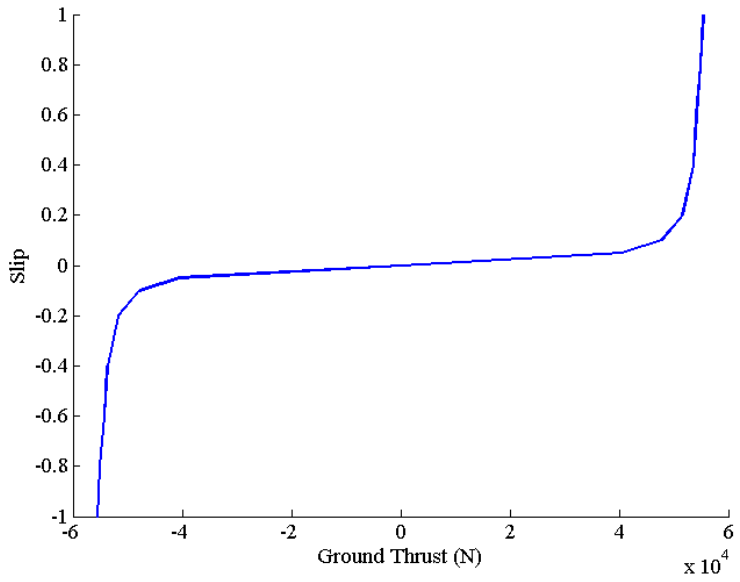

Fig. 2.11: Variation of slip of the vehicle with respect to the ground thrust

2.10 INTEGRATED MODEL OF TELE-OPERATED TRACKED VEHICLE

The models developed for the subsystems and the tracked vehicle have been integrated to obtain the complete system model for the tele-operated tracked vehicle. The integrated model is shown in Fig. 2.12. The combined planar motion dynamics of the vehicle deals with acceleration, braking, and yaw motion of the tracked vehicle. Inputs to the model are the throttle, braking, and steering, and the outputs are the time derivatives of longitudinal, lateral, and yaw displacements.

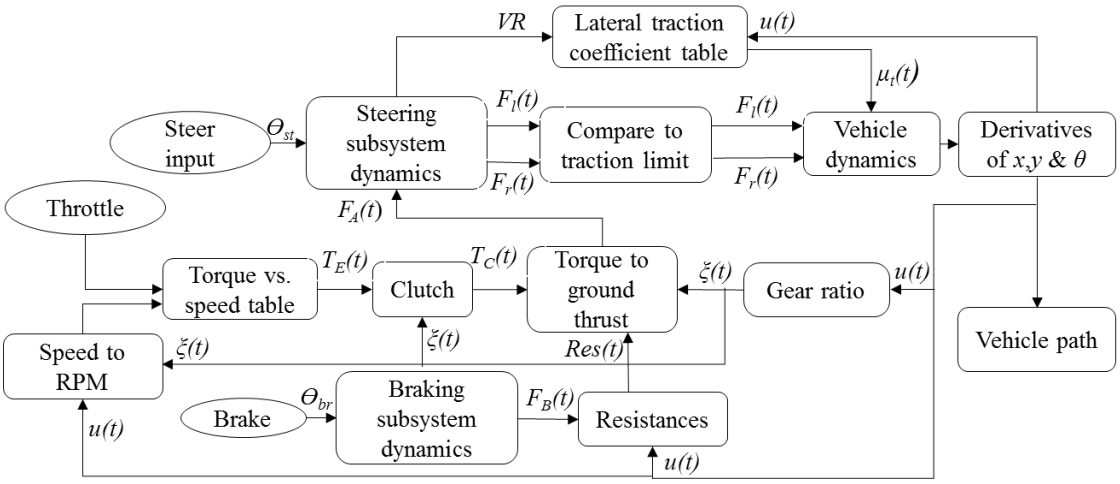

Fig. 2.12: Integrated model: Subsystems and tracked vehicle dynamics

The throttle and engine RPM are given as the inputs to the powertrain subsystem and thrust at the sprockets as the output from the powertrain subsystem. The ground thrust will be used by the steering subsystem to generate necessary thrust at the sprockets depending on the steering input. The sprocket thrusts are then compared with the maximum longitudinal traction limit to ensure that the generated longitudinal forces are within the limit. If the thrust force generated is more than the maximum longitudinal traction limit, vehicle would react only to the amount of maximum longitudinal traction limit. These force values will be used in the vehicle dynamics block to generate the time derivatives of the longitudinal, lateral, and yaw displacements.

Automatic gearshift and clutch actuation were modelled here that ensures that the gearshift takes place when the longitudinal speed reaches a particular value. However, flexibility is provided in the model to incorporate manual changes also. The integrated model is used further for simulation studies.

2.11 SUMMARY

The mathematical modeling of the various subsystems of the tele-operated tracked vehicle was provided. The assumptions made in the development of the models were stated and functioning of the subsystems was explained wherever needed. The powertrain components were modeled as lumped systems. Braking and steering subsystems were modeled for the actual vehicle configuration. Terrain dynamics has been incorporated using the available data from literature. Combined motion dynamics model for the planar motion dynamics of the tracked vehicle has been developed by integrating the subsystem models. Lower-level subsystem controller design were also explained. Simulation studies of the integrated model will be explained in the following chapter.

CHAPTER 3

SIMULATION STUDIES ON TELE-OPERATION OF TRACKED VEHICLES

The numerical simulation studies using the mathematical model developed earlier is the focus of this chapter. The subsystem models were simulated initially to understand their performance and then the integrated model simulations were carried out. Lower-level controller for the brake subsystem was designed to get the desired output response for a given input. Additionally, the simulation of a kinematic model of the tracked vehicle was carried out to compare and highlight the need for the dynamic model of the tracked vehicle for effective modelling of the tele-operated tracked vehicle.

3.1. SUBSYSTEM SIMULATION

All the three subsystems, i.e., powertrain, brake, and steering were considered for the simulation to evaluate the performance of these systems. The subsystem parameters used for the simulation are listed in Table A.1 in Appendix (A.3). The results of the simulation are presented below.

3.1.1. Powertrain Subsystem Results

The powertrain subsystem model was simulated for a time interval of 50 *s*. The model input data, i.e., throttle position and the corresponding gear changes are shown in Fig. 3.1(a). The changes in the sprocket thrust output and the engine speed variations with load are shown in Fig. 3.1(b). The fluctuations in the sprocket thrust are due to the

gearshift that takes place at different time instants. The drop in thrust before the gearshift is due to the engine speed variations. As the engine speed increases, torque output starts reducing as per the engine characteristics.

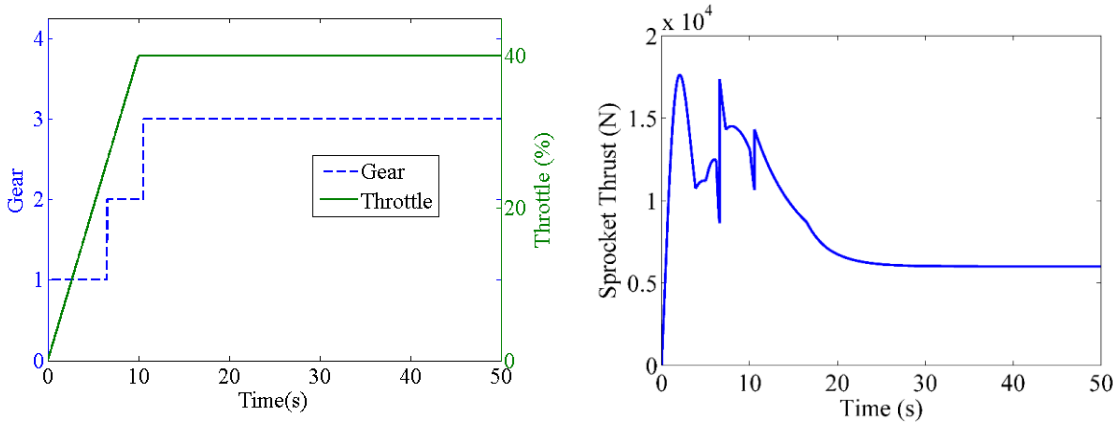

(a) Throttle input and gear shift (b) Sprocket thrust

Fig. 3.1: Powertrain subsystem - Results

3.1.2. Brake Subsystem Results

The dynamics of the brake system was simulated using a step torque input, as shown in Fig. 3.2(a) to the brake pedal. Figure 3.2(b) shows the angle swept by the links 1, 2 and 3 of the brake system (please refer to Fig. 2.5 for details).

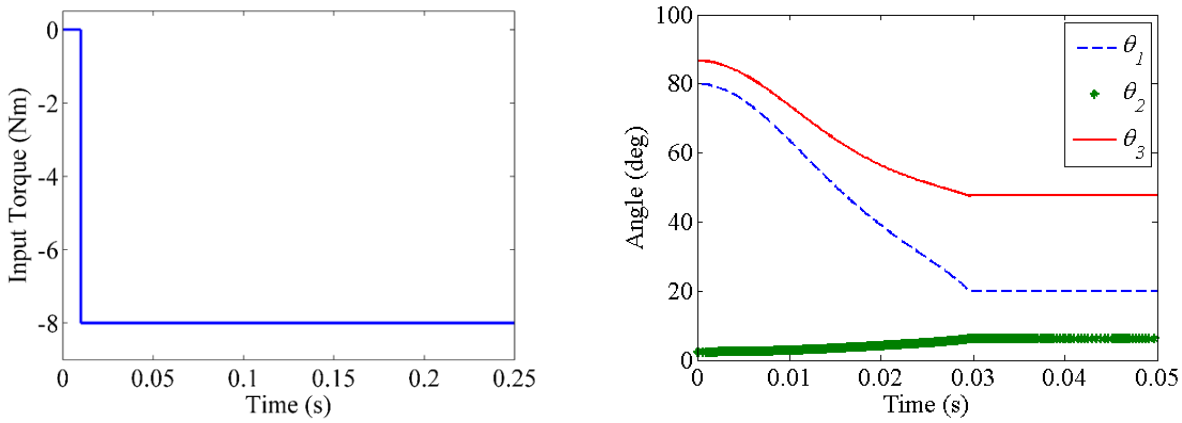

(a) Step input torque (b) Angle swept by links

Fig 3.2: Brake subsystem - Input and joint variable outputs

When the link1 reaches the maximum travel limit (20°), all the links are mechanically arrested. Figure 3.3(a) shows the displacement of the spool in the master cylinder due to the angular motion of the link3. The brake piston displacement is also shown in the same figure. Figure 3.3(b) shows the variation of hydraulic pressure in the cylinder and the force generated as a result of the hydraulic pressure rise.

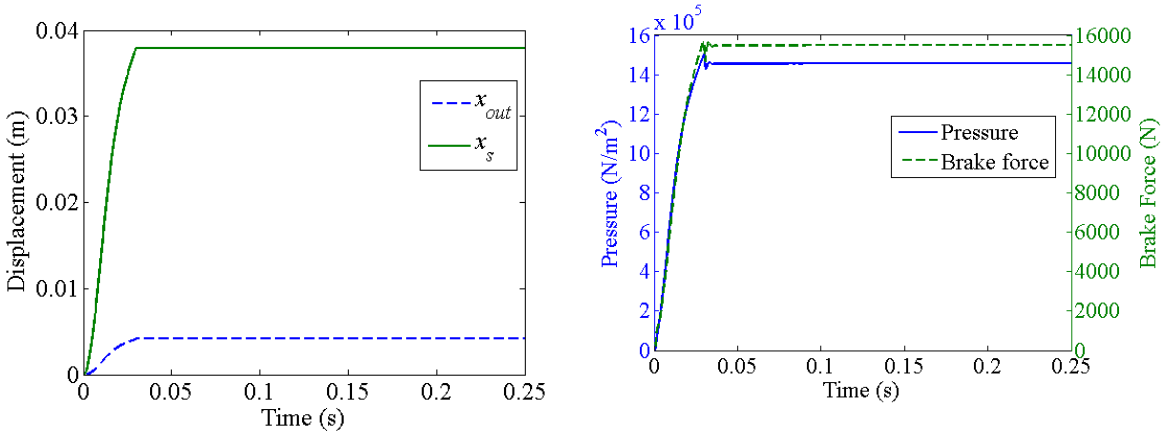

(a) Spool displacement and brake piston displacement

(b) Pressure developed and brake force generation

Fig. 3.3: Brake subsystem - Outputs

3.1.3 Brake Subsystem with Lower-level Controller

The input given in this simulation was the same as in Fig. 3.2(a). But the controller feedback gains were chosen in such a way that the brake force output is critically damped and the settling time is 0.04 *s*, as explained in section 2.7. The response of the closed loop controller for the desired brake force was plotted as shown in Fig. 3.4.

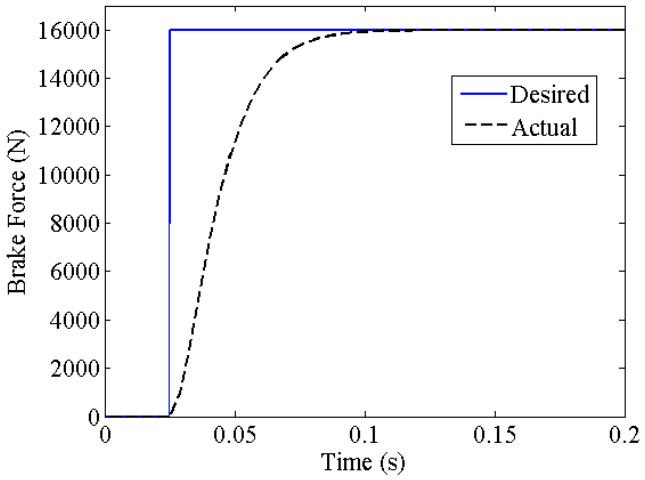

Fig. 3.4: Closed loop response of brake subsystem with controller

It can be observed from Fig. 3.4 that the response of the system can be adjusted by the careful selection of eigenvalues by following the methodological control process. The parameters chosen for the system are settling time and damping ratio. The desired eigenvalues were then found out for calculating the controller feedback gains.

3.1.4 Steering Subsystem Results

Steering system was simulated by changing the steering angle as shown in Fig. 3.5(a).

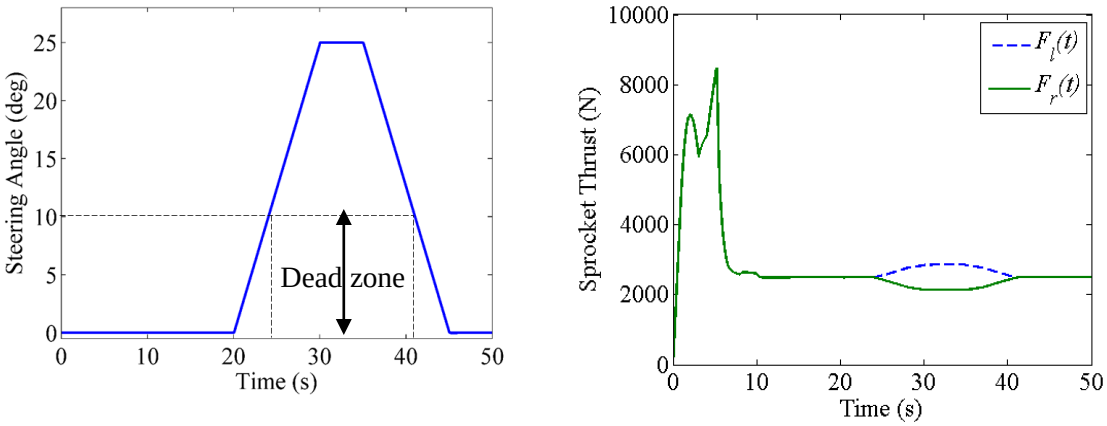

(a) Steering input (b) Left and right sprocket thrust

Fig. 3.5: Steering subsystems – Results

There is dead zone of $\pm 10°$ and as long as the steering angle is within this zone, there will not be any split force response for the steering input. Hence, a difference between the thrust of the left and right sprockets arises when the steering is increased to more than 10^0 and this is reflected in Fig. 3.5(b). The simulations results presented above for the subsystems show that the performance of the subsystems are as expected. Further simulations were carried out for the integrated model and the results are presented in the following sections.

3.2 INTEGRATED MODEL SIMULATION

The integrated model of the tele-operated tracked vehicle was simulated to study the dynamic response of the vehicle. The vehicle and tele-operation parameters used for the simulation are listed in Table A.1. The planar motion dynamics was simulated for two cases:

- Longitudinal dynamics – straight line motion test by applying throttle and brake inputs.
- Lateral dynamics – Yaw motion test by applying steering, throttle, and brake inputs.

3.2.1 Longitudinal Dynamics Results

Here, the model was simulated for longitudinal dynamics for a time interval of 40 *s*, to characterize the straight-line motion behavior. Figure 3.6(a) shows the pattern of throttle input. The simulations were carried out with different throttle inputs (at 60 % and 80 %) and brake inputs (at 50 % and 100 %). The brake was applied at the 30^{th} second as shown in Fig. 3.6(b) and the throttle was set to zero at this instant with the gear shifting to neutral position.

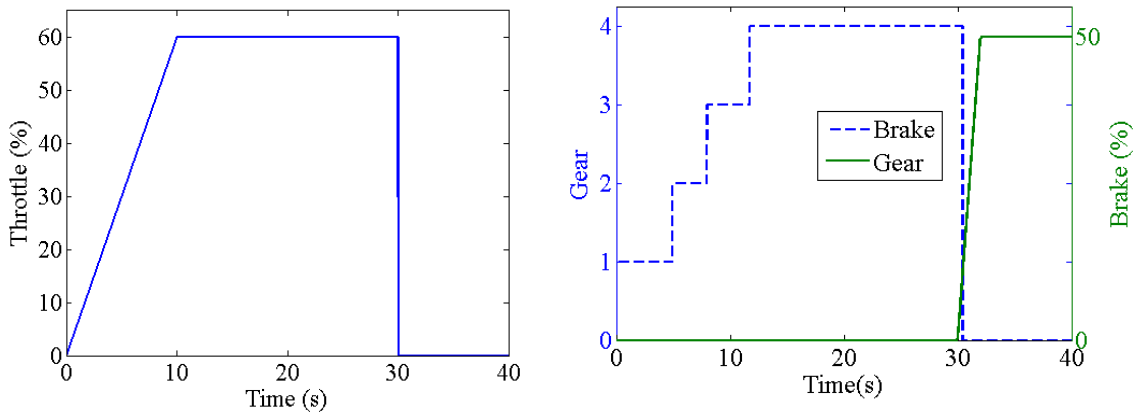

(a) Throttle input (b) Gear change and brake input

Fig. 3.6: Longitudinal dynamics – Inputs (gradual braking)

The response of the vehicle (longitudinal speed and displacement) for the longitudinal motion input is shown in Fig. 3.7. For a given throttle input, the vehicle speed increases slowly and reaches a steady state. The steady state speed depends on the throttle input. When the brake is applied, the throttle input was removed and the vehicle speed decreased with respect to the intensity of brake applied. Vehicle was stopped in 7.1 *s* with a stopping distance of 43 *m*.

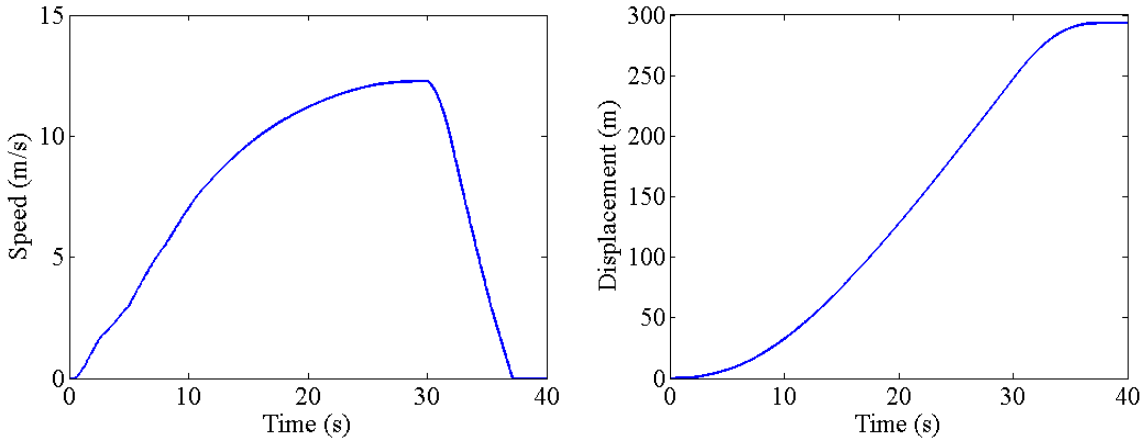

(a) Longitudinal speed (b) Longitudinal displacement

Fig. 3.7: Longitudinal dynamics – Outputs (slow braking)

Another simulation had been carried out with different driving conditions for longitudinal dynamics. Here, the throttle was increased to a maximum of 80 % and the brake was applied to the intensity of 100 % at the 30th second. The corresponding inputs are shown in Fig. 3.8.

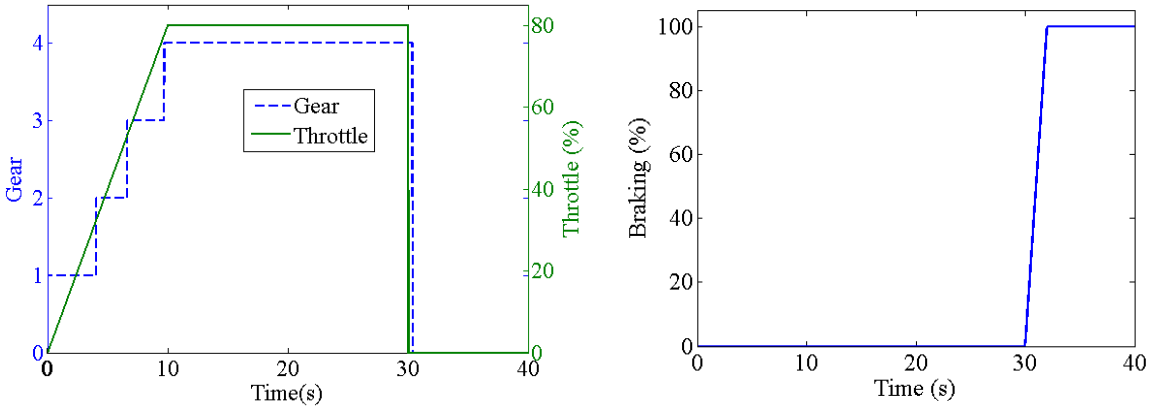

(a) Throttle input and gear change (b) Brake input

Fig. 3.8: Longitudinal dynamics – Inputs (fast braking)

The results are shown in Fig. 3.9. Due to the increased throttle input, vehicle could reach the steady state speed much faster than the previous case of throttle input 60 %.

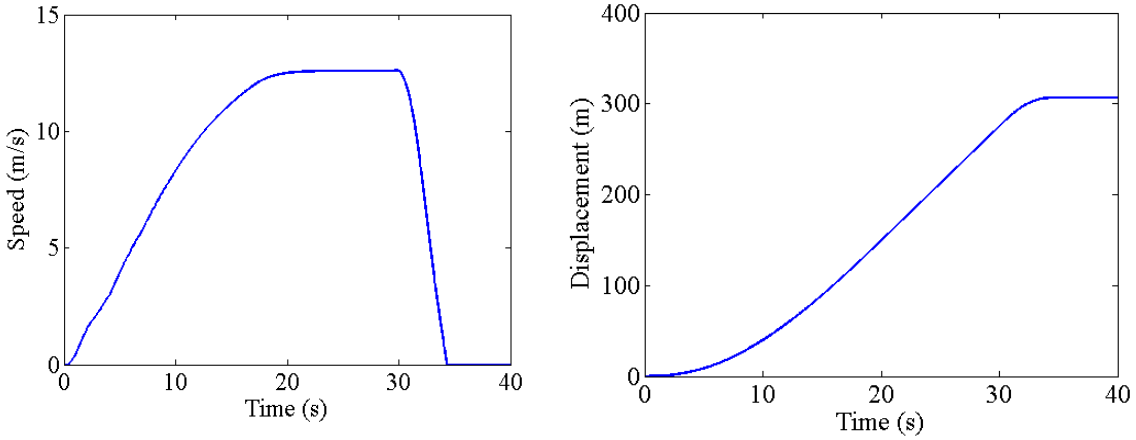

(a) Longitudinal speed (b) Longitudinal displacement

Fig. 3.9: Longitudinal dynamics – Outputs (fast braking)

Brake was applied to its maximum of 100 %, vehicle stopped in 3.5 *s* from the initial speed of 12.5 *m/s* with the stopping distance of 29 *m*.

3.2.2 Lateral Dynamics Results

The lateral dynamics of the tracked vehicle was simulated for a time interval of 50 *s*, to observe the vehicle behavior in longitudinal, lateral, and yaw motions. Figure 3.10 shows the pattern of the throttle and steering input commanded to the vehicle. In this simulation, gear was maintained in first gear. When the vehicle reaches a steady longitudinal speed, steering input, as shown in Fig. 3.10(b), was provided. Since the proposed model was developed to consider only decoupled motion of the vehicle, the throttle, braking, and steering inputs were provided in such a manner that they did not temporally overlap one another.

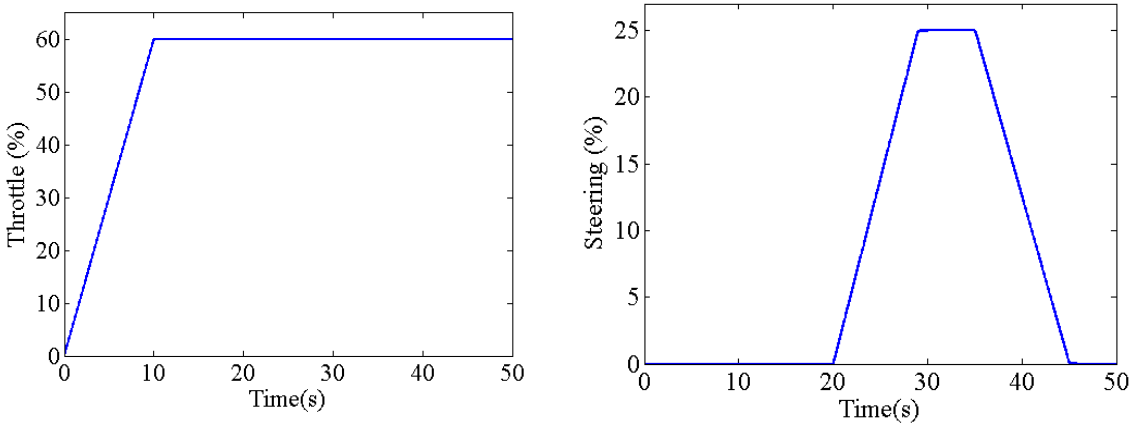

(a) Throttle input (b) Steering input

Fig. 3.10: Lateral dynamics – Inputs (Case 1)

The yaw speed and vehicle's heading angle changes are shown in Fig. 3.11. When the steering input was given, yaw speed increases and heading angle tends to change with positive slope. When the steering angle is constant, the yaw speed reaches a steady state

value and the vehicle's heading angle keep changing. Once the steering angle is brought back to zero, yaw speed also reaches zero and the vehicle does not change its heading angle and moves straight ahead, which could be seen in the displacement plots.

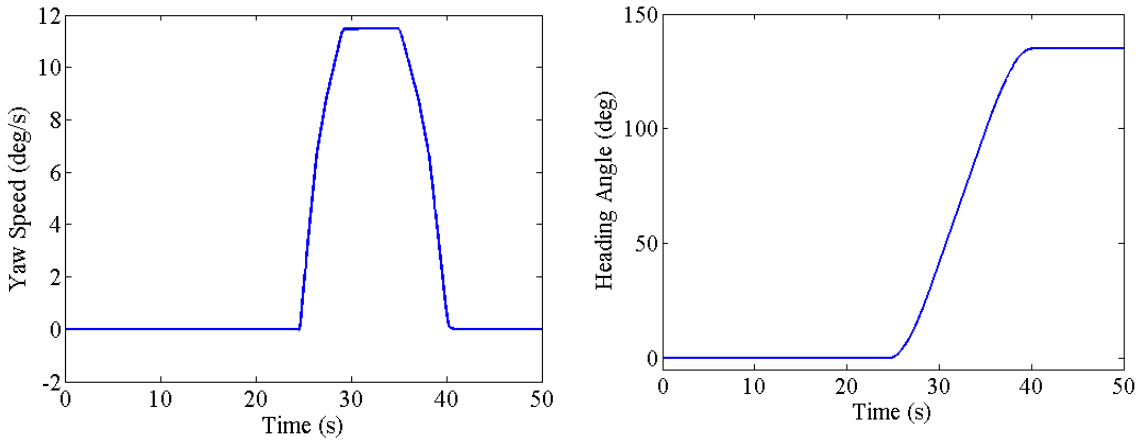

(a) Yaw speed (b) Heading angle

Fig. 3.11: Lateral dynamics – Yaw outputs (Case 1)

Figure 3.12(a) shows the longitudinal speed of the vehicle with respect to a body fixed frame. The vehicle path is plotted in Fig. 3.12(b) with respect to the global axes.

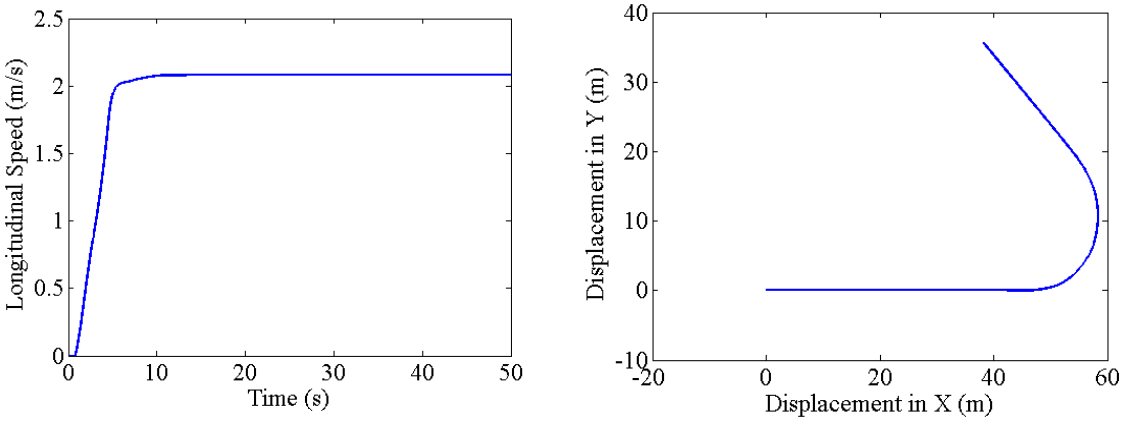

(a) Vehicle speed (b) Vehicle path

Fig. 3.12: Lateral dynamics results (Case 1)

The vehicle moves in a straight-line path before the steering input was given. It can be observed from the plots that when the steering input was given, the vehicle changed its orientation and kept the same orientation when the steering input was brought back to less than 10° as shown in Fig. 3.12(b).

Here, another simulation has been carried out for the similar test conditions with different steering rate for a time interval of 80 *s*. The steering input was provided in such a way that the vehicle would make a single lane change as shown in Fig. 3.13(b). The pattern of the throttle input given is shown in Fig. 3.13(a).

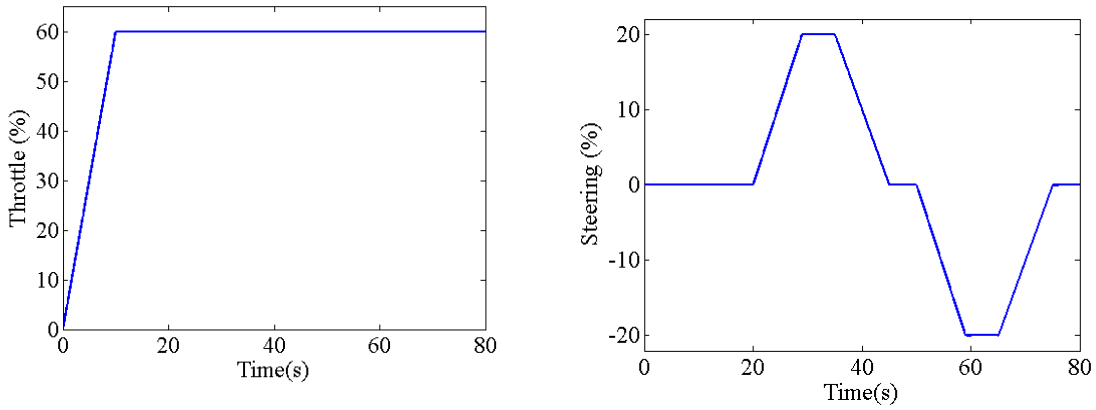

(a) Throttle input (b) Steering input

Fig. 3.13: Lateral dynamics – Inputs (Case 2)

The yaw speed and heading angle of the vehicle is obtained as shown in Fig. 3.14. Since the steering input was given in both the directions, yaw speed also changes in both positive and negative directions. Heading angle increases in positive slope when the yaw speed is in positive direction and vice versa. Finally, the heading angle comes to zero as the lane change is completed.

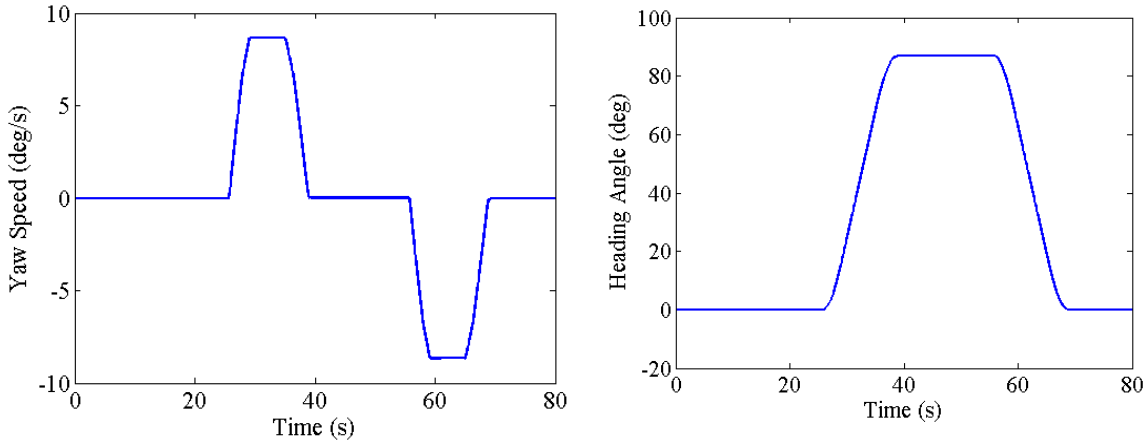

(a) Yaw speed (b) Heading angle

Fig. 3.14: Lateral dynamics – Yaw outputs (Case 2)

Longitudinal speed of the vehicle with respect to the body fixed frame is shown in Fig. 3.15(a). Vehicle path plot in Fig. 3.15(b) shows the vehicle has changed its lane by shifting away from the previous position in y-direction. It is observed from the simulation results that the vehicle behavior is in the expected pattern. This shows that the integrated model of the tracked vehicle is able to represent the vehicle dynamics under various operating conditions in the soft terrain.

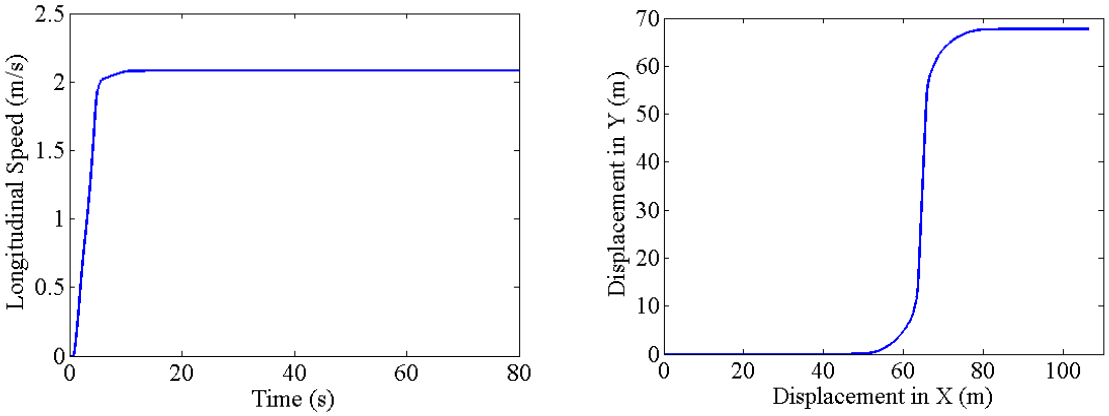

(a) Vehicle speed (b) Vehicle path

Fig. 3.15: Lateral dynamics results (Case 2)

The approximate time constant values of each subsystem and the vehicle dynamic response for acceleration, braking, and steering conditions are shown in Table 3.1. The results show that the settling time of the brake and steering subsystem is 0.036 *s*. The settling time of the vehicle dynamics response for acceleration, braking, and steering conditions are 6.3 *s*, 2.6 *s*, and 0.45 *s* respectively. It can be observed that the settling time for vehicle acceleration, braking, and steering are much higher than the corresponding subsystem's settling time. This shows that a detailed dynamic model for each subsystem may not be required for simulating the overall vehicle dynamic response. However, the subsystem models would be useful in developing "lower-level" subsystem controllers for vehicle control tasks towards its autonomous operation.

Table 3.1: Time Constant of the Subsystems and the Vehicle Response

Systems	Settling time (*s*)
Brake subsystem	0.036
Steering subsystem	0.036
Vehicle dynamics	
Acceleration	6.5
Brake	2.6
Steering	0.45

3.3 COMPARISON BETWEEN KINEMATIC AND DYNAMIC MODELS

It has been mentioned that at "low" speeds, kinematic equations are enough to describe the yaw motion of pneumatic tyred vehicles (Rajamani, 2006) instead of using a dynamic model which would increase computation time and model complexity. To understand this

better in the context of the tracked vehicle, a study was performed to find out a threshold value of the vehicle speed beyond which the dynamic model is appropriate. Beyond this threshold, kinematic equations no longer give accurate results in describing the yaw motion. The kinematic model for calculating the yaw speed of a tracked vehicle is given as (Wong, 2001)

$$\omega_z(t) = \frac{r\omega_{in}(t)(VR(t)(1-i_o(t))-(1-i_i(t)))}{B}, \quad \text{for left hand steering} \quad (3.1)$$

$$\omega_z(t) = \frac{r\omega_o(t)((1-i_o(t))-VR(t)(1-i_i(t)))}{B}, \quad \text{for right hand steering} \quad (3.2)$$

where r is the sprocket radius, $\omega_o(t)$ and $\omega_{in}(t)$ are the sprocket speed of the outer and inner tracks, VR is the speed ratio of the vehicle, $i_o(t)$ and $i_i(t)$ are the slip of the inner and outer tracks, and B is the width of the vehicle.

The above kinematic model was used for simulating the yaw motion of the tracked vehicle and the results were compared with the results from integrated dynamic model simulations. A constant radius turning test was simulated for multiple cases of vehicle speed in step of 0.05 *m/s*. Input conditions for all the test cases were maintained to be the same with a throttle input of 75 % and the steering input of 22.5 % as shown in Fig. 3.16(a), 3.17(a), and 3.18(a). The expected steady state speed of the vehicle in each case was attained by adjusting the gear ratio. Here, the comparison results are shown for three different cases of vehicle speeds where the deviation of results between the models becomes significant.

In case 1, simulation was carried out for the vehicle speed of 4 *m/s* as shown in Fig. 3.16(b). The corresponding results of yaw speed and heading angle of the vehicle are shown in Fig. 3.16(c) and 3.16(d) and the comparison between the kinematic and dynamic models are also shown. The deviation between the yaw derivatives was calculated as the Mean Absolute Percentage Error (MAPE) and was found to be around 5 % (the procedure to calculate the MAPE is explained in Appendix (A.4)).

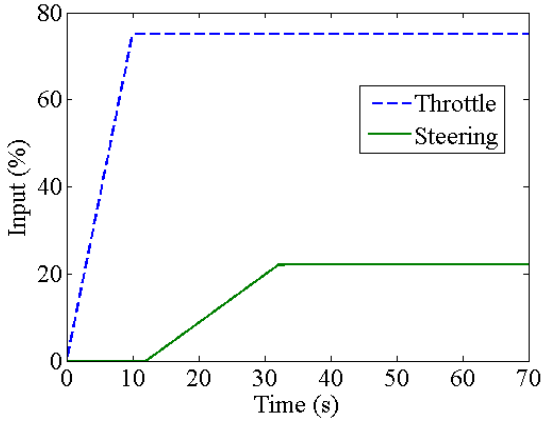

(a) Throttle and steering input

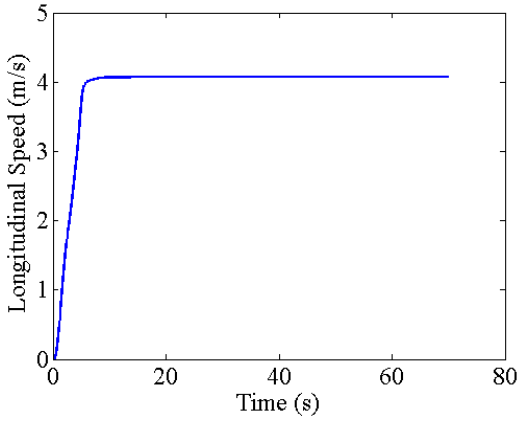

(b) Longitudinal speed

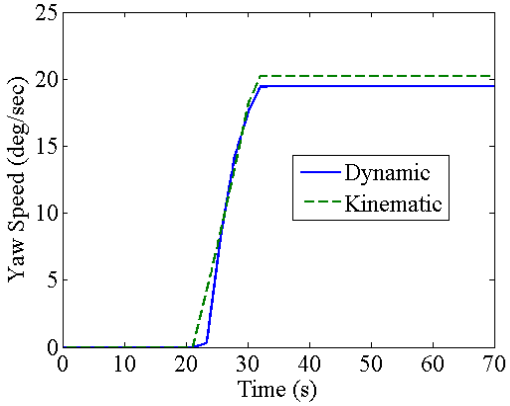

(c) Yaw speed

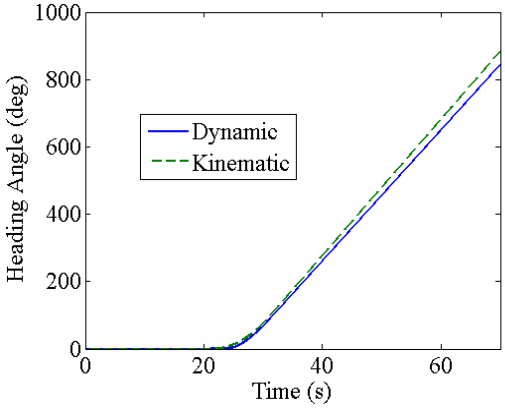

(d) Heading angle

Fig. 3.16: Lateral dynamics (Case 1)

In the second set of simulations (Case 2), the speed of the vehicle was increased to 4.15 *m/s* keeping the steering input same as in the previous case, as shown in Fig. 3.17. The

corresponding outputs are shown in Fig. 3.17(c) and 3.17(d). At this vehicle speed, it was found that the deviation between the yaw parameters calculated from the kinematic and dynamic models is about 10 %. This shows that the kinematic model is diverging from the dynamic model as longitudinal speed increases.

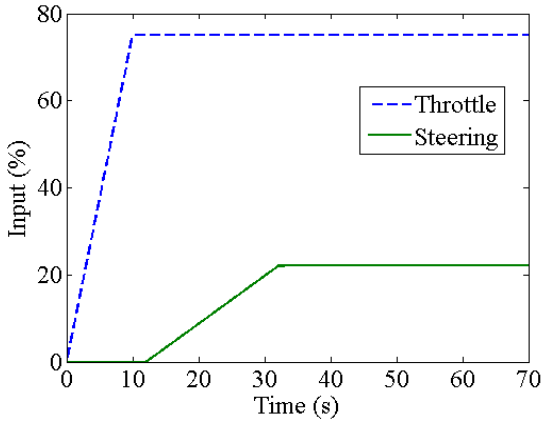

(a) Throttle and steering input

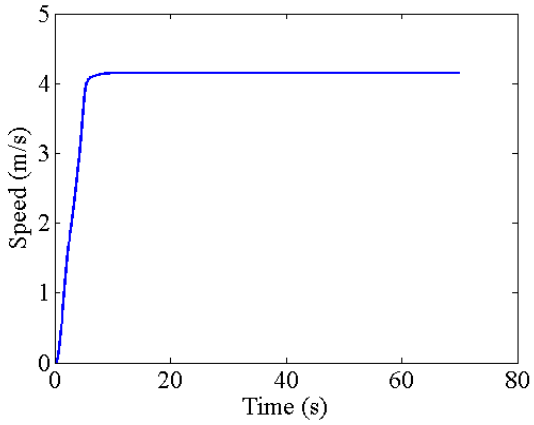

(b) Longitudinal speed

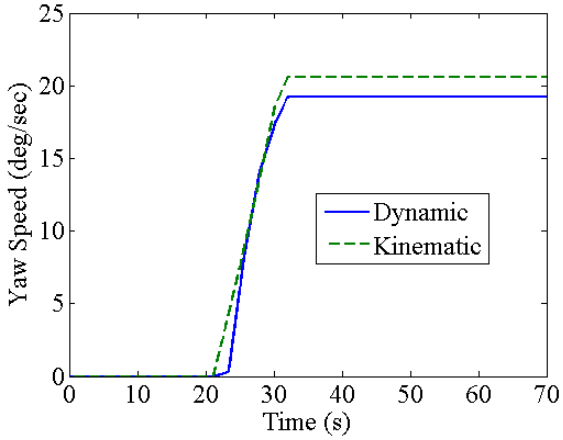

(c) Yaw speed

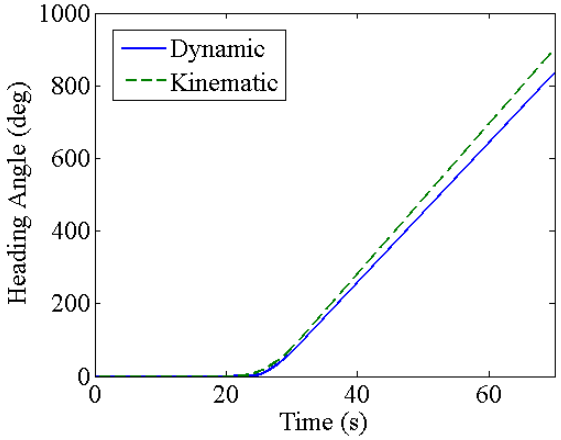

(d) Heading angle

Fig. 3.17: Lateral dynamics (Case 2)

In the simulation of case 3, the speed of the vehicle was increased to 4.25 *m/s* keeping the steering input same as in the previous case, as shown in Fig. 3.18. The corresponding yaw derivative outputs are shown in Fig. 3.18(c) and 3.18(d). At this vehicle speed, it was

found that the deviation between the yaw parameters calculated from the kinematic and dynamic models had a significant deviation, with an MAPE of 14 %. Considering MAPE of 10 % as a threshold, it is possible to infer that dynamic equations are needed for modelling the vehicle behavior when longitudinal speeds exceed 4.15 *m/s* for this vehicle under study.

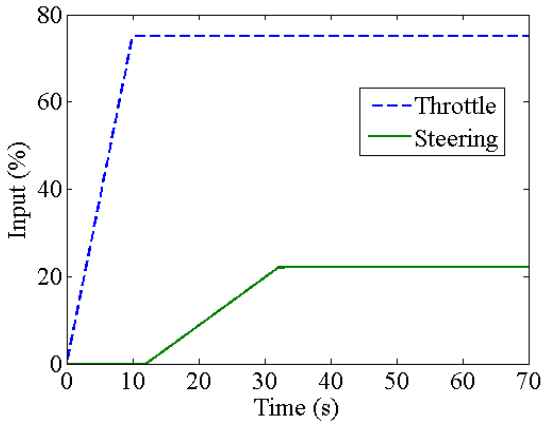

(a) Throttle and steering input

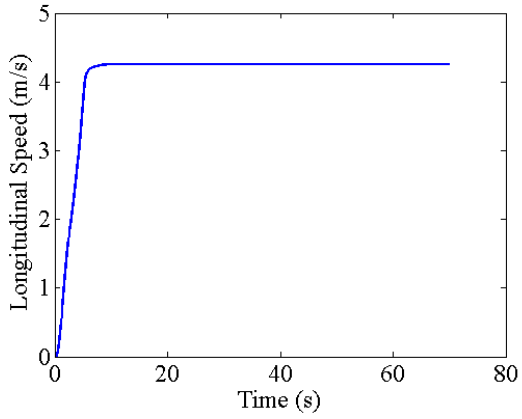

(b) Longitudinal speed

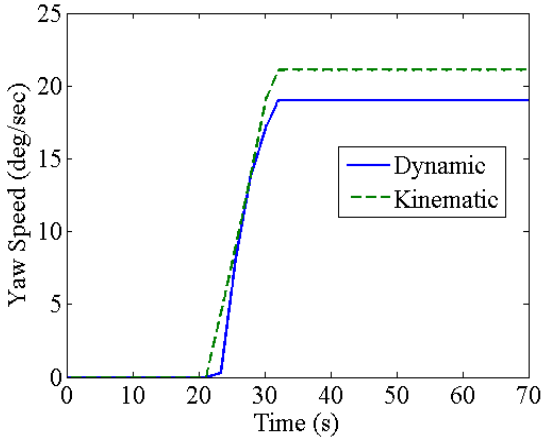

(c) Yaw speed

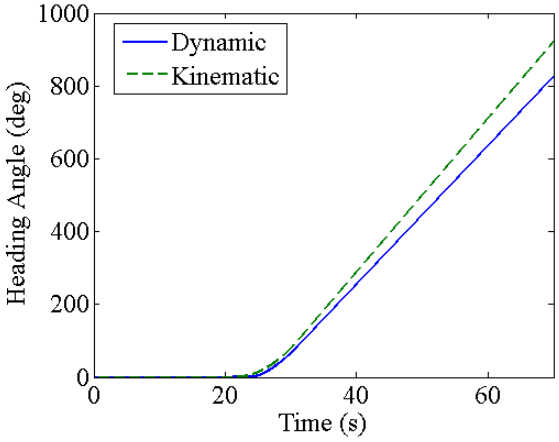

(d) Heading angle

Fig. 3.18: Lateral dynamics (Case 3)

This also shows that kinematic models may be sufficient at lower speeds to model the dynamics of the vehicle, however, at higher speeds it is necessary to have the dynamic models to predict the vehicle response.

3.4 SUMMARY

This chapter presented the numerical simulation of the subsystem models and integrated model of the tracked vehicle. The longitudinal and lateral motion dynamics of the vehicle were analyzed using simulations. As an additional step, the differences in the predicted performance of the vehicle using a kinematic model with that of the dynamic model were also studied. It was found that at lower speeds there is not much difference in the response of both the models. However, as the speed increases, the dynamic model results diverges from the kinematic model results and also it is believed that dynamic model predicts better as it captures more factors like centrifugal force and terrain dynamics. Lower level controllers for the subsystems were also implemented to get the desired brake force output. Corroboration of the simulation results of the dynamic model with the experimental results is provided in the following chapter.

CHAPTER 4

COMPARISON WITH ADAMS TRACKED VEHICLE MODEL

4.1. INTRODUCTION

In this chapter, a comparison of the proposed model results with those of a commercially available simulation software is explained. The commercially available software, Adams Tracked Vehicle (ATV), is widely used by vehicle designers for simulating vehicle performance prior to the prototyping and testing of new vehicles. The comparison was carried out here to check the accuracy of the mathematical model and to bench mark its performance.

4.2 ADAMS TRACKED VEHICLE (ATV) SOFTWARE

ATV software is generally used by designers to study the track-terrain interactions and the dynamics and motion behavior of the tracked vehicle. Forces that are generated in-between the track segments, component interfaces, and the center of mass of the vehicle can also be determined.

In order to carry out the simulation studies, a model of the tracked vehicle was developed using ATV software, as shown in Fig. 4.1. Existing tracked vehicle models in ATV were modified for this purpose. The vehicle and terrain parameters used in the numerical simulations were used in the ATV model also. The inputs to the proposed vehicle dynamics model and ATV model are the thrust of the left and right sprockets.

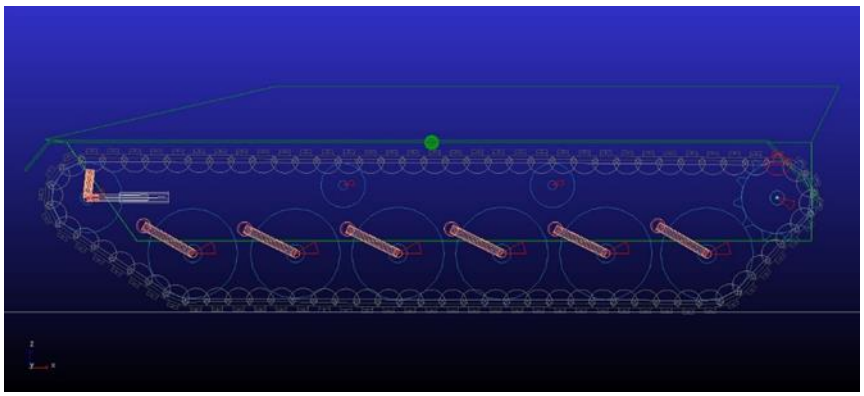

Fig. 4.1: Tracked vehicle model developed in ATV

Since the subsystem performance results cannot be obtained in the ATV, only the overall vehicle dynamics was considered for comparison. Also, since ATV has the capability of six DOF simulation, the results of simulation could capture the roll, pitch, and yaw motions along with the longitudinal, lateral, and bounce motions. However, the developed mathematical model has considered only the longitudinal, lateral, and yaw motions.

4.3 COMPARISON OF ATV AND PROPOSED MODEL RESULTS

The comparison of the performance of ATV model and the proposed model was done for four different cases. The test cases were chosen to match the cases that the vehicle would possibly encounter during its operation such as:

1. Straight line test – The acceleration and brake conditions were studied.
2. 180° and 90° turn test – To observe the behavior of the vehicle when it makes directional changes.
3. Constant radius test – To study the behavior of the vehicle when it makes a complete circle, which is usually considered as a standard test in pneumatic tyred vehicles.
4. Step steer test – Would be useful in quantifying temporal response using parameters such as time constant and settling time.

4.3.1 Straight Line Test

In order to have a fair comparison of the developed model with that of ATV, longitudinal dynamics of the tracked vehicle was simulated and compared. Figure 4.2(a) and 4.2(b) shows the inputs to the subsystems such as throttle, gear, and brake. The thrust of the left and right sprockets are the output of those subsystems as shown in Fig. 4.2(c) which were given as the input to the proposed vehicle dynamics model and the ATV model.

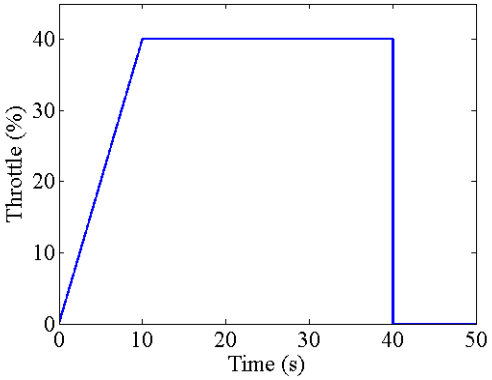

(a) Throttle input

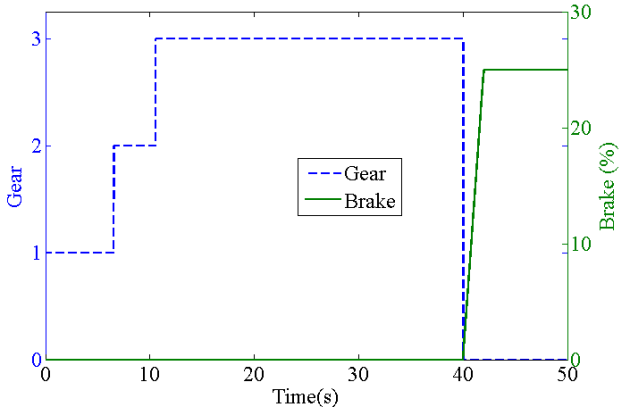

(b) Gear shifts and brake input

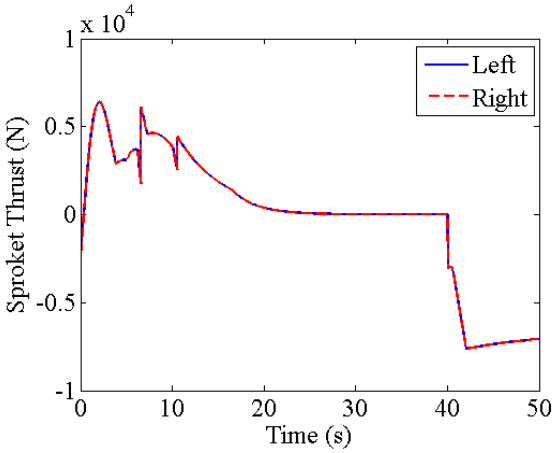

(c) Sprocket thrust from proposed model (used as input for lateral dynamics simulation)

Fig. 4.2: Straight line test – Inputs

Throttle input was given as ramp input for 10 *s* followed by a constant value input for another 30 *s*. When the brake action is initiated, the throttle was brought back to zero position as shown in Fig. 4.2(a). The corresponding gearshift is shown in Fig. 4.2(b), which changes automatically with respect to the vehicle speed. The brake was applied at the 40th second as shown in Fig. 4.2(b) and it was ramped up till 25 % and maintained at this position till the simulation was completed. The simulation results for ATV and the proposed model are shown in Fig. 4.3. Figure 4.3(a) shows the longitudinal speed and Fig. 4.3(b) shows the longitudinal displacement.

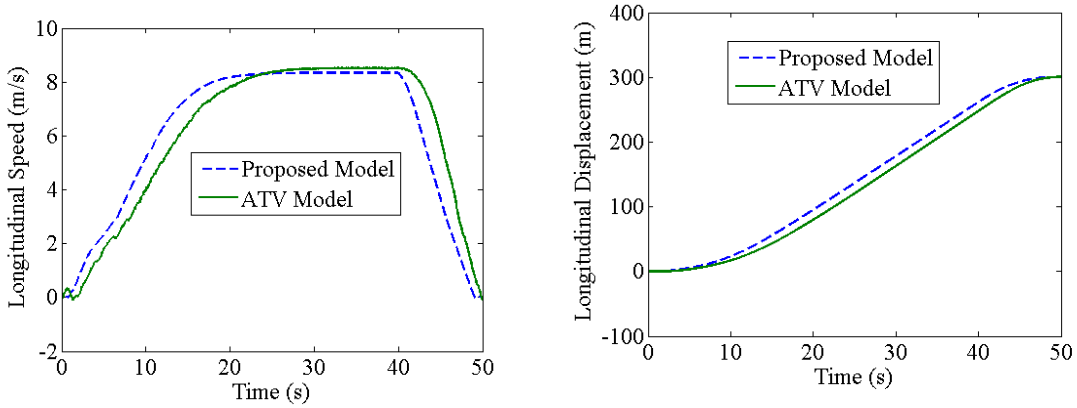

(a) Longitudinal speed (b) Longitudinal displacement

Fig. 4.3: Straight line test - Output

The ATV result shows a small fluctuation of the speed at the beginning, which may be due to the pitching effect of the vehicle, which was not addressed in the proposed model. Also, there is a small delay in the ATV response compared to the proposed model response. This could be due to the characterization of the track-slip in the case of ATV model. At the steady state speed, both responses are in very good agreement. Once the brake is applied, ATV model takes slightly longer time to settle down to zero, compared to the proposed model. A similar trend was observed in the displacement plot, where lag in the vehicle's movement is clearly seen. The ATV results show that the vehicle comes

to rest at a later time instant than that of the proposed model as seen in Fig. 4.3(a). This may also be due to the difference in characterizing the track slip between the two models (Pawar, 2016).

4.3.2 180° and 90° Turn Test

In this test, lateral dynamics of the tracked vehicle was compared when the vehicle takes 180° and 90° turns. The model was simulated for a time interval of 100 *s*. Throttle and steering inputs are shown in Fig. 4.4(a). Steering input was given only when the vehicle longitudinal speed reached a steady state value. These subsystems generate the thrust of the left and right sprocket, as outputs, which are shown in Fig. 4.4(b) and were given as the inputs to the proposed vehicle dynamics and ATV model. Steering input was given in such a way that the vehicle would take a 90° turn and then a 180° turn. When the steering input was initiated, throttle input was not changed in order to maintain the steady state longitudinal speed. Since the objective of the test was to study the transient characteristics of yaw motion, yaw test was carried out at steady state longitudinal speed.

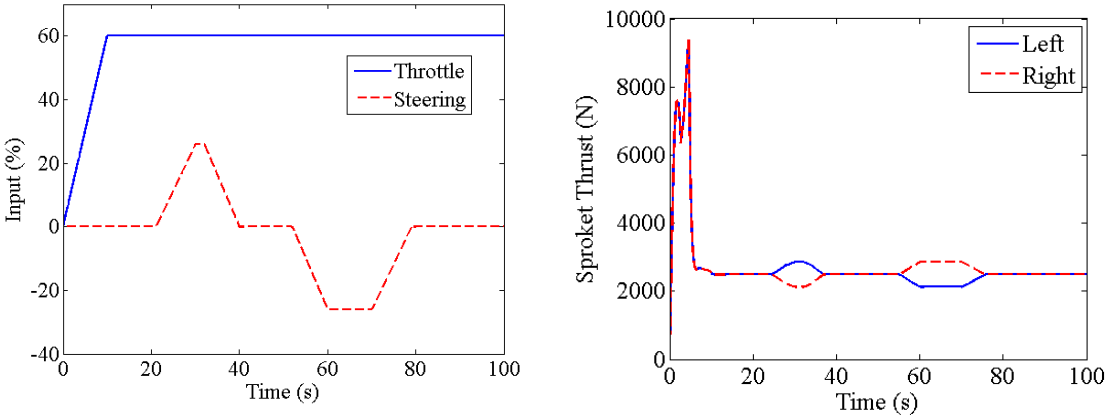

(a) Throttle and steering input (b) Left and right sprocket thrust

Fig. 4.4: 180° and 90° turn test - Inputs

The speed along X and Y axis of the global frame were compared for ATV and proposed model, and are shown in Fig. 4.5. It is seen from the plot that the ATV response is faster than the model simulation, which is in contrast with the longitudinal response shown in Fig. 4.5(a). The delay in the ATV response compared to the proposed model response could be due to the difference in characterizing track slip in the case of ATV model (Pawar, 2016). The minor oscillations in speed are mainly due to the rolling and pitching of the vehicle, captured in the ATV model. As shown in Fig. 4.5(b), the speed changes as the steering input exceeds the dead-zone value of 10°.

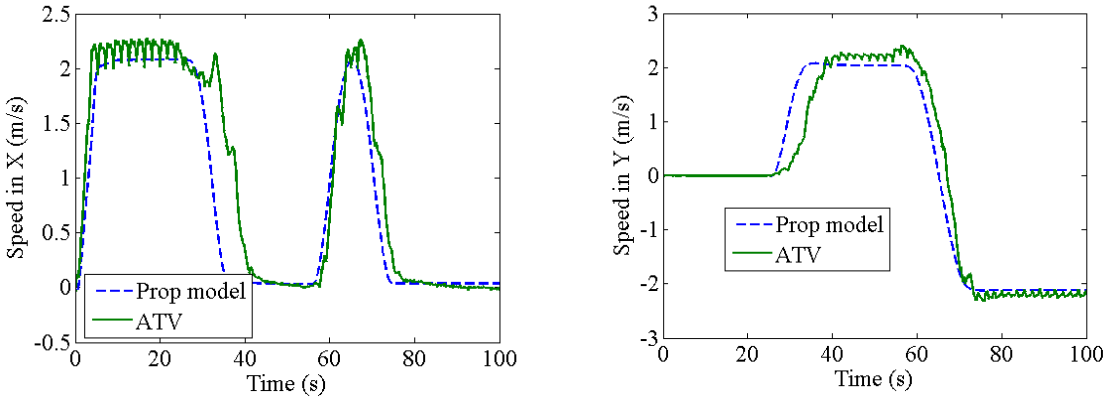

(a) Speed in global abscissa (b) Speed in global ordinate

Fig. 4.5: Vehicle speed in abscissa and ordinate axis of global coordinate system

The ATV lateral response is lagging due to the reason that the slip value in the ATV model is higher compared to the proposed model. In the proposed model, slip has been calculated as a function of sprocket thrust. Response of the ATV model in transient period is always slower compared to the proposed model. This may be due to the differences in the manner in which track slip is accounted for in the two models. However, there is a good agreement in the steady state speed. The yaw speed and vehicle path comparisons are given in Fig. 4.6 and 4.7.

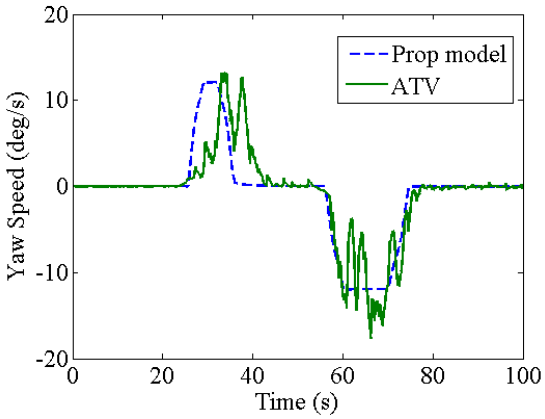

Fig. 4.6: Yaw speed

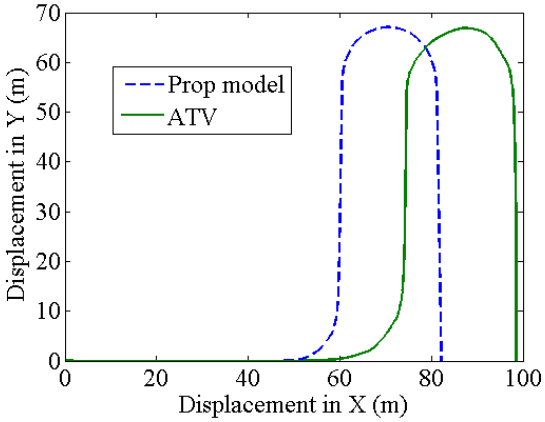

Fig. 4.7: Vehicle path

The time delay in the response has caused the deviations in the vehicle path of the vehicle. However, they show a similar pattern in the vehicle path.

4.3.3 Constant Radius Test

A constant radius test was simulated and compared here. Throttle and steering inputs were given to the powertrain and steering subsystems to produce thrust with a constant difference in the magnitude between the left and right sprockets as shown in Fig. 4.8(b). Steering input was given slowly till the sprocket thrust reaches a constant difference in magnitude between the left and right sprockets to take a constant radius turn. To avoid the transient period response time lag, steering input was ramped up slowly to reduce the differences in the response time between the models. The steering input was given only after the vehicle reaches its steady state speed. Both the inputs were given and maintained at the same value till the vehicle makes a complete circle.

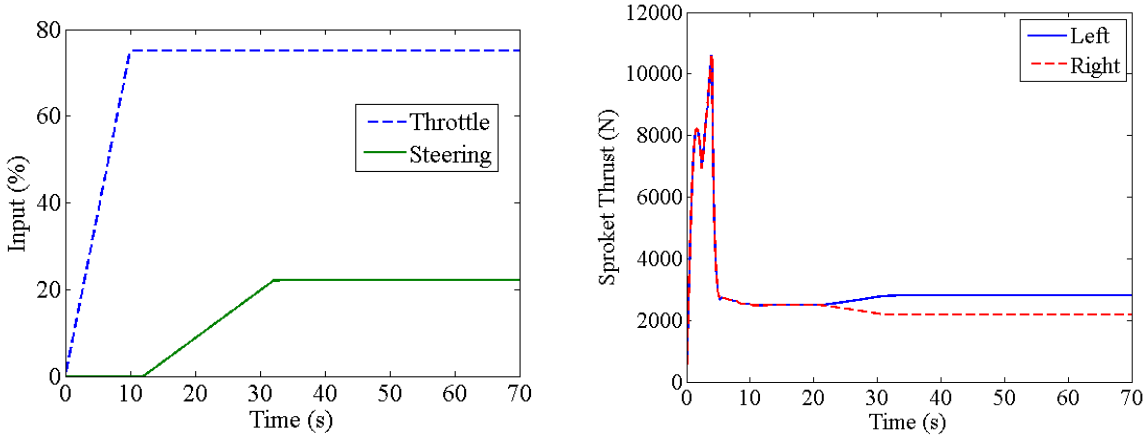

(a) Throttle and steering input (b) Left and right sprocket thrust

Fig. 4.8: Constant radius test - Inputs

Speed about X and Y axis of the global frame are shown in Fig. 4.9. As it was mentioned in the last section, slip in the ATV model is more when the vehicle is accelerated or decelerated compared to the proposed model (Pawar, 2016). Because the inputs to the ATV model was given slowly, the slip value is comparable between the proposed and ATV model.

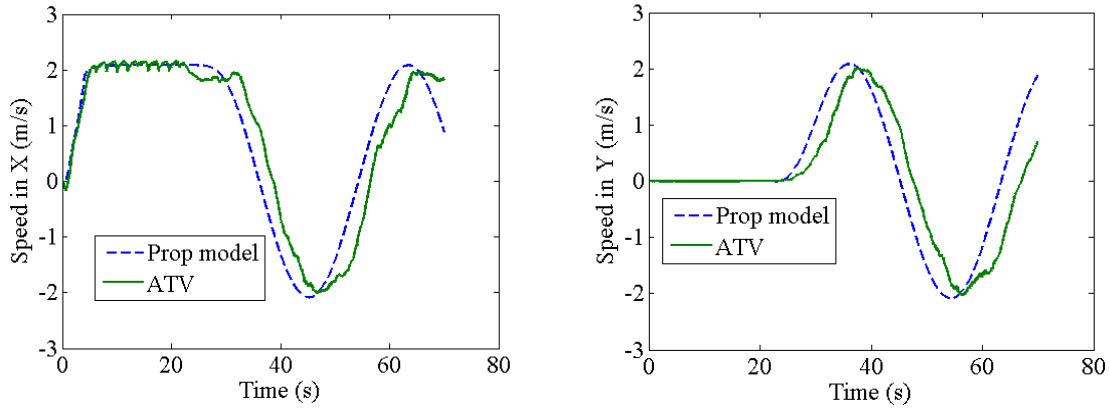

(a) Speed in global abscissa (b) Speed in global ordinate

Fig. 4.9: Vehicle speed in abscissa and ordinate axis of global coordinate system

The corresponding yaw speed plot is shown in Fig. 4.10. The oscillation in the yaw speed in ATV simulation is mainly due to the rolling and pitching motion of the vehicle, which tends the vehicle to have oscillations. The rolling and pitching motion happens due to the static simulation in ATV model (Pawar, 2016). Even though the ATV model was given inputs only to produce longitudinal, lateral, and yaw motions in the flat terrain, speed variations are observed in the roll and pith motions also.

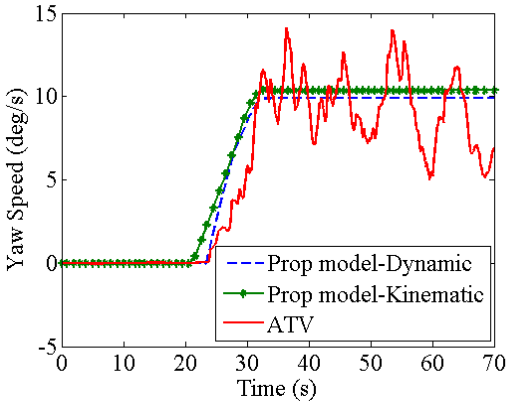

Fig. 4.10: Yaw speed

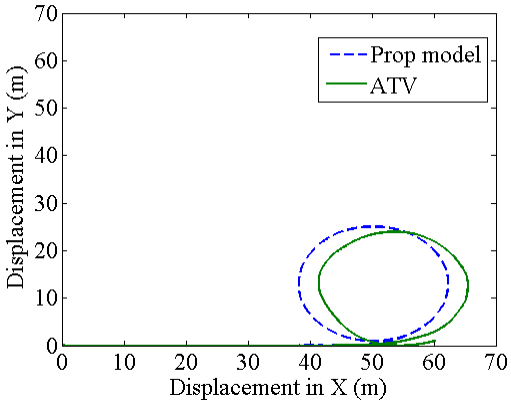

Fig. 4.11: Vehicle path

In the vehicle path plot shown in Fig. 4.11, there is a small deviation from the commanded vehicle path in both the cases. This is mainly due to the oscillations in the yaw speed.

4.3.4 Step Steer Test

In this section, a step steer test was simulated and the results were compared. The throttle and steering inputs given are shown in Fig. 4.12(a). The thrust of the left and right sprockets are the outputs of the steering and powertrain subsystems, which were given as the inputs for proposed vehicle dynamics model and ATV model as shown in Fig. 4.12(b).

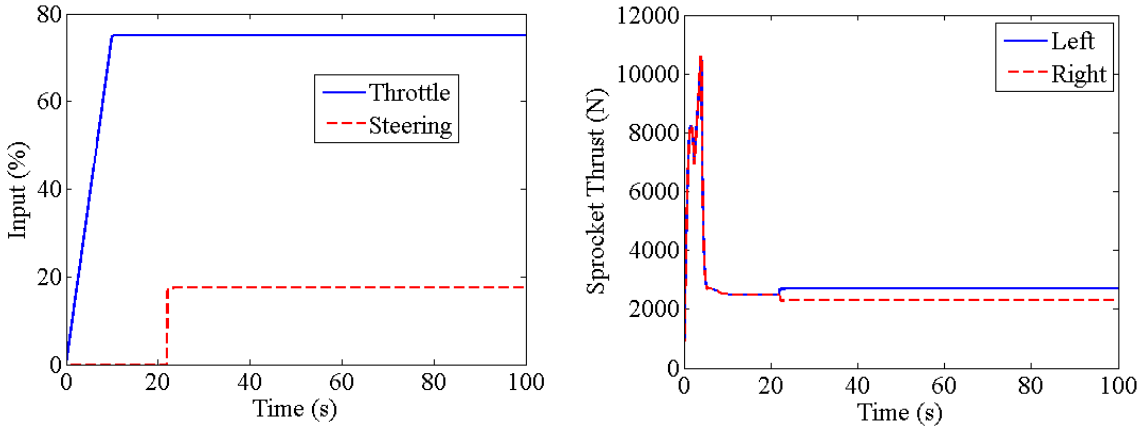

(a) Throttle and steering input (b) Left and right sprocket thrust

Fig. 4.12: Step steer test - Inputs

Speed about X and Y axis of the global frame are shown in Fig. 4.13. The lateral response time lag is more between the ATV and the proposed model compared to the previous tests due to the slow rate of steering input (Pawar, 2016). As it was mentioned in the last section, slip in the ATV model is more when the vehicle is accelerated or decelerated compared to the proposed model.

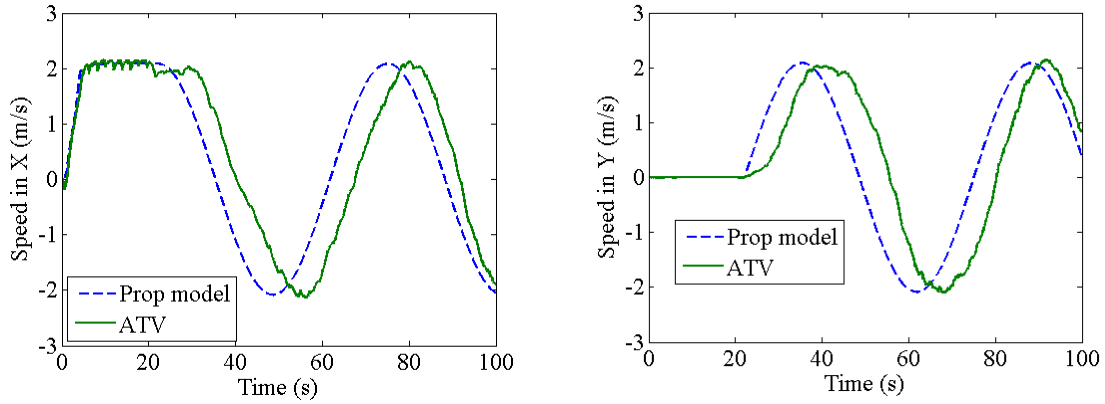

(a) Speed in global abscissa (b) Speed in global ordinate

Fig. 4.13: Vehicle speed in abscissa and ordinate axis of global coordinate system

The yaw speed plot is shown in Fig. 4.14. As seen in Fig. 4.14, the ATV model response is very sluggish due to the inherent model inability to respond to sudden steering changes and this leads to the vehicle path error shown in Fig. 4.15.

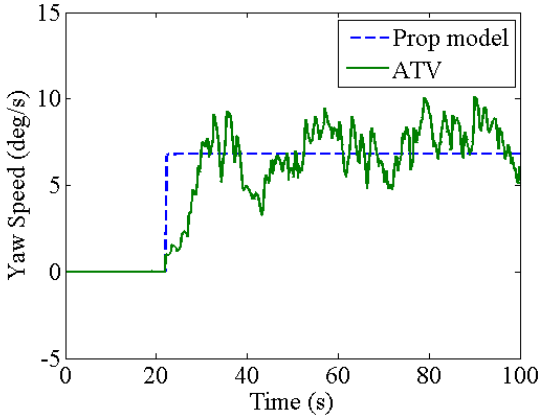

Fig. 4.14: Yaw speed

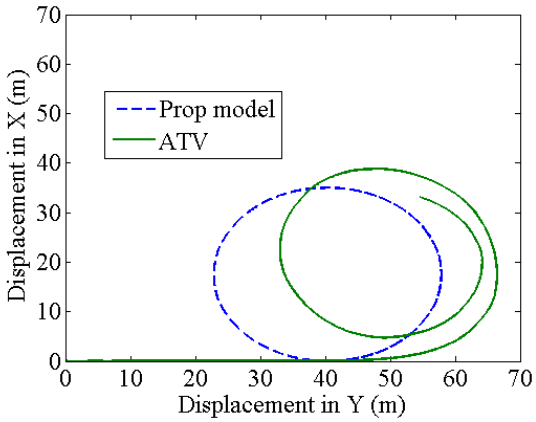

Fig. 4.15: Vehicle path

The simulation results presented above show that the developed mathematical model is comparable with the industry-standards in this field. In order to objectively compare the response of the model with that of ATV, an analysis was carried out by calculating the mean absolute percentage error. This is presented in the following section.

4.4 ERROR COMPARISON

Mean Absolute Percentage Error (MAPE) is one of the most popularly used parameters for checking the deviations between two sets of data. A quantitative analysis of the deviations between the ATV response and proposed vehicle model response for various performance parameters has been carried out using MAPE. The details of the procedure for calculating the MAPE are given in Appendix (A.4).

In order to calculate the MAPE values in the comparison test, only specific time periods have been chosen. Reasons for discarding a few time durations for calculating the MAPE values are stated here:

- When the vehicle is at rest, static simulation will be carried out at the contact between road, tracks and each wheel in ATV that results in oscillations that lead to higher MAPE values (Pawar, 2016).
- During the vehicle's turn the vehicle speed reaches zero or nearer to zero at any of the axis direction of the global frame. This situation will shoot up the error values to the maximum.

MAPE values of various test comparison between the ATV and the proposed model for various parameters are shown in Table 4.1. Here, the ATV was considered as ideal so the error values were calculated with respect to the ATV.

Table 4.1: MAPE Results Comparison Between Proposed and ATV Model

Tests	Speed in X	Speed in Y	X displacement	Y displacement	Yaw speed	Duration (*s*)
Straight line	12.7 % (1.5-47 *s*)	--	15.9 % 1.5-50 *s*	--	--	50
180° and 90° turn	29.1 % 1.5-36 *s* 16.17 % 56-70 *s*	18.6 % 25-100 *s*	18.1 % 1.5-100 *s*	22.04 % 25-100 *s*	49.36 % 25-45 *s* 31.6 % 56-75 *s*	100
Constant Radius	15.6 % 1.5-33 *s* 24.7 % 37-53 *s* 27.8 % 58-70 *s*	18.9 % 23-42 *s* 24.8 % 46-61 *s* 29.6 % 65-70 *s*	11.4 % 1.5-70 *s*	18.5 % 28-61 *s*	41.3 % 25-70 *s*	70
Step Steer	10.16 % 1.5-32 *s* 31.5 % 38-62 *s* 38.7 % 68-82 *s* 23.8 % 90–100 *s*	19.8 % 20-44 *s* 32.1 % 44-70 *s* 36.3 % 78-96 *s*	22.7 % 1.5-100 *s*	28.6 % 40-60 *s* 32.4 % 70-100 *s*	37.1 % 25-100 *s*	100

On the whole, the MAPE values were less than 35 % for all the test comparisons except for the case of yaw speed, which is around 50 %. The reason for this higher value of MAPE for yaw speed is due to the significant lag in the steering response in the ATV model during the transient period. This is mainly attributed to the numerical solver used in ATV (Pawar, 2016). The errors in displacement were also due to the initial errors in vehicle speed, as the displacement was calculated by integrating the vehicle speed.

4.5 COMPUTATION TIME COMPARISON

The proposed model is computationally less intensive in calculating the response of the vehicle for the case of longitudinal, lateral, and yaw dynamics when compared to the ATV software. It was found that the computation time for simulating the vehicle response for a time interval of 100 *s* in ATV varied from 30 *min* (for 250 time steps) to 10 *hours* (for 5000 time steps). However, the numerical simulation of the proposed model took only 10 *s* in a desktop computer for the same vehicle simulation.

Table. 4.2: Comparison of Computation Time Between the Models

Test cases with simulation time / Models	Straight run test for 41 *s* (*s*)	180 and 90 turn test for 100 *s* (*s*)	Constant radius test for 70 *s* (*s*)
Proposed model (approx.)	5	15	8
ATV software (approx.)	10800	36000	28000

4.6 SUMMARY

This chapter provided a comparison of the proposed model with the ATV model, which is considered as an industry standard for vehicle simulation. There were four standard tests considered for performance comparison. The simulation results confirmed the utility

of the model as well as its closeness to the ATV model. An analysis carried out also showed that error percentages are less than 35 %. Some of this could be attributed to the numerical solver used in ATV, particularly in the initial transient period. Computation time of the proposed model and the ATV model was compared for different test cases. As the utility and the performance of the model were established through simulation studies, the corroboration of the model with experimental analysis was carried out. Details of the experimental analysis are presented in the next chapter.

CHAPTER 5

EXPERIMENTAL ANALYSIS

5.1 INTRODUCTION

In this chapter, the experimental setup and the experiments that were carried out on the real vehicle will be explained. Corroboration of the proposed model simulation results was carried out with the experimental data. Only limited experiments were carried out due to various factors related to the constraints in the experimental vehicle, accessories that are needed to do experiments, human factors, and field restrictions.

5.2 EXPERIMENTAL SETUP

Field experiments were carried out using a BMP II (Boevaya Mashina Pehoty II) Infantry Fighting Vehicle. The experiments were carried out with the help of scientists from M/s Combat Vehicle Research and Development Establishment (CVRDE, DRDO). The block diagram of the experimental setup is shown in Fig. 5.1 and the experimental vehicle is shown in Fig. 5.2.

The experimental setup consisted of a tracked vehicle, proximity sensors with teethed wheel, absolute encoders, data acquisition devices, and a central computer. The vehicle has been made into a tele-operated vehicle using the DBW modules for actuation of brake, steering, and accelerator. These modules act as input devices for the vehicle.

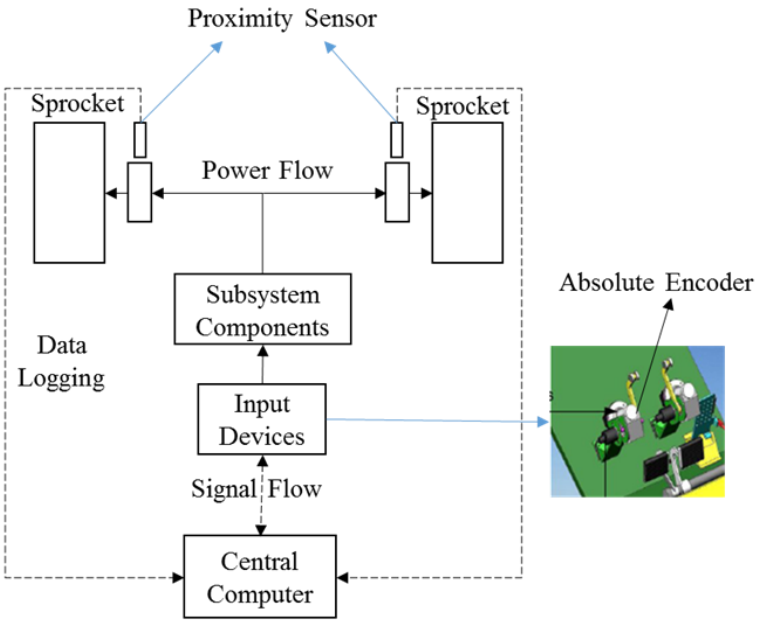

Fig. 5.1: Schematic of the experimental setup

Proximity sensors (pointing towards the teethed wheel) are attached on the drive shaft connected to the sprocket to measure the sprocket speed. Absolute encoders measure the position of the various input pedals and supply the data to the central computer.

Fig. 5.2: Experimental vehicle (courtesy: CVRDE, Chennai)

The following data were recorded during the experiments:

- Encoder values of the input devices for accelerator, brake, and steering.
- Encoders were used to calculate the sprocket speed.

5.3 RESULTS AND ANALYSIS

As explained in the previous section, only limited experimental corroboration was carried out. Experiments were carried out to analyze the longitudinal motion response of the vehicle under tele-operation. The inputs that were commanded to the experimental vehicle such as throttle, gear, steering, and clutch are shown in Fig. 5.3.

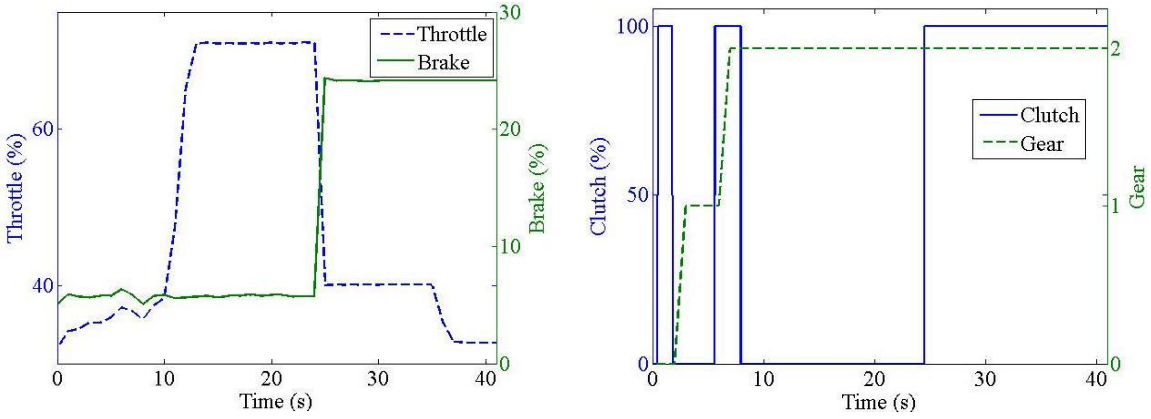

(a) Throttle and brake inputs (b) Clutch and gear inputs

Fig. 5.3: Longitudinal dynamics – Experimental inputs

Throttle input was started with 32 % and then increased to 70 % and maintained till the brake was applied. When the brake action was initiated, the throttle value was again reduced to 32 % (32 % is the minimum throttle input to be given to the vehicle to maintain the minimum engine idle speed). Figure 5.3(b) shows the gear change that took place. In this test, shifting of gear and the clutch actuation were controlled manually, clutch was applied to shift the gears. Clutching and declutching happens whenever the application of brake and shifting of gear takes place.

In order to compare the experimental results and the simulation results, same inputs were given to the proposed model, and simulations were carried out. Comparison of the results for a typical longitudinal motion experiment is shown in Fig. 5.4.

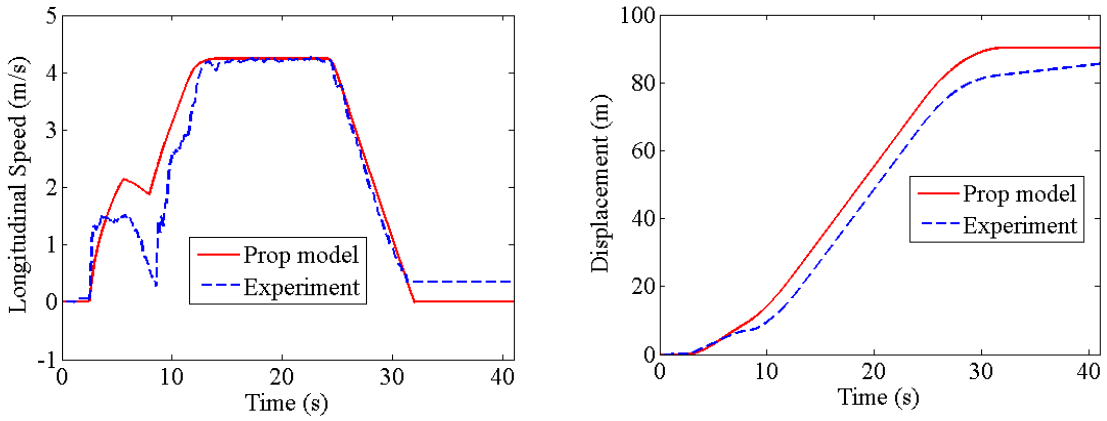

(a) Longitudinal speed (b) Longitudinal displacement

Fig. 5.4: Longitudinal dynamics outputs – Comparison between proposed model and experiment

Longitudinal speed and displacement are shown in Fig. 5.4 for the experiment and the simulation studies. It is observed from the speed plot that the experimental vehicle response is slower in comparison to the simulation results in the transient region. This is mainly due to the vehicle parameter variations and the un-modelled dynamics of the vehicle, their subsystems, and terrain. The terrain is highly sensitive to climate and seasonal variations, which were not considered in the model. At steady state condition, the vehicle speed in the experiment is matching well with the simulations. Vehicle speed profile was matching well even when the brake action was initiated and reaches the zero speed value. As seen in the results, a residual value of the vehicle speed exists in the experiments. This is due to an experimental error in the measurement of speed using the encoder. Due to unavoidable circumstances, the experiments could not be carried out with proper navigational system installed in the tracked vehicle. Longitudinal speed of

the vehicle was inferred using encoders, which does not consider the slip of the vehicle at the track-terrain interface. In order to estimate the vehicle speed by taking into account the slip, Eq. 2.57 was used to estimate the slip of the vehicle for the applied sprocket thrust at each time instant. The result of the analysis is shown in Fig. 5.5.

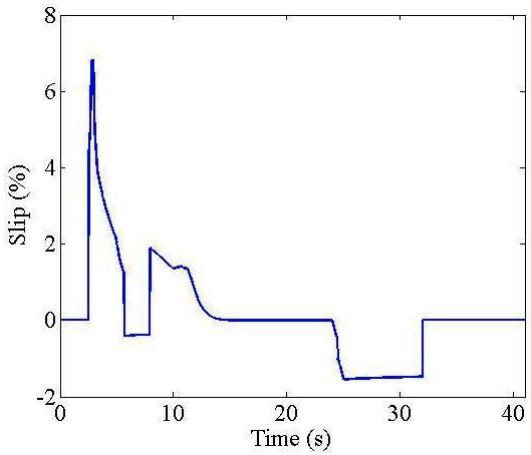

Fig. 5.5: Slip of the vehicle

The maximum slip was found to be around 7 %. When the brake was applied, it produces a slip of about 1.8 %. Hence, the accuracy of the experimental data for longitudinal speed (that was calculated using encoder data) would be subjected to these limits on longitudinal slip.

The vehicle displacement plot shown in Fig. 5.4(b) showed a similar trend of vehicle speed profile. The actual displacement of the vehicle is less than that in the simulation. This is mainly due to the low speed of the vehicle during the transient stage, resulting in less displacement. To gain a better understanding of the experimental results and its comparison, the MAPE between the experiments and simulations were calculated. The results are shown in Table 5.1. On the whole, MAPE results show that the error between the proposed model and experiment is less than 18 %. This is considered as an acceptable

range in the field of tracked vehicles. The data acquisition system used in the experiments has uncertainties that delivers non-zero speed and displacement values even when the vehicle is at rest as shown in Fig. 5.4. This causes the MAPE value to shoot up to very high values, and hence these time intervals were neglected while calculating MAPE.

The results presented above show that the mathematical model developed for the tracked vehicle was able to predict the vehicle behavior with good accuracy. This corroboration of the model with limited experiments support that the model can be used for prediction of vehicle behavior during tele-operation.

Table 5.1: MAPE Results Comparison of Proposed Model with Experiments

Straight line Test	Speed in X	X displacement	Duration
Proposed model	17.52 % (4 - 31 *s*)	17.96 % (4 - 31 *s*)	41

5.4 SUMMARY

An experimental corroboration of the mathematical model of the tracked vehicle is presented here. The results of the straight-line experiment using an experimental tele-operated tracked vehicle have shown that the mathematical model results are in good agreement with the experimental results. The maximum MAPE was less than 19 %. Experimental comparison for the lateral dynamics was not carried out due the difficulties in the sensing of vehicle position changes.

CHAPTER 6

SUMMARY AND CONCLUSIONS

6.1 SUMMARY

From the literature, it was found that there is no proper vehicle dynamics model along with subsystems dynamics model that is available for a tracked vehicle in both transient and steady state conditions. This was primarily the motivation for the research work presented in this thesis to develop a mathematical model for a tele-operated unmanned vehicle for longitudinal, lateral, and yaw motion. Mathematical models for all subsystem dynamics and vehicle dynamics were presented, along with the assumptions to simplify the model to a certain extent in order to make the model generic.

Modeling of the subsystem dynamics was done and the simulation results were shown at the end of each subsystem dynamics model. For powertrain subsystem, dynamics equations were derived separately for each component and combined together to form as a powertrain subsystem. Engine map was generated as a two-dimensional look-up table to act as the power source for entire vehicle, which relates engine speed and engine torque for different throttle inputs. Brake subsystem dynamics was modeled for the same layout for what was there in the actual vehicle. That contains three components include mechanical linkages, fluid system modeling, and band brake. Steering subsystem dynamics was developed with modification on brake subsystem since the same components were being used to obtain steering function as well. Design of lower-level subsystem controllers were implemented in the brake and steering subsystem models so that the desired output could be reached.

Modeling of vehicle system dynamics for longitudinal, lateral, and yaw motion was done and simulated with appropriate assumptions along with the terrain dynamics. Terrain dynamics was modeled by limiting the scope only to soft terrain. After modeling the vehicle dynamics, subsystem models were integrated and the simulation studies were carried out and the results were plotted for both longitudinal and lateral dynamics cases. The proposed model was developed to consider only decoupled motion of the vehicle. Hence, the throttle/braking, and steering inputs were provided in such a manner that they did not temporally overlap one another. Threshold limit to use dynamic equations instead of kinematic equations to calculate the yaw parameters were carried out and the results were presented.

The same vehicle and terrain properties were used in the ATV software to corroborate the proposed model. As the proposed model was corroborated with the ATV model, comparison studies were carried out for experimental corroboration. For experiments, a BMP II vehicle was used and the experiments were conducted only for longitudinal dynamics and the results were compared.

6.2 CONCLUSIONS

- Longitudinal dynamics model was compared with the ATV model and the experimental data. Analysis showed that the proposed model has an agreement of more than 82 % with the experimental vehicle and more than 84 % with the ATV model in straight line motion test. This shows that the proposed model is accurate enough to predict the vehicle’s longitudinal dynamics.

- Predictability of the proposed model for the lateral dynamics tests have good agreement in the period of steady state motion and reasonable in the transient periods when compared with the ATV model. On the whole it has an agreement of more than 65 % in all the cases of simulations except for the yaw speed comparison, which is more than 51 %. The MAPE value of the yaw speed is high due to too many fluctuations all along the simulation.

- The settling time of the vehicle dynamics for acceleration, braking, and steering conditions are much higher than the corresponding subsystem settling time. Hence, a detailed dynamic model for each subsystem may not be required for simulating the overall vehicle dynamic response. However, such a subsystem model would be useful in developing the "lower-level" subsystem controllers for vehicle control tasks towards its autonomous operation.

- Comparison between the kinematic and dynamic models to calculate the yaw parameters of the vehicle has shown clear advantages in using dynamic models at higher speeds. It was found that a dynamic model should be used beyond a threshold longitudinal speed of 4.15 *m/s* for the vehicle under study.

- The proposed model is computationally less intensive in calculating the response of the vehicle for the case of longitudinal, lateral, and yaw dynamics when compared to the ATV software.

6.3 FUTURE SCOPE

- The developed model is limited to soft terrains and it can be improved for hard terrain also by reconsidering the way the lateral traction coefficient and the slip was calculated. In short, the terrain dynamics model needs to be changed.

- Model can be further improved by incorporating the uncertainties in the terrain geometry and the properties. The terrain properties were modeled as time invariant and with constant parameter values. But in real case scenario, they are time variant and non-linear, which needs to be addressed.

- Model can be extended to all six DOF by considering other DOF such as pitch, roll and bounce motion.

- Coupled dynamics of the tracked vehicle can be incorporated when the vehicle encounters the situation where the combined brake and steering, or combined acceleration and steering.

- Feedback control from the base vehicle to remotely controlled vehicle can be incorporated, which will improve the controllability of the vehicle.

- Detailed model of the gear shift dynamics can be included.

- Thermodynamic model for the engine can be incorporated to predict the transient characteristics of the engine.

REFERENCES

1. **Abel, A., U. Schreiber and Schindler, J.** (2006) Engine and Gearbox Modeling and Simulation for Improving the Shifting Behavior of Powertrains with Manual or Automated Transmission. *SAE INTERNATIONAL*, Michigan, 2006.

2. **Al-Milli, S., L. D. Seneviratne and K. Althoefer** (2010) Track-terrain modelling and traversability prediction for tracked vehicles on soft terrain. *Journal of Terramechanics*, **47**(**3**), 151–160.

3. **Assanis, D., W. Bryzik, N. Chalhoub, Z. Filipi, N. Henein, D. Jung and G. Zhang** (1999) Integration and use of diesel engine, driveline and vehicle dynamics models for heavy duty truck simulation. *SAE INTERNATIONAL*, Michigan, 1999.

4. **Bodin, A.** (1999) Development of a tracked vehicle to study the influence of vehicle parameters on tractive performance in soft terrain. *Journal of Terramechanics*, **36**, 167–181.

5. **Crosheck, J. E.** (2015) Skid-steering of crawlers. *SAE INTERNATIONAL*, 1390–1404.

6. **Ehlert, W., B. Hug and I. C. Schmid** (1992) Field measurements and analytical models as a basis of test stand simulation of the turning resistance of tracked vehicles. *Journal of Terramechanics*, **29**(**1**), 57–69.

7. **Fong, T., C. Thorpe and C. Baur** (2001) Advanced interfaces for vehicle tele-operation: Collaborative control, sensor fusion displays and remote driving tools. *Autonomous Robots*, **11**, 77–85.

8. **Ghosal, A.** *Robotics: Fundamental concepts and analysis*. Oxford University Press. New Delhi, 2006.

9. **Hainsworth, D. W.** (2001). Tele-operation user interfaces for mining robotics. *Autonomous Robots*, **11**, 19–28.

10. **Janarthanan, B., C. Padmanabhan and C. Sujatha** (2009) Modeling of Diesel Engine and Automatic Transmission of a Tracked Vehicle. *SAE INTERNATIONAL*, **4970**.

11. **Janarthanan, B., C. Padmanabhan and C. Sujatha** (2012) Longitudinal dynamics of a tracked vehicle: Simulation and experiment. *Journal of Terramechanics*, **49**(**2**), 63–72.

12. **Kar, M. K.** (1987) Prediction of track forces in skid-steering of military tracked vehicles. *Journal of Terramechanics*, **24**(**1**), 75–84.

13. **Khalil, H. K.** *Non-linear systems.* Pearson. New Jersey, 2014.

14. **Kinagi, G. V., S. Pujari, R. Birkhede and D. Sonawane** (2012) Brake System Design Calculation for Light Military Tracked Vehicle. *SAE INTERNATIONAL*, **1896** (**1**).

15. **Kitano, M. and H. Jyozaki** (1976) A theoretical analysis of steerability of tracked vehilces. *Journal of Terramechanics*, **13**(**4**), 241 - 258.

16. **Kitano, M. and M. Kuma** (1977) An analysis of horizontal plane motion of tracked vehicles. *Journal of Terramechanics*, **14**(**4**), 211–225.

17. **Kuang, M. L., M. Fodor, D. Hrovat and M. Tran** (1999) Hydraulic brake system modeling and control for active control of vehicle dynamics, *Proceedings of American control conference,* June, 4538–4542.

18. **Kuo, B**. C. Automatic control systems. Eastern Economy Edition, 2010.

19. **Laughery, S., G. Gerhart and P. Muench** (2000) Evaluating Vehicle Mobility Using Bekker's Equations. T*ank-automotive and Armaments Command Conference,* Michigan, August.

20. **Lee, J. H.** (2006) A real-time simulation model for tracked vehicles. *University of Michigan*, July, 2 - 198.

21. **Li, Y. and C. Tang** (2015) Research on Coupled Dynamic Model of Tracked Vehicles and Its Solving Method. *Mathematical Problems in Engineering, 2015*.

22. **Lu, X.Y. and J. K. Hedrick** (2005) Heavy-duty vehicle modelling and longitudinal control. *Vehicle System Dynamics, 43*(9), 653–669.

23. **Ma, Z. and D. T. Akcabay** (2004) Predicting the mobility of tracked robotic vehicles. *ASME International Mechanical Engineering Congress and Exposition*, California, 1–10.

24. **Maclaurin, B.** (2007) A skid-steering model with track pad flexibility. *Journal of Terramechanics*, **44**(**1**), 95–110.

25. **Maclaurin, B.** (2011) A skid-steering model using the magic formula. *Journal of Terramechanics*, **48**(**4**), 247–263.

26. **Martinez, J. L.** (2005) Approximating kinematics for tracked mobile robots. *International Journal of Robotics Research*, **24**(**10**), 867–878.

27. **Matej, J.** (2010) Tracked mechanism simulation of mobile machine in MSC.ADAMS/View. *Research in Agricultural Engineering*, **56**(**1**), 1–7.

28. **Moghadam, M. M., R. Mardani and M. Daryanavard** (2013) Simple modeling of approximate turning characteristics of tracked mobile vehicles in steady state condition. *International Conference on Robotics and Mechatronics*, *Tehran*, 113–120.

29. **Murakami, H., K. Watanabe and M. Kitano** (1992) A mathematical model for spatial motion of tracked vehicles on soft ground. *Journal of Terramechanics*, **29**(**1**), 71–81.

30. **Ogata, K.** *Modern control engineering.* Printice Hall. New Jersey, 1991.

31. **Park, W. Y., Y. C. Chang, S. S. Lee, J. H. Hong, J. G. Park and K. S. Lee,** (2008) Prediction of the tractive performance of a flexible tracked vehicle. *Journal of Terramechanics*, **45**(**1–2**), 13–23.

32. **Pawar. D.** (2016), An email communication made to ATV support, India, dharshan.pm@csmsoftware.com.

33. **Rajamani, R.** *Vehicle Dynamics and Control*. Springer. New York, 2006.

34. **Rubinstein, D. and R. Hitron** (2004) A detailed multi-body model for dynamic simulation of off-road tracked vehicles. *Journal of Terramechanics*, **41**(**2–3**), 163–173.

35. **Schuring, D., W. Pelz and M. G. Pottinger,** (1996). A model for combined pneumatic tyredcornering and brake forces. *SAE INTERNATIONAL*, **412**.

36. **Sharon, D.** (1993) Drive by wire. *Journal of Policy Planning and Future Studies*, 491–498.

37. **Sheridan, T. B.** (1995) Tele-operation, telerobotics and telepresence: A progress report. *Control Engineering Practice*, **3**(**2**), 205–214.

38. **Shu, X. B., H. Z. Ma and X. Liu,** (2002) Transient Modeling for Heavy Tracked Vehicle Performance and Fuel Consumption. *SAE INTERNATIONAL*, **724**.

39. **Solis, J. M. and R. G. Longoria** (2008) Modeling track-terrain interaction for transient robotic vehicle maneuvers. *Journal of Terramechanics*, **45**(**3**), 65–78.

40. **Song, Z. B., Y. H. Zweiri, L. D. Seneviratne and K. Althoefer** (2008) Non-linear observer for slip estimation of tracked vehicles. *Proceedings of the Institution of Mechanical Engineers, Part D: Journal of Automobile Engineering*, **222**(**4**), 515–533.

41. **Wangl, Z. and L. Bini** (2014). Power loss analysis of tracked travelling unit of high-speed tracked vehicle. *IEEE Transportation and Electrification Conference*,

Asia-Pacific, 3–6.

42. **Wismer, R. D. and H. J. Luth** (1973) Off-road traction prediction for wheeled vehicles. *Journal of Terramechanics*, **10**(**2**), 49–61.

43. **Wong, J. Y.** (1984) An introduction to terramechanics. *Journal of Terramechanics*, **21**(**1**), 5–17.

44. **Wong, J. Y.** *Theory of Ground Vehicles (Third Edit)*. John wiley and Sons, INC, New York, 2001.
45. **Wong, J. Y. and C. F. Chiang** (2005) A general theory for skid-steering of tracked vehicles on firm ground. *Proceedings of the Institution of Mechanical Engineers, Part D: Journal of Automobile Engineering*, **215**(**3**), 343–355.

46. **Wong, J. Y. and J. P. Thomas** (1983) On the characterization of the shear stress-displacement relationship of terrain. *Journal of Terramechanics*, **19**(**4**), 225–234.

47. **Xingguo, M., Y. Tao, Y. Xiaomei and Z. Bin** (2010) Modeling and simulation of multi-body dynamics for tracked vehicle based on RecurDyn. *Proceedings of third International Conference on Intelligent Networks and Intelligent Systems*, 669–671.

LIST OF PAPERS

SUBMITTED ON THE BASIS OF THIS THESIS

I. PRESENTATIONS IN CONFERENCES

1. **Senthilkumar, D., N. Babu, T. Asokan, and S. C. Subramanian,** Tele-operation of Unmanned Tracked Vehicles: Modeling and Simulation of Planar Motion Dynamics. *International Conference on Advances in Robotics*. ACM, Goa, July, 2015.

APPENDICES

A.1 LATERAL TRACTION COEFFICIENT CALCULATION

An accurate model for predicting the lateral traction coefficient for the tracked vehicle in soft terrain is not available in the literature. A modified general theory of skid-steering of the tracked vehicle for firm ground was explained (Wong, 2001). It has been claimed that the theory can be used for soft terrains by Al-Milli *et al.* (2010).

The procedure to calculate the lateral traction coefficient for soft terrain is as follows.

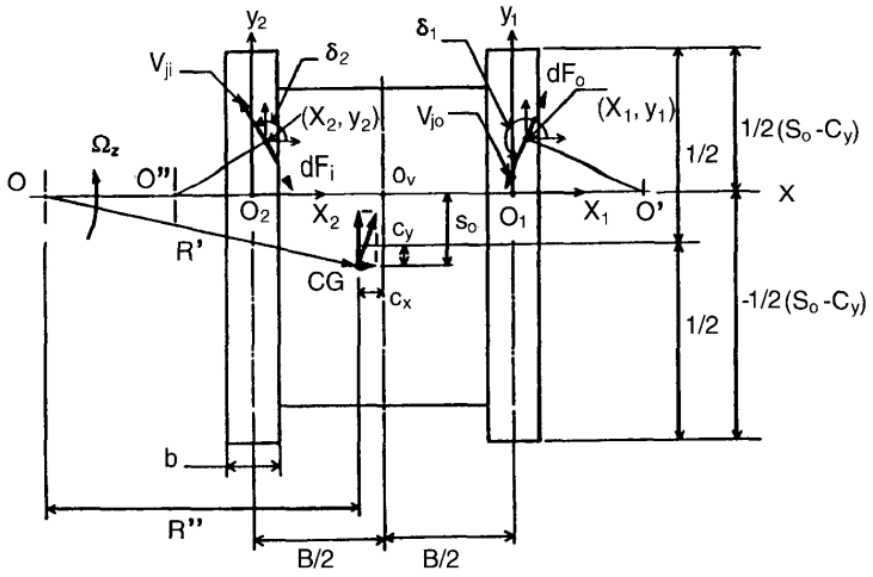

Fig. A.1: Kinematic representation of the track-terrain interface of a tracked vehicle

Wong, (2001)

According to the theory, shear speed (V_{ji}) at each element of the track-terrain interface is integrated with respect to the time to get the shear displacement. The shear displacement at the point (X_1, Y_1) in track-terrain interface for the outer track in x-axis $(j_{x0}(t))$, which is given by

$$j_{xo}(t)=\left(R(t)+\frac{B}{2}+c_x(t)+x_1\right)\left(\cos\left(\frac{\left(l/2+c_y(t)-s_o(t)-y_1\right)\omega_z(t)}{r\omega_o(t)}\right)-1\right) - y_1\sin\left(\frac{\left(l/2+c_y(t)-s_o(t)-y_1\right)\omega_z(t)}{r\omega_o(t)}\right), \quad \text{(A.1)}$$

where $c_x(t)$ and $c_y(t)$ is the distance between the C_G of the vehicle and center line of the vehicle hull in x and y directions respectively, $\omega_z(t)$ is the yaw speed of the vehicle, $\omega_o(t)$ and $\omega_i(t)$ are the angular speeds of the right and left sprocket of the vehicle respectively. The shear displacement at the point (X_1, Y_1) in track-terrain interface for the outer track in y-axis $\left(j_{yo}(t)\right)$ is given by

$$j_{yo}(t)=\left(R(t)+\frac{B}{2}+c_x(t)+x_1\right)\sin\left(\frac{\left(l/2+c_y(t)-s_o(t)-y_1\right)\omega_z(t)}{r\omega_o(t)}\right)-\left(\frac{l}{2}+c_y(t)-s_o(t)\right) + y_1\cos\left(\frac{\left(l/2+c_y(t)-s_o(t)-y_1\right)\omega_z(t)}{r\omega_o(t)}\right). \quad \text{(A.2)}$$

The resultant shear displacement $\left(j_o(t)\right)$ at point (X_1, Y_1) is given by

$$j_o(t)=\sqrt{\left(j_{xo}(t)^2+j_{yo}(t)^2\right)}. \quad \text{(A.3)}$$

The shear displacement at the point (X_2, Y_2) in track-terrain interface for the inner track in x-axis $\left(j_{xi}(t)\right)$ is given by

$$j_{xi}(t)=\left(R(t)-\frac{B}{2}+c_x(t)+x_2\right)\left(\cos\left(\frac{\left(l/2+c_y(t)-s_o(t)-y_2\right)\omega_z(t)}{r\omega_i(t)}\right)-1\right) - y_2\sin\left(\frac{\left(l/2+c_y(t)-s_o(t)-y_1\right)\omega_z(t)}{r\omega_i(t)}\right). \quad \text{(A.4)}$$

The shear displacement at the point (X_2, Y_2) in track-terrain interface for the outer track in y-axis $j_{yo}(t)$ is given by

$$j_{yo}(t) = \left(R(t) - \frac{B}{2} + c_x(t) + x_2 \right) \sin\left(\frac{\left(l/2 + c_y(t) - s_o(t) - y_2\right)\omega_z(t)}{r\omega_i(t)} \right) - \left(\frac{l}{2} + c_y(t) - s_o(t) \right) + y_2 \cos\left(\frac{\left(l/2 + c_y(t) - s_o(t) - y_2\right)\omega_z(t)}{r\omega_i(t)} \right). \quad \text{(A.5)}$$

The resultant shear displacement $(j_i(t))$ at point (X_2, Y_2) is given by

$$j_i(t) = \sqrt{\left(j_{xi}(t)^2 + j_{yi}(t)^2\right)}. \quad \text{(A.6)}$$

According to the general theory of skid-steering, the shear force developed at the interface of soft terrain is given by

$$dF_{(oj)}(t) = \left(c + \sigma_{oj} \tan\varphi\right)\left(1 - e^{-j_{oj}(t)/K}\right)dA, \quad \text{(A.7)}$$

where $\sigma_{o,i}$ is the pressure acting on the inner/outer track and *K* is the shear modulus. The moment of turning resistance on the right and left track is given by

$$M_{r(o,i)}(t) = \int_{\left(-\frac{l}{2}+c_y(t)-s_o(t)\right)}^{\left(\frac{l}{2}+c_y(t)-s_o(t)\right)} \int_{\left(-\frac{b}{2}\right)}^{\left(\frac{b}{2}\right)} y_{o,i}\left(c + \sigma_{o,i} \tan\phi\right)\left(1 - e^{-j_{o,i}(t)/K}\right)\cos\delta_{o,i}(t)\, dx_{o,i}\, dy_{o,i}. \quad \text{(A.8)}$$

The shear angle $\delta_{o,i}(t)$ are defined by

$$\cos\delta_{oj}(t) = \frac{-y_{oj}\omega_z(t)}{\sqrt{\left(\left(R(t) - \frac{B}{2} + c_x(t) + x_{oj}\right)\omega_z(t) - r\omega_{oj}(t)\right)^2 + \left(y_{oj}(t)\omega_z(t)\right)^2}}. \quad \text{(A.9)}$$

The coefficient of lateral traction is calculated by comparing Eq. 2.47 and Eq. 2.57. After rearranging the equation

$$\mu_t^{\,2}(t)+\left(\frac{4\left(M_{ro}(t)+M_{ri}(t)\right)}{Wl}\right)\mu_t(t)-\left(\frac{a_y(t)}{g}\right)^2=0. \tag{A.10}$$

By solving Eq. (A.10), for the range of speeds and the speed ratio in which the vehicle is going to be operated, the lateral traction coefficient for different vehicle speed (Fig. 2.14) was generated.

A.2 REASONS FOR NEGLECTING SOME ELEMENTS WHILE MODELING THE FLUID SYSTEM

In order to reduce the complexity in the model and to reduce the computation time, some elements in the fluid system were neglected as it has very minor contribution in calculating the output response. The details of the each are explained below:

Reason for Neglecting Resistance in hydraulic brake cylinder

According to Hagen Poiseuille's equation, pressure drop ΔP due to the major loss (pipe friction) is given as

$$\Delta P=\frac{128\mu_{hyd}a_{wc}\dot{x}_{out}}{\pi}\left(\frac{l_{mc}}{d_{mc}^{\,4}}+\frac{l_{hos}}{d_{hos}^{\,4}}+\frac{l_{br}}{d_{br}^{\,4}}\right), \tag{A.11}$$

where d_{mc} is the diameter of the master cylinder, d_{br} is the diameter of the brake cylinder, d_{hos} is the diameter of the hose which connects the master and brake cylinder, μ_{hyd} is the dynamic viscosity of the hydraulic fluid, l_{mc} is the length of the master

cylinder, l_{wc} is the length of the brake cylinder and l_{hose} is the length of the hose. After the substitution of the data sheet values in Eq. (A.11), the pressure drop in the hydraulic system due to the friction is $\Delta P = 9800\ N/m^2$. The pressure drop value was calculated for the maximum fluid discharge so that the resistance of the hydraulic system can never be more than the calculated pressure drop. But the actual pressure rise in the system is around 14 *bar* which is shown in Fig. 3.3(b). So it is reasonable to neglect the resistances in the fluid system since the pressure drop due to friction is lower when compared to the system pressure.

Reason for Neglecting the Inertia of the hydraulic fluid

Fluid inertia is governed by fluid density, fluid acceleration and the volume it occupies. Since the fluid density is a fluid property, only the fluid volume and the acceleration are the deciding factors of the inertia force. The total volume of the fluid v_{tot} that is displaced is equal to the volume of the fluid present in the master cylinder, brake cylinder and the hoses:

$$v_{tot} = v_{mc}(t) + v_{br}(t) + v_{hos}\ , \qquad \text{(A.12)}$$

where $v_{mc}(t)$ is the fluid volume occupied in the master cylinder, $v_{br}(t)$ is the fluid volume occupied in the brake cylinder and v_{hos} is the fluid occupied in the hose. By substituting the values in Eq. A.12, the total fluid volume v_{tot} was found to be $0.0001 m^3$. The mass of the fluid which is the product of fluid density and the fluid volume, was found to be 0.1 *kg*. Inertial force which is termed as inductance, which is the function of mass and acceleration of the hydraulic fluid. Since the hydraulic fluid of the brake system

is a closed system, mass of the fluid is found to be 0.1kg and the maximum acceleration of the hydraulic fluid for the brake system was determined by simulation which is 25 m/s^2. Hence the force due to the inductance of the fluid was calculated as 2.4871 *N* which is negligible with the actual force developed, was around 800 *N*. The brake piston acceleration should be around 8000 m/s^2 for the inertial force to be comparable which is infeasible. Hence, the inductance of the fluid has been neglected.

A.3 MODEL PARAMETERS

Table. A.1: Model Parameters Table

Inertia of the final drive (I_F)	0.15 $kg\text{-}m^2$
Inertia of the Engine (I_E)	0.2 $kg\text{-}m^2$
Inertia of the clutch and gear ($I_G(t)$)	0.5 $kg\text{-}m^2$
Gear Ratio ($\xi(t)$) Gear 1 Gear 2 Gear 3 Gear 4 Gear 5	 5.25 2.842 1.912 1.284 0.858
Transmission Efficiency (η)	0.8
Radius of the Sprocket (r)	0.3125 *m*
Lengths of link 1 (r_1) link 2 (r_2) link 3 (r_3)	 0.05 *m* 0.25 *m* 0.06 *m*
Ground link (r_{03})	0.255 *m*
Stiffness of the master cylinder spring (K_{mc})	6124 *N/m*
Stiffness of the brake cylinder spring (K_{wc})	55122 *N/m*
Bulk modulus of the fluid (β)	1.523741×10^8 m^5/N
stiffness of the band (K_{band})	61247 *N/m*
friction coefficient between the band and the cylinder (μ_{band})	0.85
lapping angle of the band over the cylinder (θ_{lap})	325°
mass of brake cylinder components (m_{bc})	1.8823 *kg*
Dynamic viscosity of the fluid (μ_{dyn})	0.015 $N\text{-}s/m^2$

Length of the master cylinder (l_{mc})	5 *in*
Length of the brake cylinder (l_{wc})	3 *in*
Diameter of the master cylinder (d_{mc})	7/8 *in*
Diameter of the brake cylinder (d_{wc})	2.5 *in*
breadth of the track (b)	0.3 *m*
breadth of the vehicle (B)	3.6 *m*
mass of the vehicle (m)	12868 *kg*
number of tracks (n_T)	2
number of sprocket and track wheels (n_w)	14
final drive gear ratio (ξ_F)	5.5
Inertia of the track and wheels (I_T and I_w)	0.5 *kg-m*^{2}
Yaw moment of inertia (I_{zz})	4.8126x10^7 *kg-m*^{2}
Length of the track (l)	7.2 *m*
Terrain constants k_c k_φ n	 4.37 196.72 1.6
shear modulus (K)	0.025 *m*
pressure angle (ϕ)	28°
cohesion (c)	1040 *N/m*^{2}
Traction coefficient (μ)	0.52

A.4 MAPE VALUE CALCULATION

Quantitative analysis of error deviation is done for all the variables using MAPE. MAPE parameter has been used in different situation in the above work. MAPE is defined as

$$MAPE = \frac{1}{n}\sum_{i=1}^{n}\left(\frac{\left(x_{act,i} - x_{pr,i}\right)}{x_{act,i}}100\right), \tag{A.13}$$

where n is the number of samples, $x_{act,i}$ is the actual value of the variable and $x_{pr,i}$ is the predicted value of the variable.